

THERMODYNAMIC PROPERTIES OF THE HIGH-PRESSURE PHASES IN
SOLID NITROGEN CLOSE TO PHASE TRANSITIONS

A THESIS SUBMITTED TO
THE GRADUATE SCHOOL OF NATURAL AND APPLIED SCIENCES
OF
MIDDLE EAST TECHNICAL UNIVERSITY

BY

ÖZGE AKAY

IN PARTIAL FULFILLMENT OF THE REQUIREMENTS
FOR
THE DEGREE OF DOCTOR OF PHILOSOPHY
IN
PHYSICS

NOVEMBER 2020

Approval of the thesis:

**THERMODYNAMIC PROPERTIES OF THE HIGH-PRESSURE PHASES
IN SOLID NITROGEN CLOSE TO PHASE TRANSITIONS**

submitted by **ÖZGE AKAY** in partial fulfillment of the requirements for the degree of
Doctor of Philosophy in Physics Department, Middle East Technical University
by,

Prof. Dr. Halil Kalıpçılar
Dean, Graduate School of **Natural and Applied Sciences**

Prof. Dr. Altuğ Özpineci
Head of Department, **Physics**

Prof. Dr. Hamit Yurtseven
Supervisor, **Physics, METU**

Examining Committee Members:

Prof. Dr. Bekir Sıtkı Kandemir
Physics, Ankara University

Prof. Dr. Hamit Yurtseven
Physics, METU

Prof. Dr. Hakan Altan
Physics, METU

Prof. Dr. Nizami Hasanlı
Physics, METU

Assoc. Prof. Dr. Barış Emre
Physics, Ankara University

Date: 18.11.2020

I hereby declare that all information in this document has been obtained and presented in accordance with academic rules and ethical conduct. I also declare that, as required by these rules and conduct, I have fully cited and referenced all material and results that are not original to this work.

Name, Surname: Özge Akay

Signature :

ABSTRACT

THERMODYNAMIC PROPERTIES OF THE HIGH-PRESSURE PHASES IN SOLID NITROGEN CLOSE TO PHASE TRANSITIONS

Akay, Özge

Ph.D., Department of Physics

Supervisor: Prof. Dr. Hamit Yurtseven

November 2020, 114 pages

In this thesis, the physical properties of solid nitrogen are investigated in a wide range of temperature and pressure by analyzing experimental data from the literature. For this investigation, various models are implemented to the experimental data in order to evaluate observed behavior of thermodynamic and spectroscopic properties of solid nitrogen. By means of the calculating Grüneisen parameter which depends on the volume, the pressure and temperature dependence of the Raman and IR frequencies are estimated for the internal (vibrons) and external modes (lattice) of solid nitrogen. Especially, the mean field theory based on Landau phenomenological model is used to calculate P-T phase diagram of solid nitrogen. Also by using this model, we estimate the inverse susceptibility, the entropy, the heat capacity and the thermal expansion as a function of temperature close to the phase transition. Regarding to evaluation of the thermodynamic properties, we also predict temperature dependence of the thermodynamic functions from frequency shift and volume data which are obtained from literature and we use the Pippard relations to establish linearity for thermodynamic and spectroscopic quantities. As another calculation, we calculated the frequency shift and damping constant (FWHM) as a function of pressure via the anharmonic

self energy. According to the evaluation of spectroscopic properties (frequency shift, damping constant) , we also use the pseudospin-phonon coupling (PS) and the energy-fluctuation (EF) models to obtain the damping constant as a function of temperature at constant pressures. The inverse relaxation time and the activation energy as a function of temperature are also calculated close to the phase transition. In addition to these calculations, we analyze the thermodynamic and dielectric properties at various pressures and temperatures by using the Raman frequencies of cubic gauche solid nitrogen. All these calculations indicate that the methods used for analysis can also be applied to some other molecular solids close to phase transitions.

Keywords: Vibrational Frequencies, Grüneisen Parameter, Mean Field Theory, Damping constant, solid nitrogen

ÖZ

FAZ GEÇİŞLERİ YAKININDA KATI AZOTUN YÜKSEK BASINÇ FAZLARININ TERMODİNAMİK ÖZELLİKLERİ

Akay, Özge

Doktora, Fizik Bölümü

Tez Yöneticisi: Prof. Dr. Hamit Yurtseven

Kasım 2020 , 114 sayfa

Bu tezde, katı nitrojenin fiziksel özellikleri geniş bir sıcaklık ve basınç aralığında literatürden deneysel sonuçlar analiz edilerek incelenmiştir. Bu araştırmada, katı azotun termodinamik ve spektroskopik özelliklerini değerlendirmek için deneysel verilere çeşitli modeller uygulanmıştır. Hacme bağlı olan Grüneisen parametresi hesaplanarak, katı nitrojenin iç (vibronlar) ve dış modları (lattice) için Raman ve IR frekanslarının basınç ve sıcaklık bağımlılığı tahmin edilmiştir. Katı nitrojenin P-T faz diyagramını hesaplamak için özellikle Landau fenomenolojik modeline dayanan ortalama alan teorisi kullanılmıştır. Ayrıca bu modeli kullanarak, ters duyarlılığı, entropiyi, ısı kapasitesini ve ısı genleşmeyi faz geçişine yakın sıcaklığın bir fonksiyonu olarak tahmin ettik. Termodinamik özelliklerin değerlendirilmesiyle ilgili olarak, termodinamik fonksiyonların sıcaklık bağımlılığını da literatürden elde edilen frekans kayması ve hacim verilerinden tahmin ettik ve termodinamik ve spektroskopik büyüklükler için doğrusal ilişkiyi oluşturmak için Pippard bağıntılarını kullandık. Başka bir hesaplama olarak, harmonik olmayan öz enerji yoluyla basıncın bir fonksiyonu olarak frekans kayması ve sönümleme sabitini (FWHM) hesapladık. Spektroskopik özelliklerin (fre-

kans kayması, sönümlleme sabiti) değlerlendirmesine göre, sönümlleme sabitini sabit basınçlarda sıcaklığın bir fonksiyonu olarak elde etmek için sanki spin-fonon birleştirme (PS) ve enerji dalgalanması (EF) modellerini de kullandık. Ters gevşeme süresi ve sıcaklığın bir fonksiyonu olarak aktivasyon enerjisi de faz geçişine yakın olarak hesaplandı. Bu hesaplamalara ek olarak, çeşitli basınç ve sıcaklıklarda termodinamik ve dielektrik özelliklerini kübik gauche katı nitrojenin Raman frekansları kullanılarak analiz edildi. Tüm bu hesaplamalar, analiz için kullanılan yöntemlerin, faz geçişlerine yakın diğer bazı moleküler katılara da uygulanabileceğini göstermektedir.

Anahtar Kelimeler: Titreşim Frekansları, Grüneisen Parametresi, Ortalama Alan Teorisi, Sönüm Sabiti, Katı Azot

To myself

ACKNOWLEDGMENTS

I would like to express my sincere gratitude to Prof. Dr. Hamit Yurtseven for his continuous guidance, encouragement, support, advice and supervision throughout this study. I would like to thank to Prof. Dr. Bekir Sıtkı Kandemir, Prof. Dr. Hakan Altan, Prof. Dr. Nizamı Hasanlı and Assoc. Prof. Dr. Barış Emre for their judgments and helpful critics as the thesis committee. I would like to express my deepest appreciation to my family for their love, support and faith in me. I would like to my best friend Simge Ateş. She has always encouraged me to keep on, no matter what problem was. I would like to thank officemates for their supports and friendship during hard times of PhD. programme. I would also like to thank Şengül Ersoy for her sincere friendship. Last but not least, I owe an appreciation to my dear friend Ahmet Sefer for his heartening attitude , valuable help and support.

TABLE OF CONTENTS

ABSTRACT	v
ÖZ	vii
ACKNOWLEDGMENTS	x
TABLE OF CONTENTS	xi
LIST OF TABLES	xiii
LIST OF FIGURES	xviii
CHAPTERS	
1 INTRODUCTION	1
1.1 Phase and Phase transitions	1
1.2 Properties of Solid Nitrogen	2
1.3 Phase Diagram of Solid Nitrogen	3
2 THEORY	7
2.1 Classification of Phase transition	7
2.2 Landau Phenomenological Theory	9
2.3 Mean Field Theory	11
2.3.1 Calculations of the Landau Energy in the Mean Field Theory	11
2.4 Grüneisen Parameter	13
2.5 Damping Constant	14

2.6	Pippard Relations	18
2.7	Anharmonic Self Energy	19
3	CALCULATIONS AND RESULTS	21
3.1	"Calculations of the Raman and IR frequencies from the volume data at high pressures in Solid nitrogen."	21
3.2	"Calculation of the phase diagrams for the fluid-solid and solid-solid ($\delta - \delta_{loc} - \epsilon$) transitions in molecular nitrogen by using mean field model."	29
3.3	"Calculation of the thermodynamic functions using a mean field model for the fluid-solid transition in nitrogen."	37
3.4	"Raman bandwidths calculated for the librational (α -phase) and internal (ϵ , δ_{loc} and δ phases) modes in N_2 using pseudospin-phonon coupling (PS) and energy-fluctuation (EF) models"	42
3.5	"Calculation of the thermodynamic functions from the Raman frequency shifts close to the ϵ - δ_{loc} - δ phases transitions and Pippard relations in nitrogen."	50
3.6	"Calculation of the Raman frequency and linewidth of vibrons using anharmonic self energy model for the ϵ - δ_{loc} - δ phases in nitrogen." .	60
3.7	"Calculation of the inverse relaxation time and the activation energy as a function of temperature for the Raman modes close to the phase transitions in solid nitrogen."	66
3.8	"Calculations of the temperature and pressure dependence of the thermodynamic quantities and analysis of the dielectric properties by using the Raman frequencies of cubic gauche nitrogen."	77
4	CONCLUSIONS	95
	REFERENCES	99

LIST OF TABLES

TABLES

Table 3.1	Values of the coefficients to Eq.(3.2) fitted to the observed volume data[30] for solid nitrogen.	22
Table 3.2	Values of the coefficients according to Eq.3.1 fitted to the observed Raman and IR frequencies [20] for the lattice modes indicated within the pressure interval for solid nitrogen.	23
Table 3.3	Values of the coefficients according to Eq.3.1 fitted to the observed Raman and IR frequencies [20] for vibrons indicated within the pressure interval for solid nitrogen.	26
Table 3.4	Values of the coefficients of the pressure-dependent term $A(P)$ according to Eq.3.5 for the lattice modes within the pressure intervals indicated for nitrogen.	26
Table 3.5	Values of the coefficients of the pressure-dependent term $A(P)$ according to Eq.3.5 for the vibrons within the pressure intervals indicated for nitrogen.	27
Table 3.6	Values of the fitted parameters within the pressure intervals indicated for the fluid-solid transition[53] and the melting curves[92] according to Eq.3.13, and for the solid-solid transitions of $\delta - \delta_{loc}$ and $\delta_{loc} - \epsilon$ [23] according to Eq.3.35 in N_2	32

Table 3.7	Values of the slope(dP/dT) within the temperature and pressure intervals according to the equations indicated for the transitions in N_2 . T_c and P_c denote maximum (T_m, P_m) values for the melting curve and fluid–solid transition (Fig.3.8). dT/dP values are calculated at 300 K for the $\delta - \delta_{loc}$ and $\delta_{loc} - \epsilon$ transitions in N_2	33
Table 3.8	Values of the coefficients a_2 , which were obtained by fitting Eq.(3.54) ($a_2=0$) to the experimental T-P data for the solid N_2 -liquid N_2 transition [54,53] within the temperature and pressure intervals indicated. Values of the transition temperature (T_t) and pressure (P_t) in Eq.(3.54), are also given here.	38
Table 3.9	Values of the coefficients a_0 , a_1 and a_2 (Eq.3.58) and, of the a,b and c (Eq.3.59) with the ν_0 and T_c values for the Raman modes of E_g for the transition of $\alpha - \beta$ [86] and ν_1 for the transition of $\epsilon - \delta_{loc} - \delta$ [23] at the pressures indicated within the temperature intervals in solid nitrogen. .	43
Table 3.10	Values of the coefficients a_0 , a_1 and a_2 (Eq.3.57) and of the a,b and c (Eq.3.58) with the ν_0 and T_c values for the frequency difference ($\nu_1 - \nu_2$) of the ν_1 and ν_2 for the transition of $\epsilon - \delta_{loc} - \delta$ [23] at the pressures indicated within the temperature intervals in solid nitrogen.	45
Table 3.11	Values of the coefficients calculated according to the Eqs.2.34 and 2.36 for the E_g librational mode of the α -phase ($P=0$) in solid nitrogen. . .	47
Table 3.12	Values of the coefficients calculated according to the Eqs.2.34 and 2.36 for the ν_1 mode for the phases of ϵ , δ_{loc} and δ ($P=18$ GPa) in solid nitrogen.	47
Table 3.13	Values of the coefficients calculated according to the Eqs. 2.34 and 2.36 for the frequency difference ($\nu_1 - \nu_2$) for the phases of ϵ , δ_{loc} and δ at constant pressures in solid nitrogen.	48
Table 3.14	Values of the coefficients calculated according to the Eq.3.62 for the vibrons indicated in solid nitrogen.	52

Table 3.15 Values of the coefficients calculated according to the Eq.3.65 for the phase transitions indicated in solid nitrogen.	52
Table 3.16 Calculated dP/dT values by using Eq.3.65 and the values of the slope dP/dT and the intercept of $(1/V)(dV/dT)$ (Eq.7) derived from the Pippard relations (Eqs.3.66 and 3.67) for the vibrons of solid nitrogen. . .	54
Table 3.17 Values of the fitted parameters according to Eq.3.68 for the fluid-solid transition[53] in nitrogen.	56
Table 3.18 Values of the fitted parameters according to Eq.3.70 for the fluid-solid transition[53] and melting curve[92] in nitrogen.	56
Table 3.19 Values of the dP/dT and the $(1/V)(dV/dT)$ according to the Pippard relations (Eqs.3.66 and 3.67) for the fluid-solid transition in nitrogen. . . .	57
Table 3.20 Values of the parameters for the Raman frequencies of the vibrons ν_1 , ν_2 and ν_{22} according to Eq.2.46 by using the observed data [23] within the temperature intervals indicated for the phases of ϵ , δ_{loc} and δ (P=18 GPa) in solid nitrogen.	62
Table 3.21 Values of the parameters for the frequency difference ($\nu_1-\nu_2$) of the Raman internal modes ν_1 and ν_2 according to Eq.2.46 by using the observed data [23] within the temperature intervals at constant pressures indicated for the phases of ϵ , δ_{loc} and δ in the solid nitrogen.	62
Table 3.22 Values of the parameters for the linewidths, of the vibrons ν_1 , ν_2 and ν_{22} according to Eq.2.47 by using the observed data [23] within the temperature intervals indicated for the phases of ϵ , δ_{loc} and δ (P= 18 GPa) in solid nitrogen.	64
Table 3.23 Values of the parameters for the linewidths, of the frequency difference ($\nu_1-\nu_2$) of the Raman internal modes ν_1 and ν_2 according to Eq.2.47 by using the observed data [23] within the temperature intervals at constant pressures indicated for the phases of ϵ , δ_{loc} and δ in the solid nitrogen.	65

Table 3.24 Values of the activation energy (E_a) and the attempt relaxation time (τ_0), which were extracted from Eq.3.73 for the E_g librational mode [86] in the solid nitrogen (P=0).	68
Table 3.25 Values of the activation energy (E_a) and the attempt relaxation time (τ_0), which were extracted from Eq.3.73 for the internal modes of ν_1 , ν_2 and ν_{22} in the solid nitrogen (P=18 GPa).	68
Table 3.26 Values of the activation energy (E_a) and the attempt relaxation time (τ_0), which were extracted from Eq.3.74 for the difference in the frequency shifts ($\nu_1 - \nu_2$) of the Raman internal modes ν_1 and ν_2 within the temperature intervals for the phases at constant pressures indicated in N_2 by using the observed frequency and linewidth data [23].	73
Table 3.27 Values of the activation energy (E_a) with the coefficients A,B and C which were extracted by fitting (Eq.3.74) to the observed FWHM for the E_g mode at P=0 [86] and for the internal modes of ν_1 , ν_2 and ν_{22} at P=18 GPa [23] within the temperature intervals indicated in the solid nitrogen.	73
Table 3.28 Values of the activation energy E_a with the coefficients A,B and C which were extracted from Eq.3.74 by fitting to the observed FWHM data [23] for the difference in the frequency shifts ($\nu_1 - \nu_2$) of the Raman internal modes ν_1 and ν_2 at constant pressures within the temperature intervals indicated in the solid nitrogen.	74
Table 3.29 Values of the coefficients V_0 , α and β (Eq.3.75) at the pressures indicated for the cubic gauche solid nitrogen.	77
Table 3.30 Values of the fitted parameters for the the temperature dependence of the isothermal compressibility $\kappa_T=(1/B)$ (Eq.3.77) with the thermal expansion α_P at 295 K and the slope dP/dT of the transition line in the P-T phase diagram for the cubic gauche nitrogen.	79
Table 3.31 Values of the coefficients e_0, e_1, e_2 at constant pressures indicated (Eq.3.78) for cubic gauche solid nitrogen.	80

Table 3.32 Values of the coefficients b_0 , b_1 and b_2 (Eq.3.81) and b'_0 , b'_1 and b'_2 (Eq.3.83) for various pressures for the cubic gauche solid nitrogen.	81
Table 3.33 Values of the coefficients V_0 , α and β (Eq.3.75) at the pressures indicated for the cubic gauche solid nitrogen.	82
Table 3.34 Values of coefficients a_0 , a_1 , a_2 for the Raman and infrared modes in the phases indicated according to Eq.(3.85) and the coefficients of the additional term $A(P)$ which were determined by fitting Eq.(3.88) to the observed frequency data[28] for the cubic gauche solid nitrogen.	86
Table 3.35 Values of the coefficients b_0 , b_1 and b_2 by using the volume-pressure (V-P) data [46] according to Eq.(3.86) within the pressure range indicated for cubic gauche solid nitrogen.	86
Table 3.36 Values of coefficients a_0 , a_1 , a_2 for the frequencies of zone-center phonon modes according to Eq.(3.85) by using the observed data [42]. . .	86
Table 3.37 Values of the coefficients b_0 , b_1 and b_2 using the volume-pressure (V-P) data [101] according to Eq.(3.86) with V_0 within the pressure range indicated for cubic gauche solid nitrogen.	88

LIST OF FIGURES

FIGURES

Figure 1.1	Typical phase diagram for pure substance.	2
Figure 1.2	Schematic representation of the observed T-P phase diagram of solid nitrogen. Shaded areas are noncrystalline and liquid phases[30]. . .	5
Figure 1.3	Polymeric forms of solid nitrogen[41].	5
Figure 2.1	The changes in thermodynamic quantities due to first order phase transition. G are continuous in the transition, but the first derivatives of G (V and S) are discontinuous[62]	8
Figure 2.2	The changes in thermodynamic quantities due to second order phase transition. First derivatives of G are continuous, but some second derivatives (C_p) diverge[62]	9
Figure 2.3	Landau free energy at different temperatures for second order phase transition[69].	13
Figure 3.1	Pressure dependence of the isothermal mode Grüneisen parameter (γ_T) calculated for lattice modes indicated according to Eq.3.3 by using the observed data for the Raman and IR frequencies [20] and volume[30] of solid nitrogen.	23
Figure 3.2	Pressure dependence of the isothermal mode Grüneisen parameter (γ_T) calculated for lattice modes indicated according to Eq.3.3 by using the observed data for the Raman and IR [20] and volume [30] of solid nitrogen.	24

Figure 3.3	Pressure dependence of the isothermal mode Grüneisen parameter (γ_T) calculated for lattice modes indicated according to Eq.3.3 by using the observed data for the Raman and IR frequencies[20] and volume [30] of solid nitrogen.	24
Figure 3.4	Pressure dependence of the isothermal mode Grüneisen parameter (γ_T) calculated for vibrons indicated according to Eq.3.3 by using the observed data for the Raman and IR frequencies[20] and volume [30] of solid nitrogen.	25
Figure 3.5	Pressure dependence of the isothermal mode Grüneisen parameter (γ_T) calculated for vibrons indicated according to Eq.3.3 by using the observed data for the Raman and IR frequencies[20] and volume [30] of solid nitrogen.	25
Figure 3.6	Raman and IR frequencies calculated for the lattice modes(red squares) indicated as a function of pressure according to Eq.3.4 for solid nitrogen. Observed data (black squares)[20] are also given here.	27
Figure 3.7	Raman and IR frequencies calculated for the vibrons(red squares) indicated as a function of pressure according to Eq.3.4 for solid nitrogen. Observed data (black squares)[20] are also given here.	28
Figure 3.8	Calculated phase diagram of N_2 in the melting region according to Eq.(3.6) by using the mean field model. Observed data (squares)[53] and (circles)[92] with the uncertainties are also given for the fluid-solid transition in nitrogen.	32
Figure 3.9	Calculated phase diagram of N_2 for the transitions of $\delta_{loc} - \epsilon$ and $\delta_{loc} - \epsilon$ according to Eq.3.35 using the experimental data [23].	37
Figure 3.10	Variation of the order parameter ψ (normalized) with the temperature (a) and the pressure (b) at the transition pressures of $P_t = 74.3$ GPa and $P_t = 106.9$ GPa by using the observed T-P data (circles) [54] and (squares) [53], respectively, for the solid –liquid transition in N_2 according to Eq.3.52 through Eq.3.54.	39

Figure 3.11	Inverse susceptibility χ_{ψ}^{-1} of the order parameter ψ as a function of temperature (a) and pressure (b) at the transition pressures of $P_t=74.3$ GPa and $P_t=106.9$ GPa by using the observed T-P data (circles) [54] and (squares) [53] respectively, for the solid –liquid transition in N_2 according to Eq.3.55.	40
Figure 3.12	Entropy S (normalized) calculated from the free energy (Eq.11) as a function of temperature at the transition pressures of $P_t=74.3$ GPa and $P_t=106.9$ GPa by using the observed T-P data (circles) [54] and (squares) [53] respectively, for the solid –liquid transition in N_2	40
Figure 3.13	Heat capacity C_v (normalized) calculated from the free energy (Eq.3.56) as a function of temperature at the transition pressures of $P_t=74.3$ GPa and $P_t=106.9$ GPa by using the observed T-P data (circles) [54] and (squares) [53] respectively, for the solid –liquid transition in N_2	41
Figure 3.14	Thermal expansion α_p (normalized) as function of temperature at the transition pressures of $P_t=74.3$ GPa and $P_t=106.9$ GPa using the observed T-P data (circles) [54] and (squares) [53] respectively, for the solid –liquid transition in N_2	41
Figure 3.15	Isothermal compressibility κ_T (normalized) as a function of temperature at the transition pressures of $P_t=74.3$ GPa and $P_t=106.9$ GPa by using the T-P data (circles) [54] and (squares) [53] respectively, for the solid –liquid transition in N_2	42
Figure 3.16	Raman frequency calculated for the Raman modes of E_g by using Eqs.(3.57) and (3.58) through Eq. (3.59) for the α phase ($P=0$) with the observed data [86] in solid nitrogen.	44
Figure 3.17	Raman frequency calculated for the internal mode of ν_1 by using Eqs.(3.57) and (3.58) through Eq. (3.59) for the ϵ , δ_{loc} and δ phases ($P=18$ GPa) with the observed data [23] in solid nitrogen.	45

Figure 3.18	Raman frequency calculated for the frequency difference ($\nu_1 - \nu_2$) of the ν_1 and ν_2 by using Eqs.(3.57) and (3.58) through Eq. (3.59) for the ϵ , δ_{loc} and δ phases at constant pressures with the observed data [23] in solid nitrogen.	46
Figure 3.19	Damping constant (linewidth) calculated from Eqs.2.34 and 2.36 for the E_g mode for the α -phase (P=0) with the observed data[86] in solid nitrogen.	49
Figure 3.20	Damping constant (linewidth) calculated from Eqs.2.34 and 2.36 for the ν_1 mode of the ϵ , δ_{loc} and δ phases at constant pressures with the observed data [23] in solid nitrogen.	49
Figure 3.21	Damping constant (linewidth) calculated from Eqs.2.34 and 2.36 for the frequency difference ($\nu_1 - \nu_2$) for the phases of ϵ , δ_{loc} and δ at constant pressures with the observed data [23] in solid nitrogen.	50
Figure 3.22	Temperature dependent thermal expansion calculated from Eq.3.61 for the Raman modes of ν_1 , ν_2 and ν_{22} for the phases of ϵ , δ_{loc} and δ in solid nitrogen.	53
Figure 3.23	Temperature dependent isothermal compressibility calculated from Eq.3.63 for the Raman modes of ν_1 , ν_2 and ν_{22} for the phases of ϵ , δ_{loc} and δ in solid nitrogen.	53
Figure 3.24	Difference in the heat capacity calculated from Eq.3.64 for the Raman modes of ν_1 , ν_2 and ν_{22} for the phases of ϵ , δ_{loc} and δ in solid nitrogen.	54
Figure 3.25	$(C_p - C_v)/V$ versus $\alpha_P T$ for the phases of ϵ , δ_{loc} and δ in solid nitrogen according to the Pippard relation (Eq.3.66).	55
Figure 3.26	Thermal expansion (α_p) versus the isothermal compressibility (κ_T) for the phases of ϵ , δ_{loc} and δ in solid nitrogen according to the Pippard relation (Eq.3.67).	55

Figure 3.27	Isothermal compressibility (κ_T) at various pressures calculated according to Eq.3.69 for the two different observed V-P data (circle[53] and square[54]).	57
Figure 3.28	Thermal expansion (α_P) at various pressures calculated according to Eq.3.63 for the two different observed T-P data (circle[92] and square[53]).	58
Figure 3.29	Difference in the heat capacity at various pressures calculated according to Eq.(3.64) for the fluid-solid transition in nitrogen.	58
Figure 3.30	($C_p - C_v$) versus $V\alpha_P$ as a function of pressures according to the Pippard relation (Eq.3.66).	59
Figure 3.31	Thermal expansion (α_P) versus isothermal compressibility (κ_T) as a function of pressures according to the Pippard relation (Eq.3.67) at two different pressure interval.	59
Figure 3.32	Temperature dependence of the Raman frequency for the vibron ν_1 as a function of temperature (P=18.5 GPa) according to Eq.2.46 which was fitted to the experimental data [23] for the phases of ϵ , δ_{loc} and δ in the solid nitrogen.	61
Figure 3.33	Temperature dependence of the Raman frequency for the vibrons ν_2 and ν_{22} as a function of temperature (P=18.5 GPa) according to Eq.2.46 which was fitted to the experimental data [23] for the phases of ϵ , δ_{loc} and δ in the solid nitrogen.	61
Figure 3.34	Temperature dependence of the Raman frequency shifts ($\nu_1 - \nu_2$) for the Raman internal modes ν_1 and ν_2 as a function of temperature at constant pressures according to Eq.2.46 which was fitted to the experimental data [23] for the phases of ϵ , δ_{loc} and δ in the solid nitrogen. . . .	64
Figure 3.35	Temperature dependence of the linewidths for vibrons ν_1 , ν_2 and ν_{22} as a function of temperature (P=18.5 GPa) according to Eq.2.47 which was fitted to the experimental data [23] for the phases of ϵ , δ_{loc} and δ in the solid nitrogen.	65

- Figure 3.36 Temperature dependence of the difference in the linewidths for the corresponding to the frequency difference ($\nu_1 - \nu_2$) of vibrons ν_1 and ν_2 as a function of temperature at four constant pressures indicated according to Eq.2.47 which was fitted to experimental data [23] for the phases of ϵ , δ_{loc} and δ in the solid nitrogen. 66
- Figure 3.37 Temperature dependence of the inverse relaxation time (τ^{-1}) calculated according to Eq.3.72 for the E_g mode of solid nitrogen (α phase, $P=0$) by using the observed data [86]. 68
- Figure 3.38 The temperature dependence of the inverse relaxation time (τ^{-1}) calculated according to Eq.3.72 for the ν_1 and ν_2 modes for the ϵ , δ_{loc} and δ phases in N_2 ($P=18$ GPa) by using the observed data [23]. Vertical lines denote the phase boundaries (at T_c) between the two phases. 69
- Figure 3.39 Relaxation time (logarithmic) as a function of the inverse temperature for the E_g mode according to Eq.3.73 in the solid nitrogen (α phase, $P=0$). Solid line represents the best fit (Eq.3.73) to the values given. 69
- Figure 3.40 Relaxation time (logarithmic) as a function of the inverse temperature for the ν_1 and ν_2 modes according to Eq.3.73 in the N_2 (ϵ , δ_{loc} and δ phases, $P=18$ GPa). Vertical lines denote the phase boundaries (at T_c) between the two phases. 70
- Figure 3.41 Temperature dependence of the inverse relaxation time (τ^{-1}) calculated according to Eq. (3.73) for the frequency shifts $\nu_1 - \nu_2$ of the internal modes ν_1 and ν_2 by using the observed Raman frequency and FWHM data[23] at constant pressures indicated in the solid nitrogen. In the ϵ phase (c), solid line is the best fit (Eq.3.72) to the τ^{-1} values. Vertical lines denote the phase boundaries (at T_c) between the two phases. 71

Figure 3.42 Relaxation time (logarithmic) as a function of the inverse temperature for the difference in the frequency shifts ($\nu_1 - \nu_2$) of the internal modes ν_1 and ν_2 by using the observed Raman frequency and FWHM data [23] according to Eq.(3.73) at constant pressures indicated in the solid nitrogen. Solid lines represent the best fit (Eq.3.74) to the values. Vertical lines denote the phase boundaries (at T_c) between the two phases. 72

Figure 3.43 Temperature dependence of the linewidth of the E_g line of the α phase ($P=0$) in N_2 . Solid line represents best fit (Eq.3.74) to the experimental data [86]. 75

Figure 3.44 Temperature dependence of the FWHM of the internal modes of the ν_1 and ν_2 for the phases of ϵ , δ_{loc} and δ ($P=18$ GPa) in N_2 . Solid lines represent best fit (Eq.3.74) to the observed FWHM data [23]. Vertical lines denote the phase boundaries (at T_c) between the two phases. 75

Figure 3.45 Temperature dependence of the FWHM of the $\nu_1 - \nu_2$ of the internal modes of the ν_1 and ν_2 for the phases of ϵ , δ_{loc} and δ at constant pressures indicated in N_2 . Solid lines represent best fit (Eq.3.74) to the observed FWHM data [23]. Vertical lines denote the phase boundaries (at T_c) between the two phases. 76

Figure 3.46 Temperature dependence of volume at various pressures (0,35,125 and 250 GPa) for the cubic gauche solid nitrogen. 78

Figure 3.47 Time dependence thermal expansion (α_P) calculated through Eq.3.75 at various pressures for the cg-N. 78

Figure 3.48 Temperature dependence of the isothermal compressibility κ_T calculated (3.79) at the pressures indicated for the cubic gauche nitrogen. 79

Figure 3.49 Temperature dependence of the bulk modulus $B(T)$ according to $B(T)=1/\kappa_T$ (Eq.3.79) at the pressures indicated for the cubic gauche nitrogen. 80

Figure 3.50	Heat capacity (C_P) as a function of temperature by using the calculated $V(T)$ and C_v data[28] through Eq.3.82 at the pressures indicated for the cubic gauche nitrogen.	81
Figure 3.51	Thermal expansion κ_T/κ_0 as a function of pressure (T=295 K), which was calculated according to Eq.3.79 for cubic gauche solid nitrogen.	83
Figure 3.52	Thermal expansion α_P as a function of pressure (T=295 K), which was calculated according to Eq.3.79 for cubic gauche solid nitrogen.	84
Figure 3.53	Heat capacity as a function of pressure (T=295 K) which was calculated according to Eq.3.82 for cg-N.	84
Figure 3.54	Grüneisen parameter γ as a function of pressure, which was calculated according to Eq.3.80 for the cubic gauche solid nitrogen.	85
Figure 3.55	Isothermal mode Grüneisen parameter γ_T as a function of pressure which was calculated using Eq.3.84 for the optic modes indicated in cg-N.	87
Figure 3.56	Calculated frequencies of the optic modes as a function of pressure through Eq.3.87 with the observed data only [45] for the cg-N.	87
Figure 3.57	Static frequency dielectric constant as a function of frequency for the pressure dependent optic modes [28] in the cg-N.	88
Figure 3.58	The Raman frequencies (ν^2) [45] as a function of the elastic anisotropy(A) [12] due to the elastic constant c_{11} , c_{12} and c_{44} in the pressure range of 0-360 GPa (a) and 0-100 GPa (b).	89
Figure 3.59	Static frequency dielectric constant as a function of Variation of the frequency shifts $(1/\nu)(\partial\nu/\partial P)$ as derived from the Raman frequencies as a function of elastic anisotropy (A) for the Raman frequencies of the zone-center phonon modes in cubic gauche nitrogen. for the pressure dependent optic modes [28] in the cg-N.	90

Figure 3.60	Static frequency dielectric constant as a function of the frequency for the pressure dependent optic modes [28] in the cg-N. Solid lines represent the best fits to the values given.	92
Figure 3.61	High frequency dielectric constant as a function of the frequency for the pressure dependent optic modes [28] in the cg-N. Solid lines represent the best fits to the values given.	93
Figure 3.62	Colo-cole plot of the optic modes at various pressures [28] for the cg-N. Solid lines represent the best fits to the values given.	93

CHAPTER 1

INTRODUCTION

1.1 Phase and Phase transitions

The relation between macroscopic (mechanical) and microscopic properties of matter is an essential topic for condensed matter physics. In order to build the bridge between microscopic attitude of atoms and observed macroscopic attitude of bulk matter, the phase transition is a key issue since every material shows different properties at different phases according to thermodynamic conditions that it is subjected. Hence, before investigating the phase transition of materials, we should mention to understand the nature of phases. Phase is a homogeneous state where it shows same macroscopic properties determined under the specified external conditions such as temperature, pressure, electric fields. In the same phase, substance exhibits an equilibrium state in which physical and chemical properties are uniform. Generally, most of the materials shows four main phases that is solid, liquid, gas and plasma. In each state, material is different in density, entropy, free energy, heat capacity etc. Every matter has a variety of atomic arrangement that can be observed with different properties regarding phases at certain pressures and temperatures. These different orientations of their molecules provide to gain material to new optical, electrical and mechanical features. In the same solid or liquid material, these distinct arrangements can be observed. What it means that matter can possess several solid or liquid phases at different pressures and temperatures. For instance, under high pressure, the crystalline substance in the solid phase, can change its molecular arrangement to another one hence it has another solid phase [1] Actually, phase transition modifies not only atomic arrangement but also electric properties of materials such as ferromagnetism and superconductivity. However, the important question why the materials undergo

phase transition (change of state). The phase transition occurs when a phase becomes unstable as a result of changing thermodynamic conditions. In nature, there are different phase transitions. One of the most common phase transitions is the change of water into ice (solidification) or melting. Another one is that at above certain temperature (Curie temperature), magnets cannot attract steel or iron pieces anymore. Phase diagram is used to state the different phases in which a substance can exist. It is a kind of chart with the two coordinate system. Generally, these two coordinates are pressure and temperature as depicted in Fig. 1.1. while through the solid lines two phases coexist, triple point represents that three phases (solid, liquid and vapor) can exist together in an equilibrium state.

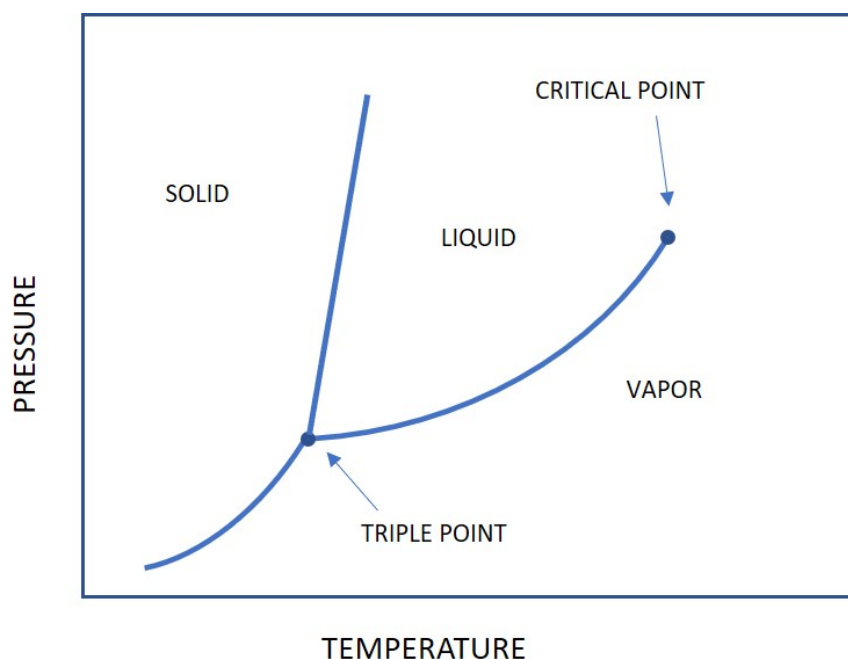


Figure 1.1: Typical phase diagram for pure substance.

1.2 Properties of Solid Nitrogen

In order to examine phase transitions, crystalline systems are preferred. To discover the structures and space groups of molecular crystals at various temperatures and pressures, intermolecular potentials can give a lot of information. Generally, because of complex interactions between atoms, simple diatomics such as H_2 , N_2 , I_2 are preferred to investigate [2, 3]. Among them, solid nitrogen is an ideal diatomic

molecule since it serves highly efficient properties in order to investigate intermolecular interaction behaviors physically and chemically at high pressures, densities and temperatures [4]. One of them is that solid nitrogen is a first-row element which has a strong triple bond $N \equiv N$ between atoms [5], and also dimolecular nitrogen is one of the elements which have a greatest binding energy. For that reason, solid nitrogen can remain stable up to extreme pressures and temperatures. After H_2 , it has a shortest bond length about 1.09 Å [6, 7]. The other importing feature is its transition from molecular phase to non-molecular (polymeric) phase at which there is a single bond between nitrogen atoms under any compression [6–9]. At moderate pressures and temperatures, there is a strong covalent bond between N atoms, however, under any high pressures, nitrogen undergoes a transition to mono atomic phase. This transition is an essential to discover barely noticeable differences between intermolecular interactions in condensed matter. Also during this distortion, a large amount of energy is released so that molecular nitrogen has a huge binding energy [10–12]. Because of its low atomic number, its facilitating to theoretical calculations is the other important reason why solid nitrogen is used widely in the theoretical and experimental molecular interactions studies such as Raman spectroscopy, infrared absorption, NMR, density functional theory, x-ray, diamond anvil cell (DAC) [13, 14]. Besides this simplifying, solid nitrogen has a rich phase diagram under a wide temperature and pressure range [15–17].

1.3 Phase Diagram of Solid Nitrogen

With the advent of diamond-cell and some computational methods (MD, DFT, Monte Carlo simulations), investigating of intermolecular transitions and spectroscopy of materials become more possible and accessible. Hence, research interest of analyzing structures of molecular crystals at high pressures and temperatures have increased [18]. According to the experimental [19–24] and theoretical [7, 13, 14, 25–29] studies in the literature, solid nitrogen has nine phases shown in Fig.1.2 [30]. Solid nitrogen in each phase represents different orientational structures. And these different structures can be defined by means of space groups. Space group is described symmetry of crystals. There are 230 space groups for crystal systems. According to space

group, the first step is to determine the geometry of unit cell, then whether there are reflection conditions should be checked for centred lattices, glide planes and screw axes respectively. The information of all possible space groups can be found out in the literature [31]. Although solid nitrogen shows different behavior in different phases, all phases are insulators with a large band gap. At low temperature and pressure below 3500 atm, α ordered cubic phase exists [16]. Its space group is Pa3. There are four atoms per unit cell. Molecular motion is rotational describing a sphere in three dimensions. When the temperature is increased up to 63 K, β phase occurs [32, 33]. Its structure is disordered hexagonal and space group is P63/mmc [34]. In this phase, molecules can rotate in two dimensions as disks. Beyond 3.5 kbar, tetragonal γ phase occurs [15, 35]. It is an ordered tetragonal phase and its space group is P42/mnm. It is stable in the pressure interval which is 0.4 – 1.9 GPa. There is a triple point among the α , β and γ phases at 44.5 K and 4.7 kbar as seen in the phase diagram of nitrogen (Fig. 1.2). At room temperature and $P > 4.5$ GPa, solid N_2 has cubic disordered δ phase as determined by the x-ray diffraction [36–38]. Its space group is Pm3n. When the pressure is increased or temperature is decreased, δ_{loc} occurs and it is considered on as a partly ordered modification of the δ phase. $\epsilon - N_2$ that is rhombohedral phase with eight oriented molecules per unit cell (R3c) exists below 40 GPa with increasing temperature [39, 40]. At higher pressure up to 100 GPa, a rhombohedral ζ phase occurs [41] with the space group R3c. $\iota - N_2$ and $\theta - N_2$ phases appear at around 65 GPa with 750 K and at around 69 GPa with 850 K, respectively [16, 22]. A high pressure phase $\eta - N_2$ has been detected at around 200 GPa with 300 K by Raman [18, 42] and another high pressure phase κ has been investigated around 150 GPa by optical spectroscopic techniques [20]. Polymeric solid nitrogen gains different structure and properties according to temperature, pressure or synthesized methods. Cubic gauche, black phosphorus, α -arsenic and chainlike are important polymeric forms of solid nitrogen as shown in Fig. 1.3 [43]. Among these polymeric forms of solid nitrogen, cubic gauche is the important one due to its low energy about 0.86 eV/atom [7, 43–46].

In the literature, various physical properties of solid nitrogen have been investigated experimentally and theoretically as pointed above. Some of these studies are as follows: Medina et al. [17] have obtained Raman frequency and linewidth data for the E_g and B_{1g} librational modes in the α phase of solid nitrogen. It has been reported

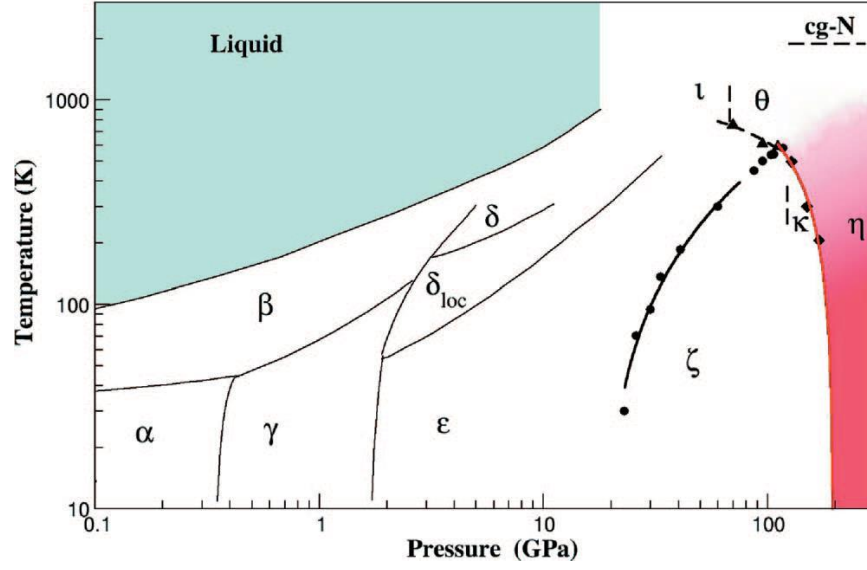


Figure 1.2: Schematic representation of the observed T-P phase diagram of solid nitrogen. Shaded areas are noncrystalline and liquid phases[30].

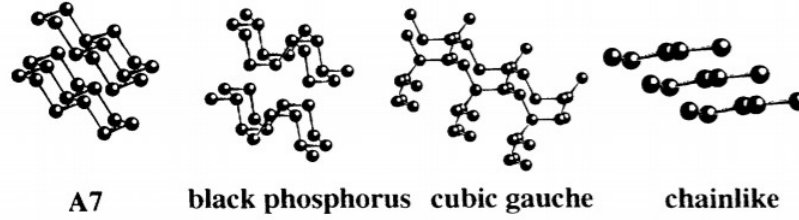


Figure 1.3: Polymeric forms of solid nitrogen[41].

that Tassini et al [23] have measured the Raman frequency and FWHM (linewidth) data for the ν_1 and ν_2 internal modes at various temperatures for the ϵ , δ_{loc} and δ phases of solid nitrogen. Transition of the molecular solid nitrogen to polymeric forms (cubic-gauche) has been found experimentally by Eremest et al. [47, 48] and this transformation has been also confirmed theoretically [43–46, 49, 50]. Regarding phase transitions, at room temperature the $\delta - \epsilon$ transition has been observed at around 17 GPa as obtained by Raman spectroscopy [42] and x-ray studies [51]. Besides vibrational properties, thermodynamic features of solid nitrogen have been reported in the literature. Its thermal expansivity [52, 53], heat capacity [54, 55] and isothermal compressibility [56] have been studied.

In this dissertation, we analyzed experimental results from the literature and calculated physical properties of solid nitrogen at wide pressures ($0 < P < 300$ GPa) and

temperatures ($0 < T < 1000$ K). We predicted the Raman and IR frequencies of solid nitrogen at high pressures (at 160 GPa) through the Grüneisen parameter and its volume. By obtaining phase line equations, we calculated phase diagram of solid nitrogen by using mean field theory and we obtained some thermodynamic quantities as functions of pressure and temperature. Also, we examined the thermodynamic quantities of solid nitrogen by means of the Pippard relations. The Raman bandwidths (FWHM) of the solid nitrogen was predicted for the librational and internal modes in various phases of solid nitrogen by using pseudospin-phonon coupling (PS), energy fluctuation (EF) and anharmonic self energy models near the phase transitions. Finally, we calculated the inverse relaxation time and the activation energy as a function of temperature for the Raman modes close to phase transitions in solid nitrogen.

As included the general information about the phases and phase transitions of pure substance; phases, phase diagram of solid nitrogen and some previous studies on solid nitrogen in this chapter, in Chapter 2, an outline of the theoretical background about physical quantities and methods, which we are used in our calculations is given. In Chapter 3, we present our calculations and the results which we have obtained during this thesis preparation process. With the articles published [57–61] and some articles submitted to the journals. Finally, we summarize our all calculations and results in chapter 4. Future work and applications are discussed in Chapter 4, conclusion.

CHAPTER 2

THEORY

2.1 Classification of Phase transition

In nature, we can observe so many phase transitions which are extreme variations of properties in the thermodynamic behaviors of the physical systems. Solid-solid transition in crystals, conducting-superconducting in metals, and paramagnetic-ferromagnetic transition in magnets can be some of examples for phase transitions. Moreover, phase transition is used in so many technical and industrial systems such as steam generator of a nuclear power plant, metallurgical operations and food systems [62]. Although these phase transitions show specific thermodynamic properties, they can be classified in accordance with thermodynamic characteristics of them and there are different classifications systems. Modern classification and Ehrenfest classifications are most familiar of them. In this dissertation, Ehrenfest classification that depends on the discontinuity of the thermodynamic potentials with respect to thermodynamic variable that is temperature, pressure, volume or order parameter is preferred because of its convenience and reliability. Ehrenfest states in 1993 that phase transitions can be classified as a first order (discontinuous) transition, second order (continuous) transition and higher order transition by considering thermodynamic potentials [63] .

First order phase transition

In this case, the first derivative of thermodynamic potentials as a function of some thermodynamic variables (temperature, pressure) is discontinuous. Hence according to first order phase transition (discontinuous phase transition) , all the thermodynamic

quantities such as volume, enthalpy, entropy are discontinuous as given in Eq. 2.1 [64].

$$S = - \left(\frac{\partial G}{\partial T} \right)_p \quad V = \left(\frac{\partial G}{\partial P} \right)_T \quad H = T \left(\frac{\partial G}{\partial T} \right) \quad (2.1)$$

G is the Gibbs free energy. Liquid-solid phase transition is familiar examples for first order phase transitions. Fig.2.1 exhibits the behavior of the some thermodynamic quantities in the first order phase transitions [64].

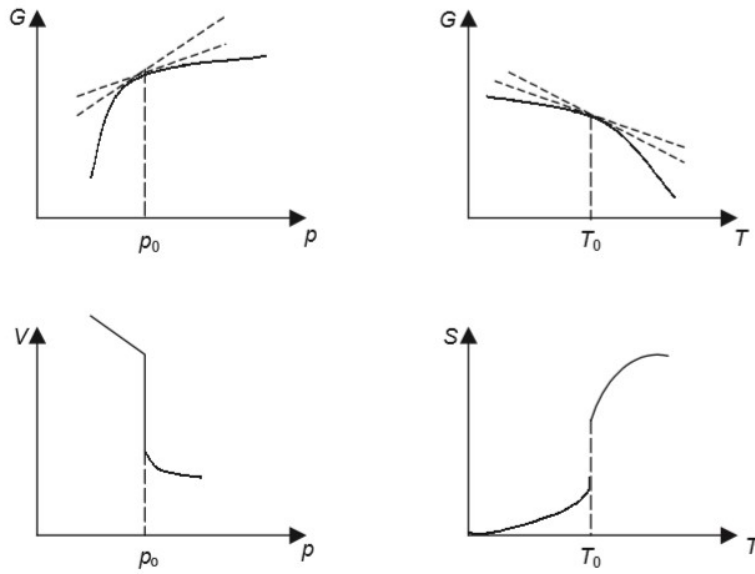


Figure 2.1: The changes in thermodynamic quantities due to first order phase transition. G are continuous in the transition, but the first derivatives of G (V and S) are discontinuous[62]

Second order phase transition

According to second order phase transitions (continuous phase transition), thermodynamic quantities are continuous but the first derivatives of thermodynamic quantities are discontinuous. For example, isobaric specific heat and isothermal compressibility are discontinuous thermal quantities for second order phase transition as given in Eq.

2.2 [64].

$$C_p = T \left(\frac{\partial S}{\partial T} \right) \quad K_T = -\frac{1}{V} \left(\frac{\partial V}{\partial P} \right) \quad (2.2)$$

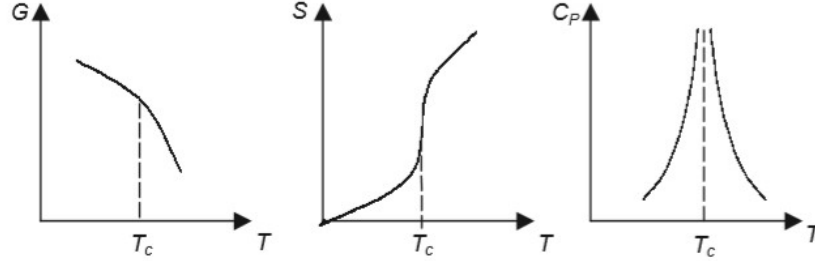


Figure 2.2: The changes in thermodynamic quantities due to second order phase transition. First derivatives of G are continuous, but some second derivatives (C_p) diverge[62]

Ferromagnetic transition [65] and superconducting transition [66] can be examples for this kind of transition. In higher order transitions (multicritical transitions), the potential energy is continuous but the third and higher derivatives of the potential energy with respect to variables are discontinuous and reduced to zero at the transition point [62,64]

2.2 Landau Phenomenological Theory

Although Ehrenfest's classification is very valuable to exhibit similarities and differences between phase transitions, it is not sufficient to clarify all phenomena related to phase transitions. Indeed, in the most of the phase transitions, a symmetry change occurs. Hence, the symmetry change is also considered while studying phase transitions. In 1937, a new approach was presented by L.D.Landau [67]. He suggested a new concept (order parameter) accompanied with the change of symmetry with the phase transition [67]. Order parameter is a physical quantity affected by changing of thermodynamic variables. For instance, when the pressure increases or decreases, the order parameter is also varied. Order parameter is different physical quantity depending on the different phase transitions. For example while in magnetic tran-

sition, order parameter is magnetization, change of density can be used as an order parameter in liquid-solid transitions [68] Generally, order parameter is defined zero or non-zero due to high symmetry phase (disordered) and low symmetry phase (ordered) respectively. Generally, to investigate the thermodynamic properties such as the free energy, entropy or isothermal compressibility of the systems, the Schrödinger equation should be solved. For this purpose, so many numerical and long calculations should be made. For example, for crystals, density of states must be calculated by using dispersion relation that is used for the expression that the solutions of Schrödinger equation for the microscopic states are labeled by k . Then, thermodynamic properties can be obtained by using density of states [69]. However, Landau [67] proposed that, in the vicinity of the transition, free energy can be expressed as an expansion in terms of order parameter as Eq.2.3

$$F(\psi, T, P) = a_0 + \frac{1}{2}a_2\psi^2 + \frac{1}{3}a_3\psi^3 + \frac{1}{4}a_4\psi^4 + \frac{1}{5}a_5\psi^5 \dots \quad (2.3)$$

where ψ is an order parameter, a_0, a_2, a_3, a_4 and a_5 are constants as a function pressure and temperature. Generally, a_0 does not depend on the order parameter. However, while a_2 depends on temperature or pressure strongly, a_3, a_4 (it can be positive or negative) and a_5 are nearly independent of temperature or pressure [70]. Since in the transition region, order parameter is very small, we can expand free energy as a function of order parameter. By minimizing the free energy in terms of order parameter ($\partial F / \partial \psi = 0$), we can easily get the value of the order parameter. After calculating order parameter and free energy $F(\psi, T, P)$, other thermodynamic quantities can be obtained by using the expression below

$$\text{Entropy} \quad S = - \frac{\partial F}{\partial T} \quad (2.4)$$

$$\text{Heat Capacity} \quad C_P = - T \left(\frac{\partial^2 F}{\partial T^2} \right) \quad (2.5)$$

$$\text{Inverse susceptibility} \quad \chi_\psi^{-1} = \frac{\partial^2 F}{\partial \psi^2} \quad (2.6)$$

2.3 Mean Field Theory

Mean field theory is a kind of approximation theory to convert many body problems to one-body problems [71]. According to this theory, all interactions between the atoms can be considered average interaction between them. Hence, difficult calculations can be solved by considering this average approximation. The mean field approach can be applied for free energy calculations in the Landau phenomenological theory.

2.3.1 Calculations of the Landau Energy in the Mean Field Theory

The main idea of Landau theory is to construct the free energy of the system in the transition region of the phase transition. In order to calculate free energy, a suitable order parameter should be chosen and certain boundary conditions [72] should be applied due to the properties of the systems. Phase transition is defined as a first order and second order transition according to whether symmetry is broken or not.

First Order Phase Transition

As stated in Eq.2.3, free energy can be expanded in terms of the order parameter by using Taylor expansion. Higher order terms can be neglected since order parameter is very small and little effect around the transition region. First order transition should be analyzed in two different cases according to the conservation of symmetry.

Symmetric case:

Because of the symmetry of the system, only even terms are taken into account, but quartic term must be negative [71]

$$f = \frac{1}{2}a_2\psi^2 + \frac{1}{4}a_4\psi^4 + \frac{1}{6}a_6\psi^6 \quad (2.7)$$

where $a_4 < 0$, $a_6 > 0$ and $a_2 = a'_2(T - T_c)$ with constant a'_2 and T_c is the transition temperature. By using the stability condition ($\partial f / \partial \psi = 0$),

$$f = a_2\psi + a_4\psi^3 + a_6\psi^5 = 0 \quad (2.8)$$

The solutions of equations(Eq.2.8) are

$$\psi = 0 \quad \text{for } T > T_c$$

and

$$\psi = \pm \left[\mathbf{a}_2 + (\mathbf{a}_4^2 - 4\mathbf{a}_2\mathbf{a}_6)^{1/2} / 2\mathbf{a}_6 \right]^{1/2} \quad (2.9)$$

Since a_4 is negative and a_6 is positive, at $T > T_c$, the order parameter has a single solution that is $\psi = 0$. However, below transition temperature, there are three solutions with $\psi = 0$ and Eq. 2.9.

Asymmetric case:

According to the asymmetric case, cubic term is also used to calculate free energy because the system does not have a symmetry [71].

$$\mathbf{f} = \frac{1}{2}\mathbf{a}_2\psi^2 + \frac{1}{3}\mathbf{a}_3\psi^3 + \frac{1}{4}\mathbf{a}_4\psi^4 \quad (2.10)$$

Again by minimizing free energy with respect to order parameter, we have

$$\psi = 0$$

and

$$\psi = - \left[\mathbf{a}_3 \pm (\mathbf{a}_3^2 - 4\mathbf{a}_2\mathbf{a}_4)^{1/2} \right] / (2\mathbf{a}_4) \quad (2.11)$$

as solutions of Eq.2.11 At high temperatures ($T > T_c$), zero order parameter is the only solution because nonzero solutions become complex since $a_2 = a'_2(T - T_c)$. However, below the transition temperature ($T < T_c$), Eq.2.11 gives nonzero solutions.

Second Order Phase Transition

In the second order phase transition, free energy has a symmetry,

$$\mathbf{f}(\psi, \mathbf{T}) = \mathbf{f}(-\psi, \mathbf{T}) \quad (2.12)$$

and in order to preserve symmetry, odd terms are not allowed to calculate the free energy given by

$$\mathbf{f} = \frac{1}{2}\mathbf{a}_2\psi^2 + \frac{1}{4}\mathbf{a}_4\psi^4 \quad (2.13)$$

and a_4 must be positive [71]. By minimizing free energy under the boundary condition

$$\left(\frac{\partial f}{\partial \psi}\right) = 0 = a_2\psi + a_4\psi^3 \quad (2.14)$$

solutions are

$$\psi = 0$$

and

$$\psi = - \pm (-2a_2/a_4) \quad (2.15)$$

ψ is zero for the disordered phase above T_c and below transition temperature, Eq. 2.13 gives the real solution for the second order phase transition as showed in Fig. 2.3 [71]

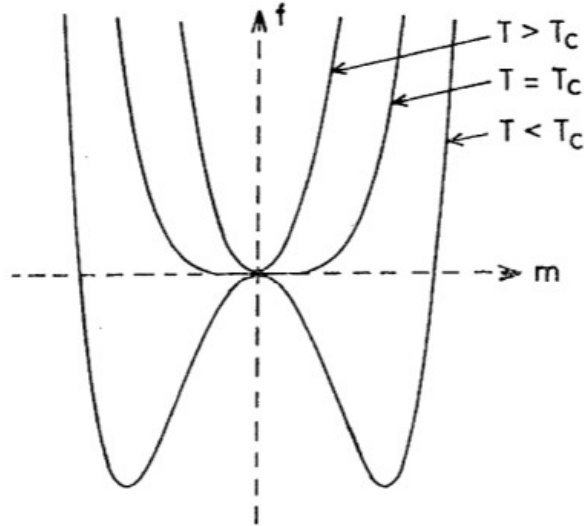


Figure 2.3: Landau free energy at different temperatures for second order phase transition[69].

2.4 Grüneisen Parameter

Grüneisen parameter is a unitless quantity defined by Grüneisen in 1912 [74] and it is an important quantity to investigate thermoelastic properties of matters at high temperatures and pressures. Actually, Grüneisen parameter is considered as a measure of anharmonicity of the crystals since at high pressures and temperatures, anharmonic

term of potential energy becomes dominant [75]. Basically, there are two ways to define Grüneisen parameter denoted by γ [76]. One of them is microscopically representation given as

$$\gamma_j = -\frac{d \ln(\nu_j)}{d \ln(V)} \quad (2.16)$$

where ν_j is the vibrational frequency for mode j and V is volume of the material. Macroscopic (thermodynamic) definition of Grüneisen parameter consists of familiar thermodynamic quantities such as heat capacity (C_v), isothermal expansion (α_T) and bulk modulus (κ_T) is expressed by

$$\gamma_{TH} = -\frac{\alpha_T \kappa_T V}{C_v} \quad (2.17)$$

Grüneisen parameter can also be defined as isobaric (γ_p) and isothermal (γ_T) Grüneisen parameter according to its dependence on temperature and pressure as given by Eq.2.18 and 2.19, respectively,

$$\gamma_P = -\frac{V (\partial \nu / \partial T)_P}{\nu (\partial V / \partial T)_P} \quad (2.18)$$

$$\gamma_P = -\frac{V (\partial \nu / \partial T)_T}{\nu (\partial V / \partial T)_T} \quad (2.19)$$

2.5 Damping Constant

In 1972, Yamada et al. [77] used an Ising spin-phonon system to explain the temperature dependence of phonons by setting the macroscopic Hamiltonian. Hamiltonian including antisymmetric part that clarifies to coupling between phonons and spin, is described by Yamada et al. [77] as follows:

$$\mathbf{H} = \frac{1}{2} \sum_{\vec{k}s} \left(\vec{p}_{\vec{k}s} \vec{p}_{\vec{k}s}^* + \omega_{\vec{k}s}^2 \mathbf{q}_{\vec{k}s} \mathbf{q}_{\vec{k}s}^* \right) - \frac{1}{2} \sum_{ij} \mathbf{J}_{ij} \sigma_i \sigma_j - \sum_{\vec{k}s} \sum_i \frac{\omega_{\vec{k}s}}{\sqrt{N}} \mathbf{g}_{\vec{k}s} \mathbf{q}_{\vec{k}s} \sigma_i \mathbf{e}^{i \vec{k} \cdot \vec{r}_i} \quad (2.20)$$

where $q_{\vec{k}s}$ is the coordinate of phonon with the wave vector \vec{k} for s mode, $\vec{p}_{\vec{k}s}$ is the momentum of phonon, $\omega_{\vec{k}s}$ is the characteristic frequency of phonon, J_{ij} is the pair interaction energy between σ_i and σ_j , $g_{\vec{k}s}$ is the coupling constant between spin and phonon and σ_i is the Ising spin variable. N is the number of unit cell in the molecular system. To simplify Eq.2.20, $q_{\vec{k}s}$ is transformed by using canonical

transformation [78]:

$$q_{\vec{k}s} = Q_{\vec{k}s}^* + \sum_j \frac{1}{\sqrt{N}} \frac{1}{\omega_{\vec{k}s}} g_{\vec{k}s} \sigma_j e^{-i\vec{k} \cdot \vec{r}_j} \quad (2.21)$$

The normalized Hamiltonian can be written as

$$\mathbf{H} = \frac{1}{2} \sum_{\vec{k}s} \left(\vec{p}_{\vec{k}s} \vec{p}_{\vec{k}s}^* + \omega_{\vec{k}s}^2 \mathbf{Q}_{\vec{k}s} \mathbf{Q}_{\vec{k}s}^* \right) + \sum_{ij} \mathbf{J}_{\text{eff}}(\vec{r}_{ij}) \sigma_i \sigma_j \quad (2.22)$$

where J_{eff} is the effective pair interaction between spins given by,

$$J_{eff} = -\frac{1}{2} \left(J_{ij} + \sum_{\vec{k}s} \frac{1}{N} g_{\vec{k}s} g_{\vec{k}s}^* e^{i\vec{k} \cdot \vec{r}_{ij}} \right) \quad (2.23)$$

The first term denotes the direct coupling energy and the second term is indirect interaction between spins [77]. By using Fourier transforms of the Ising spin variable denoted by σ_i ,

$$\sigma(\vec{k}) = \frac{1}{\sqrt{N}} \sum_i \sigma_i e^{i\vec{k} \cdot \vec{r}_i} \quad (2.24)$$

the total Hamiltonian is provided with the $\sigma(\vec{k})$ as follows:

$$\mathbf{H} = \frac{1}{2} \sum_{\vec{k}s} \left(\vec{p}_{\vec{k}s} \vec{p}_{\vec{k}s}^* + \omega_{\vec{k}s}^2 \mathbf{Q}_{\vec{k}s} \mathbf{Q}_{\vec{k}s}^* \right) - \frac{1}{2} \sum_{ij} \mathbf{J}_{\text{eff}}(\mathbf{k}) \sigma(\vec{k}) \sigma(-\vec{k}) \quad (2.25)$$

with

$$J_{eff}(\vec{k}) = j(\vec{k}) + \sum_{\vec{k}s} g_{\vec{k}s}^* g_{\vec{k}s} \quad (2.26)$$

In Eq.2.25, the first term is the anharmonic part (H_A), the second term is the interaction of a phonon and pseudospin Hamiltonian (H_{int}) by using Ising pseudospin-phonon coupled model, respectively. Under phase transition, only interaction is the Hamiltonian part considered due to domination of the energy in the molecular systems. Matsushita [79] has improved the Hamiltonian due to Yamada et al. [77] by using the Ising pseudospin-phonon coupled model for the interaction between more than one phonon and pseudospin. He explained the behavior of frequency and linewidth (damping constant) in terms of the temperature under phase transition by considering Hamiltonian of a pseudospin-phonon coupled system in molecular crystals. Mat-

sushita expressed Hamiltonian with the temperature dependence of phonon as

$$\begin{aligned}
H = & \frac{1}{2} \sum_{\vec{k}\nu} \left[\vec{P}(\vec{k}\nu) \vec{P}^*(\vec{k}\nu) + \omega^2(\vec{k}\nu) Q(\vec{k}\nu) Q^*(\vec{k}\nu) \right] \\
& - \frac{1}{2} \sum_q J_{eff}(q) \sigma(q)^* \sigma(q) + \sum_{\vec{k}q\nu\nu'} K_{1,eff}(\vec{k}q\nu\nu') \sigma(q) Q^*(\vec{k}\nu) Q(\vec{k} - q\nu') \\
& + \sum_{\vec{k}q'\nu\nu'} K_{2,eff}(\vec{k}q'q\nu\nu') \sigma(q) \sigma(q') Q^*(\vec{k}\nu) Q(\vec{k} - q - q'\nu') + H_A \quad (2.27)
\end{aligned}$$

where $J_{eff}(q)$ is the effective exchange energy of pseudospins which is defined as

$$J_{eff}(q) = J(q) + \sum_{\nu} |g(q\nu)|^2. \quad (2.28)$$

While $K_{1,eff}$ shows the interaction between two phonons ($k\nu$) and ($k - q, \nu'$) and one pseudospin with wave vector q , $K_{2,eff}$ represents the interaction between two ($k\nu$) and ($k - q - q', \nu'$) and two pseudospins with the wave vectors q and q' respectively. Eq.2.27 is the basic Hamiltonian described by Matsushita [79] to investigate the temperature dependence of damping constant and frequency of phonons due to their dynamical behavior. The damping constant of phonon derived by Matsushita [79] is given as

$$\begin{aligned}
\Gamma(\vec{k}\nu) = & \sum_{q\nu'} \frac{|K_1(\vec{k}, q, \nu, \nu')|^2}{8\omega\omega_0(k - q, \nu')} \times \left\{ \left[\frac{n(\omega_0(\vec{k} - q\nu'))}{n\omega - (\omega_0(\vec{k} - q\nu'))} + 1 \right] \right. \\
& \times S(q, \omega - \omega_0(\vec{k} - q, \nu')) + \left[\frac{n(\omega_0(\vec{k} - q\nu'))}{n(\omega - \omega_0(\vec{k} - q\nu'))} + 1 \right] \\
& \left. \times S(q, \omega + \omega_0(\vec{k} - q, \nu')) \right\} \quad (2.29)
\end{aligned}$$

where $K_1(k, q, \nu, \nu')$ is an effective coupling constant of the ($k\nu$) and ($k - q, \nu'$) phonons and pseudospin with the wave vector q and $S(q, \omega)$ is the dynamic scattering function of the pseudospins. Laulicht and Luknar [80] made simpler Eq.2.29 by means some assumptions:

- (a) $\Gamma(\vec{k}\nu, \omega)$ can be nearly equal to $\Gamma(\vec{k}\nu, \omega_\nu)$, ω_ν is the peak frequency and $\omega_\nu = \omega_0(\vec{k}, \nu) \cong \omega_0(\vec{k} - q, \nu)$.
- (b) K_1, ω 's and n 's are almost independent on q and temperature in the vicinity of transition temperature T_c .

(c) Integral can be used instead of summation on q .

(d) $S(q, \omega_\nu(\vec{k}) - \omega_\nu(\vec{k} - q)) \approx S(q, 0)$ since $S(q, \nu)$ is the Debye type function below T_c .

(e) All terms of $S(q, \omega_\nu - \omega_0)$ are zero.

According to all assumptions given above, damping constant was derived by Laulicht [81]

$$\Gamma_{sp}(\omega_\nu) = A \int S(q, \omega) \left(\frac{n(\omega_\nu)}{n(\omega + 1)} + 1 \right) d^3q + B \quad (2.30)$$

where

$$S(q, \omega) = (n(\omega) + 1) \frac{\chi(q, 0) \omega \tau_q}{1 + (\omega \tau_q)^2} \quad (2.31)$$

In Eq.2.30, A and B are weakly temperature dependent constant, τ_q denotes the relaxation time and χ is dielectric susceptibility. Also, Laulicht [81] assumed that $n(\omega) + 1 \sim (kT/(\hbar\omega))$, $(\omega \tau_q)^2 < 1$ and $\frac{n(\omega_\nu)}{n(\omega+1)} < 1$ for $\omega \cong 0$. So, under this assumption, damping constant can be written as

$$\Gamma_{sp}(\omega_\nu) = \frac{AkT}{\hbar} \int \chi(q, 0) \tau_q d^3q + B \quad (2.32)$$

Lahajnar et al. [82] have defined general dielectric susceptibility by using dynamic Ising model in the random phase approximation as

$$\chi(q, 0) = \frac{C(1 - P^2) \tau_q}{T \tau} \quad (2.33)$$

where P is the order parameter, C is the Curie constant and τ is the proton correlation time. Then using all calculations of Lahajnar et al [82], the temperature dependent of damping constant near T_c can be written as [80, 82]

$$\Gamma_{sp} = \Gamma_0 + A(1 - P^2) \ln \left(\frac{T_c}{T - T_c(1 - P^2)} \right) \quad (2.34)$$

Here Γ_0 is a background damping constant and A is constant.

A different approach to evaluate Γ_{sp} has been presented by Schaack and Winterfelt [83] due to pseudospin phonon interaction. As a result of pseudospin-phonon coupling, the phonon frequencies ($\omega_p \hbar$) undergoes a shift which is proportional to order parameter (P). Then the broadening due to energy fluctuation of the mode has been expressed as

$$\Gamma_{sp}^2 = \frac{k\tau\chi(q, 0)}{V} \quad (2.35)$$

where V is the volume of the crystal. By using the dielectric susceptibility for a dynamic Ising model (Eq.2.33), damping constant is simply obtained as

$$\Gamma_{sp} = \Gamma'_0 + A' \left(\frac{T(1 - P^2)}{T - Tc(1 - P^2)} \right)^{1/2} \quad (2.36)$$

As explained in Eq.2.34, Γ'_0 and A' are background damping constant and constant, respectively. As a conclusion, in order to calculate and analyze the temperature dependence of damping constant, pseudospin-phonon coupling (PS) and energy fluctuation (EF) models can be used for molecular crystal systems.

2.6 Pippard Relations

Pippard relations are essentially phenomenological equations proposed by Pippard [84]. He derived these relations on the basis of the cylindrical approximation of pressure and temperature dependence of the entropy (S) close to the λ transition given as [85]

$$S(P, T) = S_0 + aT + f\left(T \left(\frac{dP}{dT} \right)_\lambda - P\right) \quad (2.37)$$

Here, S_0 and a are constants. By using this approximation, Pippard suggested two equations as given below: First equation shows the linear relation between the heat capacity ($C_p - C_v$) and thermal expansion (α_p)

$$C_p = TV\alpha_p \left(\frac{dP}{dT} \right) + T \left(\frac{dS}{dT} \right)_\nu \quad (2.38)$$

where $T \left(\frac{dS}{dT} \right)_\nu$ corresponds to C_v at constant volume, $\frac{dP}{dT}$ is the variation of pressure with temperature.

Second equation gives the linear relation between thermal expansion (α_p) with the isothermal compressibility (κ_T) expressed as

$$\alpha_p = \frac{dP}{dT} \kappa_T + \frac{1}{V} \frac{dV}{dT} \quad (2.39)$$

where as Eq.2.37, $\frac{dP}{dT}$ is the variation of pressure with temperature and $\frac{dV}{dT}$ is the variation of volume with temperature. Pippard relations are very useful equations in order to calculate thermodynamic quantities of thermodynamic systems and compare the linear variation of them as a function of pressures and temperatures. Hence, by using these two Pippard relations, we analyzed and established the linear relation

between C_p with α_P (Eq.2.38) and α_P with κ_T (Eq.2.39) for solid nitrogen. And also, we predict dP/dT values for the fluid-solid, solid-solid phase transitions of molecular nitrogen from these linear relations of thermodynamic functions.

2.7 Anharmonic Self Energy

Based on the harmonic approximation, there is no phonon interaction in crystals systems and lifetimes of phonons are infinite. However, within the real crystal, interactions between phonons occur and are considered as anharmonic interactions which contribute to the potential energy of crystals [86]. These anharmonic (renormalized) interactions are owing to quadric and cubic components of the total expanded crystal potentials with respect to atomic displacement [87]. The number of renormalized phonons can be defined as occupation numbers (n) of all the phonons in the system and to add one phonon k to the system (n_k to $n_k + 1$). This required energy can be expressed as

$$\hbar\omega_k + \hbar\omega_2 k(\text{quartic}) + \hbar\omega_2 k(\text{cubic}) \quad (2.40)$$

where $\hbar\omega_k$ and $\hbar\omega_2 k$ are first order and second order phonon energy, respectively and depend on the occupation number of all the phonons. By using the second order perturbation theory, energy shift can be obtained as a complex and it is written as

$$\hbar\Delta\omega(\lambda) = \hbar\Delta(\lambda) - i\hbar\Gamma(\lambda) \quad (2.41)$$

Here $\Delta(\lambda)$ is a frequency shift, $2\Gamma(\lambda)$ denotes a linewidth at half intensity of the corresponding Raman line (FWHM) and λ is a phonon mode with a particular wave vector [87]. While the cubic and quartic anharmonic terms contribute the frequency, only cubic anharmonic terms contribute to the linewidths (inverse phonon lifetimes). By considering cubic and quartic terms of the second order phonon energy, frequency

shift can be expressed as

$$\begin{aligned} \hbar\Delta_\lambda = & 12 \sum_{\lambda'} \Phi_{\lambda,-\lambda,\lambda',-\lambda'} (2n'_\lambda + 1) - \frac{18}{\hbar} \sum_{\lambda',\lambda''} \left\{ |\Phi_{\lambda,\lambda',\lambda''}|^2 \left[\frac{(n_{\lambda'} + n_{\lambda''} + 1)}{(\omega_\lambda + \omega_{\lambda'} + \omega_{\lambda''})} \right. \right. \\ & + \frac{(n_{\lambda'} - n_{\lambda''})}{(\omega_\lambda + \omega_{\lambda'} - \omega_{\lambda''})} + \frac{(n_{\lambda''} - n_{\lambda'})}{(\omega_\lambda - \omega_{\lambda'} + \omega_{\lambda''})} - \left. \frac{(n_{\lambda'} + n_{\lambda''} + 1)}{(\omega_\lambda - \omega_{\lambda'} - \omega_{\lambda''})} \right] + \\ & \left. 2\Phi_{\lambda,-\lambda,\lambda''}\Phi_{\lambda',-\lambda',-\lambda''} \frac{(2n_\lambda + 1)}{\omega_{\lambda''}} \right\} \end{aligned} \quad (2.42)$$

and linewidth that consists of only cubic components of the second order phonon energy is defined as

$$\begin{aligned} \hbar\Gamma_\lambda = & \frac{18\pi}{\hbar} \sum_{\lambda',\lambda''} |\Phi_{\lambda,\lambda',\lambda''}|^2 \{ (n_{\lambda'} + n_{\lambda''} + 1) \delta(\omega_\lambda - \omega_{\lambda'} - \omega_{\lambda''}) \\ & + (n_{\lambda'} - n_{\lambda''}) [\delta(\omega_\lambda + \omega_{\lambda'} - \omega_{\lambda''}) - \delta(\omega_\lambda - \omega_{\lambda'} + \omega_{\lambda''})] \} \end{aligned} \quad (2.43)$$

where $\Phi_{\lambda,\lambda',\lambda''}$ represents the potential energy coefficient and n_λ is the occupation number at the equilibrium it is expressed as

$$n_\lambda = \frac{1}{\exp(\hbar\omega_\lambda/k_B T) - 1} \quad (2.44)$$

In Eq.2.44, ω_λ is the harmonic frequency and k_B is the Boltzmann constant [87]. The frequency shift can be expressed as [87],

$$\Delta_\lambda = C(\lambda) + \sum_{\lambda'} C(\lambda, \lambda') n(\lambda') \quad (2.45)$$

In this equation, $C(\lambda)$ and $C(\lambda, \lambda')$ are temperature independent factors and they rely on cubic and quartic interactions [88]. By assuming that the Raman mode interacts only with one other excitation, its Raman frequency can be written as

$$\omega(T) = \omega_1 + \frac{\omega_2}{e^{\hbar\omega_0/k_B T} - 1} \quad (2.46)$$

where $\omega_0(\lambda')$ is the harmonic frequency of vibron, ω_1 and ω_2 are constants [88]. Also by assuming that vibron attracts with a second excitation to produce a third one, the temperature dependence of the bandwidth can be given as

$$\Gamma(\lambda) = \Gamma_1(\lambda) \left[\frac{1}{e^{\hbar\omega_0/k_B T} - 1} - \frac{1}{e^{(\omega - \omega')/k_B T} - 1} \right] \quad (2.47)$$

In Eq.2.47, ω , ω' and $\omega'' = \omega + \omega'$ denotes to the Raman frequencies of vibron (ω) and the other two excitations (ω' and ω'') [88]. $\Gamma_1(\lambda)$ is the background linewidth and we take that $\Gamma_1(\lambda)$, $\Gamma_2(\lambda)$ are the temperature independent. As mentioned above, only cubic terms are considered while calculating the Raman linewidth [88].

CHAPTER 3

CALCULATIONS AND RESULTS

3.1 "Calculations of the Raman and IR frequencies from the volume data at high pressures in Solid nitrogen."

Raman and IR frequencies of molecular structures can be calculated by using statistical models through observed data from the literature. In this study, we calculate the pressure dependence of the Raman and IR frequencies of the lattice and internal modes of solid nitrogen up to 160 GPa at room temperature. We used observed frequency data [20] for the high-pressure phases of ϵ , ξ , κ and cg-N solid nitrogen. By using experimental volume data [30] and the Raman and IR frequencies, Grüneisen parameter at constant temperature (γ_T) for the lattice and internal modes, are calculated at various pressures. First of all, by fitting experimental Raman and IR frequencies (ν) and crystal volume (V) as a function of pressure of solid nitrogen through quadratic equations which can be defined as

$$\nu_T(P) = a_0 + a_1P + a_2P^2 \quad (3.1)$$

and

$$V_T(P) = b_0 + b_1P + b_2P^2 \quad (3.2)$$

respectively, where a_0 , a_1 , a_2 and b_0 , b_1 , b_2 are constants, pressure dependence of isothermal mode Grüneisen parameter (γ_T) which defines the anharmonicity of the systems is obtained according to,

$$\gamma_T(P) = -\frac{V(P)(\partial\nu/\partial P)_T}{\nu(P)(\partial V/\partial P)_T} \quad (3.3)$$

Also, we can obtain the Raman frequencies by using Eq.3.3 with the pressure dependent additional term $A(P)$

$$\gamma_T(P) = A(P) + \nu_0 \exp \left[-\gamma_T(P) \ln \left(\frac{V_T(P)}{V_0} \right) \right] \quad (3.4)$$

where ν_0 and V_0 denote the values of the Raman frequency and volume at $P=0$ and $T=300$ K. The pressure-dependent term can also be assumed as

$$A(P) = a + bP + cP^2 \quad (3.5)$$

with constants a, b and c , which can be obtained by fitting to the experimental data for the Raman frequencies. We analyzed the observed data for the crystal volume and the experimental frequencies at various pressures due to Eqs.(3.1) and (3.2), respectively, and we obtained the coefficients (a_0, a_1, a_2 and b_0, b_1, b_2) as given in Table 3.1(Eq.3.2), Table 3.2 (Eq.3.1) for lattice modes and Table 3.3 (Eq.3.1) for vibrons within the pressure intervals studied. We added the $a_3 P^3$ term in Eq 3.1 in order to obtain the best fit for the lattice modes of ν_{IV} and ν_{VI} and the vibrons of ν_{2d} and ν_{2f} . Value of the coefficient a_3 is given for relevant lattice modes and vibrons in Table 3.2 and Table 3.3 respectively. Then, we computed isothermal mode Grüneisen parameter (Eq.3.3) by using values of coefficients (Tables 3.1–3.3) for the lattice modes and vibrons. Figs.3.1–3.3 show the change of (γ_T) with the pressure for the lattice modes at room temperature. We plotted (γ_T) as a function of pressure as indicated in Figs.3.4 and 3.5 for vibrons of solid nitrogen.

Table 3.1: Values of the coefficients to Eq.(3.2) fitted to the observed volume data[30] for solid nitrogen.

$V(\text{\AA}^3)$	$b_0(\text{\AA}^3)$	$b_1(\text{\AA}^3/GPa)$	$b_2 \times 10^{-4}(\text{\AA}^3/GPa^2)$
Solid N_2	11.75	-0.076	2.58

We were then able to predict the Raman and IR frequencies of those modes for the phases of ϵ, ξ, κ and cg-N solid nitrogen by the means of Eq.3.4. By fitting observed frequency data [20] for the lattice modes and vibrons with respect to Eq.3.4, the coefficients of $A(P)$ were obtained as given in Tables 3.4 and 3.5, respectively. We also added cubic polynomial term dP^3 to Eq.3.5 for the lattice modes of ν_{IV} and ν_{VI} and the vibrons of ν_{2d} and ν_{2f} as implemented to Eq.3.1 for the observed frequency data

Table 3.2: Values of the coefficients according to Eq.3.1 fitted to the observed Raman and IR frequencies [20] for the lattice modes indicated within the pressure interval for solid nitrogen.

ν (cm^{-1})	a_0 (cm^{-1})	a_1 (cm^{-1}/GPa)	$-a_2 \times 10^{-2}$ (cm^{-1}/GPa^2)	$a_3 \times 10^{-4}$ (cm^{-1}/GPa^3)	Pressure interval P(GPa)
ν_I	309.9	4.61	0.88	-	42.9<P<139.8
ν_{II}	308.5	4.91	1.23	-	80.4<P<160.1
ν_{III}	195.5	4.82	1.05	-	24.7<P<111.0
ν_{IV}	204.5	4.72	2.80	0.86	42.9<P<110.5
ν_V	70.2	4.28	1.15	-	60.7<P<124.1
ν_{VI}	20.3	4.71	4.45	1.62	23.4<P<110.5

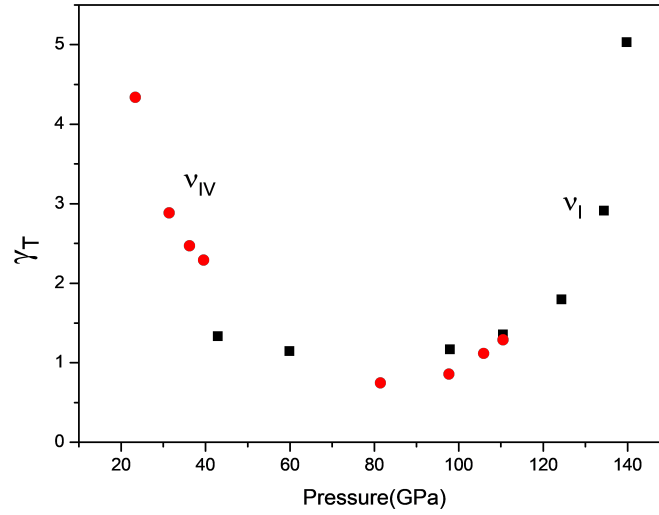


Figure 3.1: Pressure dependence of the isothermal mode Grüneisen parameter (γ_T) calculated for lattice modes indicated according to Eq.3.3 by using the observed data for the Raman and IR frequencies [20] and volume[30] of solid nitrogen.

fitting ($a_3 P^3$). At the end of the study, we calculated Raman and IR frequencies of solid nitrogen by using Eq.3.4 and depicted for the lattice modes and vibrons as a function of pressures in Figs.3.6 and 3.7, respectively, with the observed data [20, 30].

For the calculations provided, the pressure induced change in the isothermal mode

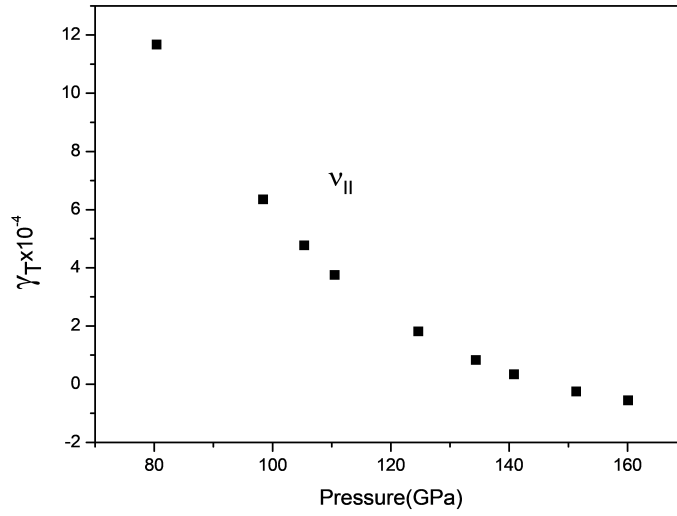


Figure 3.2: Pressure dependence of the isothermal mode Grüneisen parameter (γ_T) calculated for lattice modes indicated according to Eq.3.3 by using the observed data for the Raman and IR [20] and volume [30] of solid nitrogen.

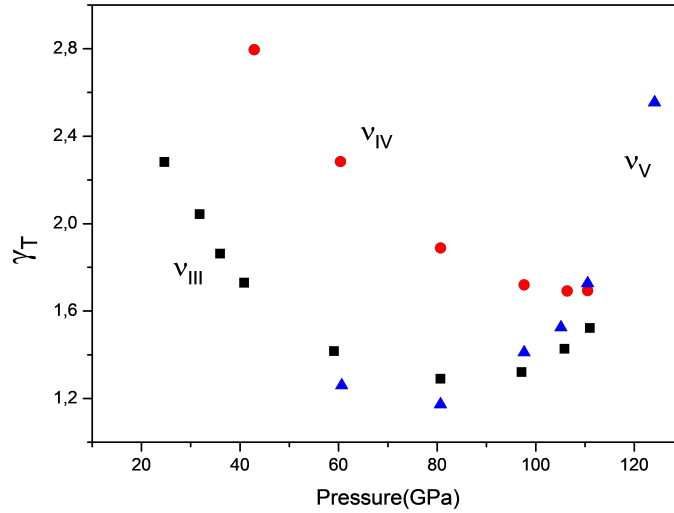


Figure 3.3: Pressure dependence of the isothermal mode Grüneisen parameter (γ_T) calculated for lattice modes indicated according to Eq.3.3 by using the observed data for the Raman and IR frequencies[20] and volume [30] of solid nitrogen.

Grüneisen parameter (γ_T) represented in Figs.3.1-3.5 for the Raman and IR frequencies of the lattice modes and the vibrons ν_1 and ν_2 in solid nitrogen. According to our results, calculated (γ_T) values of the lattice modes ν_I and ν_{VI} (Fig.3.1) and ν_V (Fig.3.3

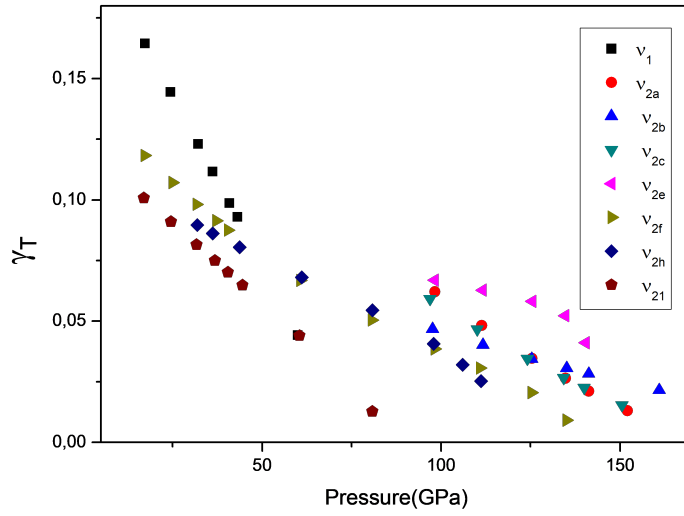


Figure 3.4: Pressure dependence of the isothermal mode Grüneisen parameter (γ_T) calculated for vibrons indicated according to Eq.3.3 by using the observed data for the Raman and IR frequencies[20] and volume [30] of solid nitrogen.

increase with increasing pressure in the pressure interval 60 to 140 GPa except that (γ_T) value of the lattice mode ν_{VI} decreases from 20 to 60 GPa. Grüneisen parameter (γ_T) related the vibrons (ν_1 and ν_2) is reduced (Figs.3.4 and 3.5) with increasing pressure with the exception of the ν_{2g} and ν_{2d} modes. While the (γ_T) values for the ν_{2g} mode increase (Fig.3.5b) as the pressure increases, for the ν_{2d} mode the (γ_T) values decrease first then start to increase about 100 GPa (Fig. 3.5c). According to Sherman's studies where he predicts that at high pressures, (γ_T) values approach to 1 for molecular crystals, our (γ_T) calculations show nearly good agreement with his

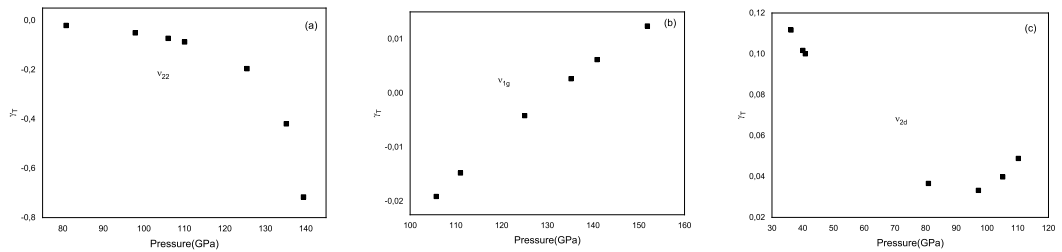


Figure 3.5: Pressure dependence of the isothermal mode Grüneisen parameter (γ_T) calculated for vibrons indicated according to Eq.3.3 by using the observed data for the Raman and IR frequencies[20] and volume [30] of solid nitrogen.

Table 3.3: Values of the coefficients according to Eq.3.1 fitted to the observed Raman and IR frequencies [20] for vibrons indicated within the pressure interval for solid nitrogen.

ν (cm^{-1})	a_0 (cm^{-1})	a_1 (cm^{-1}/GPa)	$-a_2 \times 10^{-3}$ (cm^{-1}/GPa^2)	$a_3 \times 10^{-5}$ (cm^{-1}/GPa^3)	Pressure interval P(GPa)
ν_I	2335.6	3.26	22.18	-	17.3<P<60.0
ν_{2a}	2368.4	1.30	3.76	-	98.3<P<152.0
ν_{2b}	2402.0	0.65	1.19	-	97.7<P<141.2
ν_{2c}	2378.6	1.16	3.26	-	96.9<P<150.5
ν_{2d}	2307.4	3.60	33.27	1.12	36.2<P<110.2
ν_{2e}	2321.1	1.87	6.48	-	98.2<P<140.4
ν_{2f}	2323.1	2.20	13.14	2.51	17.2<P<141.3
ν_{2g}	2493.7	-0.91	-3.46	-	105.8<P<140.9
ν_h	2343.1	1.78	7.24	-	31.9<P<111.2
ν_{21}	2331.1	1.88	10.72	-	17.0<P<80.8
ν_{22}	2389.4	0.80	10.72	-	80.8<P<139.4

Table 3.4: Values of the coefficients of the pressure-dependent term A(P) according to Eq.3.5 for the lattice modes within the pressure intervals indicated for nitrogen.

$A(P)$	a (cm^{-1})	b (cm^{-1}/GPa)	$c \times 10^{-3}$ (cm^{-1}/GPa^2)	$d \times 10^{-4}$ (cm^{-1}/GPa^3)	Pressure interval P(GPa)
ν_I	214.44	0.637	23.70	-	42.9<P<139.8
ν_{II}	-0.64	4.924	-12.32	-	80.4<P<160.1
ν_{III}	-154.17	7.698	-46.97	-	24.7<P<111.0
ν_{IV}	48.53	-2.873	109.49	-7.35	42.9<P<110.5
ν_V	-59.64	4.117	-9.24	-	60.7<P<124.1
ν_{VI}	-16.04	4.376	-31.45	0.67	23.4<P<110.5

prediction for lattice modes and vibrons [89, 90]. In the last part, we calculated Raman and IR frequencies of lattice modes and vibrons studied above by means of Eq.3.4 and we plotted with the observed data for the lattice modes (Fig.3.6) and vibrons (Fig.3.7). According to Figs.3.6 and 3.7, we obtained the same behavior of the calculated frequencies by the change against pressure with the experimental ones,

Table 3.5: Values of the coefficients of the pressure-dependent term $A(P)$ according to Eq.3.5 for the vibrons within the pressure intervals indicated for nitrogen.

$A(P)$	a (cm^{-1})	b (cm^{-1}/GPa)	$c \times 10^{-3}$ (cm^{-1}/GPa^2)	$d \times 10^{-4}$ (cm^{-1}/GPa^3)	Pressure interval P(GPa)
ν_I	0.63	-0.013	21.50	-	17.3<P<60.0
ν_{2a}	-29.45	0.714	0.66	-	98.3<P<152.0
ν_{2b}	-4.19	0.140	2.58	-	97.7<P<141.2
ν_{2c}	-24.31	0.596	0.73	-	96.9<P<150.5
ν_{2d}	7.17	-0.493	43.79	-3.03	36.2<P<110.2
ν_{2e}	353.78	-6.066	28.90	-	98.2<P<140.4
ν_{2f}	-23.46	1.603	-17.09	0.95	17.2<P<141.3
ν_{2g}	-456.35	13.592	-80.58	-	105.8<P<140.9
ν_h	39.84	-1.494	14.79	-	31.9<P<111.2
ν_{21}	1.97	-0.107	11.30	-	17.0<P<80.8
ν_{22}	-5561.67	117.863	-618.09	-	80.8<P<139.4

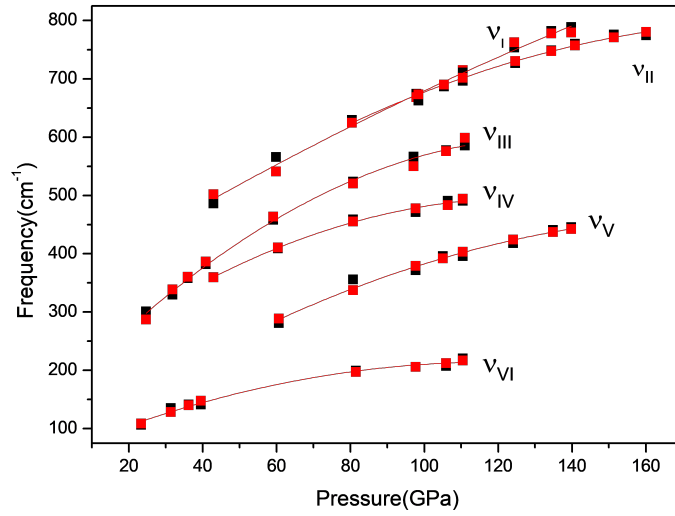


Figure 3.6: Raman and IR frequencies calculated for the lattice modes (red squares) indicated as a function of pressure according to Eq.3.4 for solid nitrogen. Observed data (black squares)[20] are also given here.

which increase with pressure up to 160 GPa except that ν_2 mode starts to decrease after 80 GPa, which is not shown in Fig.3.7. Also, at around 100 GPa, ν_2 mode

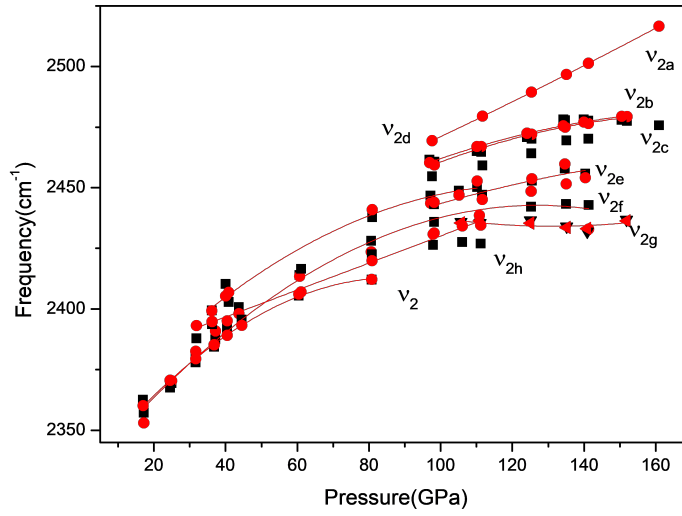


Figure 3.7: Raman and IR frequencies calculated for the vibrons (red squares) indicated as a function of pressure according to Eq.3.4 for solid nitrogen. Observed data (black squares)[20] are also given here.

splits out as it softens during the phase transition from the ϵ to the ξ phase in solid nitrogen. This softening concerns with the increasing of the vibrational coupling or the weakening of the intramolecular bonding between molecules [49, 91, 92]. As pointed out previously [14], due to the interactions between high pressure-induced molecules, pressure-induced decomposition creates a polymeric phase called a cubic gauche [43]. When we compared with the Fig.3.6 and Fig.3.7, the external (lattice) modes are more sensitive than internal (vibrons) modes against the compression [93].

3.2 "Calculation of the phase diagrams for the fluid-solid and solid-solid ($\delta - \delta_{loc} - \epsilon$) transitions in molecular nitrogen by using mean field model."

Phase diagram is the convenient way to describe the phases and phase transitions of materials in terms of temperature and pressure as pointed out in Chapter 2. In this study, we derived phase line equations in order to calculate phase diagrams using the mean field theory for the models of the solid-fluid and the solid-solid transitions of the $\delta - \delta_{loc} - \epsilon$ in nitrogen. To obtain phase line equations, free energy expanded in terms of order parameter was analyzed. Pressure and temperature dependent coefficients in the expansion of the free energy were obtained by the means of fitting of the phase like equations to the experimental data from the literature [23, 55, 94] As mentioned in Chapter 2, according to mean field theory, there are two kinds of phase transitions depending on the transition type. These are first order and second order phase transitions. In these calculations, we predicted phase diagrams of nitrogen by considering the first order fluid-solid transition and, the second order $\delta - \delta_{loc}$ and the first order $\delta_{loc} - \epsilon$ transitions.

Fluid-solid transition

To describe the fluid-solid transition of nitrogen, the free energy expanded in terms of order parameter η with the cubic term was used as given by

$$F_s = a_2\eta^2 + a_3\eta^3 + a_4\eta^4 \quad (3.6)$$

where a_2, a_3 and a_4 are the temperature and pressure dependent coefficients and we assumed $a_2 > 0$, $a_3 < 0$ and $a_4 > 0$ for the first order phase transition. By applying two boundary conditions:

- 1) minimizing free energy with respect to order parameter ($\partial F / \partial \eta = 0$),
- 2) no ordering in liquid phase ($F_S = F_{fluid} = 0$), we then get order parameter as

$$\eta = -\frac{2a_2}{a_3} = -\frac{a_3}{2a_4} \quad (3.7)$$

Hence, we obtained the phase line equation for the first order fluid-solid phase transition in molecular nitrogen as

$$a_3^2 = 4a_2a_4 \quad (3.8)$$

We assumed that a_2 and a_3 are the temperature and pressure dependent, respectively, while a_4 is constant as given below :

$$a_2 = a_{20}(T - T_m) \quad (3.9)$$

$$a_3 = a_{30}(P - P_m) \quad (3.10)$$

$$a_4 = a_{40} \quad (3.11)$$

where T_m and P_m represent the temperature and pressure at the melting point, respectively. By substituting Eqs.3.9 and 3.10 into Eq.3.8, phase line equation was obtained as functions of pressure and temperature

$$a_{30}^2(P - P_m) = 4a_{20}a_{40}(T - T_m) \quad (3.12)$$

We expand Eq.3.12 as expressed in Eq.3.13,

$$f(T, P) = T - \alpha_1 - \alpha_2P + \alpha_3P^2 = 0 \quad (3.13)$$

where

$$\alpha_1 = T_m + \frac{a_{30}^2 P_m^2}{4a_{20}a_{40}} \quad (3.14)$$

$$\alpha_2 = -\frac{a_{30}^2 P_m}{2a_{20}a_{40}} \quad (3.15)$$

$$\alpha_3 = -\frac{a_{30}^2}{4a_{20}a_{40}} \quad (3.16)$$

Eq.3.13 was then fitted to the experimental phase diagram data and the values of a_1 , a_2 and a_3 were predicted at the maximum values of $T_m=1769.4$ K and $P_m=74.3$ GPa on the melting line [55] for the fluid-solid transition in nitrogen as given in Table 1. We plot the calculated phase diagram and experimental data with the uncertainties [55] as depicted in Figure 3.8 for the fluid-solid transition in N_2 . Also another observed P-T [94] data taken from the literature were fitted through Eq.3.13 in order to calculate

the coefficients of phase line equation. For the coefficients we used the maximum values of $T_m=1920$ K and $P_m=50$ GPa we assumed that

$$a_2 = a_{20}(T - T_m) \quad (3.17)$$

$$a_3 = a_{30}(T - T_m) \quad (3.18)$$

$$a_4 = a_{40}(P - P_m) \quad (3.19)$$

Again by inserting Eqs.3.17–3.19 into Eq.3.8, we get

$$a_{30}^2(T - T_m) = 4a_{20}a_{40}(P - P_m) \quad (3.20)$$

By expanding Eq.3.20, we get Eq.3.8 with the $a_3 = 0$, where

$$\alpha_1 = T_m - \left(\frac{4a_{20}a_{40}}{a_{30}^2}\right)P_m \quad (3.21)$$

and

$$\alpha_2 = \frac{4a_{20}a_{40}}{a_{30}^2} \quad (3.22)$$

Then, Eq.3.13 was fitted to the observed linear melting line according to the two pressure intervals and the coefficients a_1 (Eq.3.21), a_2 (Eq.3.22) were determined as given in Table 3.6. This is plotted in Fig.3.8. for the melting temperature with the observed data [94]. In Eq. 3.13, to get the best fit from experimental data, we took a_3 as a zero. Regarding to the first order fluid-solid transition in nitrogen, we obtained that the temperature increases with increasing pressure up to about 90 GPa in the melting region as mentioned experimentally [55]. When we look at the change in the temperature of melting, there is a linear increase up to a maximum point where the temperature is 1920 K and the pressure is 50 GPa . However after this point, a sharp linear decrease occurs down to 1400 K and 71 GPa as obtained experimentally [94].Table 3.7 gives us the dT/dP values of melting temperature according to linear fit with the pressure and temperature intervals.The negative slope value in Fig.3.8 implies that the liquid is denser than the underlying solid as stated previously [94].

Also, the sharpness of the changes in the melting temperature can be an evidence of first order liquid-liquid polymer transition [94] that supports the molecular dynamic simulations [14]. The reason why the experimental data taken from Refs. [55]

Table 3.6: Values of the fitted parameters within the pressure intervals indicated for the fluid-solid transition[53] and the melting curves[92] according to Eq.3.13, and for the solid-solid transitions of $\delta - \delta_{loc}$ and $\delta_{loc} - \epsilon$ [23] according to Eq.3.35 in N_2 .

$f(T, P)$	α_1 (K)	$\alpha_2 \times 10^{-2}$ (K/GPa)	$\alpha_3 \times 10^{-5}$ (K/GPa ²)	Pressure interval P(GPa)
<i>Fluid – solid transition</i>	43.6	-7.1	4.80	15.9<P<74.3
<i>Melting curve</i>	200.98	3599.0	-	0.2<P<49.7
	4.924	-12.32	-	49.5<P<71.2
$\delta_{loc} - \epsilon$	-4.44	4.12	3.11	3.9<P<21.4
$\delta - \delta_{loc}$	-1.98	3.78	3.84	5.5<P<33.6

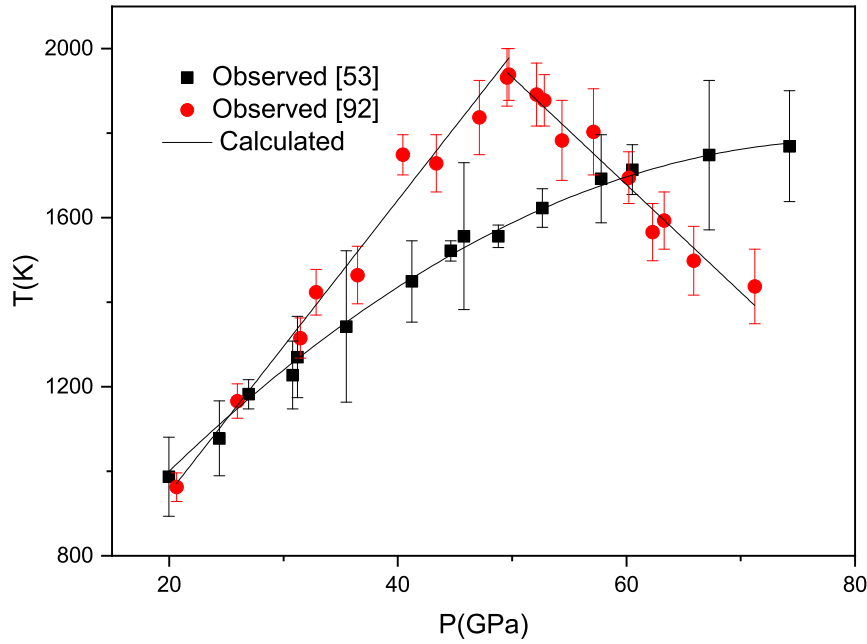


Figure 3.8: Calculated phase diagram of N_2 in the melting region according to Eq.(3.6) by using the mean field model. Observed data (squares)[53] and (circles)[92] with the uncertainties are also given for the fluid-solid transition in nitrogen.

and [94] are different because of the difference in methods used, which are Raman spectroscopy and visual observations from laser speckle motion for the melting curve [94]. When compared the calculated data with the experimental ones [55, 94], there is a good agreement between them so that mean field theory is adequate to analyze

Table 3.7: Values of the slope(dP/dT) within the temperature and pressure intervals according to the equations indicated for the transitions in N_2 . T_c and P_c denote maximum (T_m, P_m) values for the melting curve and fluid –solid transition (Fig.3.8). dT/dP values are calculated at 300 K for the $\delta - \delta_{loc}$ and $\delta_{loc} - \epsilon$ transitions in N_2 .

Transition in N_2	T_c (K)	P_c (GPa)	dT/dP (K/GPa)	Temperature Interval(K)	Pressure Interval(GPa)	Reference No.	Equation No.
<i>Melting Curves</i>	1920.0	50.0	$34.6(T < T_c)$	$74.57 < T < 1939.0$	$0.2 < P < 49.7$	92	3.13
			$-25.5(T < T_c)$	$1437.3 < T < 1932.2$	$49.5 < P < 71.2$		
<i>Fluid – solid</i>	1746.7	74.0	-0.0638	$816.0 < T < 1769.41$	$15.9 < P < 74.3$	53	3.13
$\delta_{loc} - \epsilon$	300.0	10.72	16.7	$181.2 < T < 463.3$	$3.9 < P < 21.4$	23	3.35
$\delta - \delta_{loc}$	300.0	17.35	16.4	$100.4 < P < 534.8$	$5.5 < P < 33.6$	23	3.35

the phase transition in nitrogen.

$\delta - \delta_{loc} - \epsilon$ transitions

In this section , we analyzed solid – solid transitions of $\delta - \delta_{loc} - \epsilon$ in solid nitrogen as a two separate transitions of $\delta - \delta_{loc}$ and $\delta_{loc} - \epsilon$ using mean field models. For the $\delta - \delta_{loc}$ transition, while δ is a disordered phase, δ_{loc} is a partially-ordered phase. Hence, this transition was assumed to be of a second order. For this calculation, we used disorder parameter (σ) and order parameter (κ) for the disordered δ phase and partially-ordered δ_{loc} phase, respectively. The expansion of the free energy in terms of the disorder parameter and order parameter could be represented as

$$F_{\delta-\delta_{loc}} = b_2\kappa^2 + b_4\kappa^4 + c_2\sigma^2 + c_4\sigma^4 + d\sigma^2\kappa^2 \quad (3.23)$$

Here, b_2, b_4, c_2, c_4 were assumed to depend on the pressure and temperature and d is the coupling constant. Since $\delta - \delta_{loc}$ transition is considered as a second order, all coefficients are taken positive. Due to the symmetry reasons and positive free energy reason, we considered only even terms in the Eq.3.23. By taking derivation of Eq.3.23 with respect to the order parameter κ and disorder parameter σ , we find

$$\frac{\partial F}{\partial \kappa} = 2\kappa(b_2 + 2b_4\kappa^2 + d\sigma^2) \quad (3.24)$$

and

$$\frac{\partial F}{\partial \sigma} = 2\sigma(c_2 + 2c_4\sigma^2 + d\kappa^2) \quad (3.25)$$

For the disordered phase δ , ordered parameter κ was taken as zero ($\kappa = 0$). Under this condition, the solution of Eq.3.24 was obtained as

$$\sigma_2 = -\frac{b_2}{d} - \frac{2b_4}{d}\kappa^2 \quad (3.26)$$

Also, solution for Eq.3.25, $\sigma=0$ was defined for the δ_{loc} phase with the nonzero order parameter κ . By substituting Eq.3.26 into the solution of Eq.3.25, the order parameter κ was obtained as

$$\kappa_2 = \frac{2b_2c_4 - c_2d}{d_2 - 4b_4c_4} \quad (3.27)$$

For this calculation, the free energy Eq.(3.23) was arranged in terms of the order parameter κ as follows:

$$\mathbf{F}_{\delta-\delta_{loc}} = \frac{b_2}{d} \left(\frac{b_2c_4}{d} - c_2 \right) + \frac{2b_4}{d} \left(\frac{b_2c_4}{d} - c_2 \right) \kappa^2 + b_4 \left(\frac{4b_4c_4}{d^2} - 1 \right) \kappa^4 \quad (3.28)$$

Phase line equation was derived from Eq.3.28 by applying condition for as given the second order transition

$$\frac{2b_4}{d} \left(\frac{b_2c_4}{d} - c_2 \right) = 0 \quad (3.29)$$

By assuming pressure and temperature dependence of coefficients as

$$b_2 = b_{20}(T - T_c) \quad (3.30)$$

$$b_4 = b_{40}(T - T_c) \quad (3.31)$$

$$c_2 = c_{20}(P - P_c) \quad (3.32)$$

$$c_4 = c_{40}(T - T_c) \quad (3.33)$$

with the constant d , we obtained temperature and pressure dependence of the phase line equation (Eq.3.29) as

$$2b_{20}c_{40}(T - T_c)^2 = c_{20}d(P - P_c) \quad (3.34)$$

where T_c and P_c are the critical temperature and pressure, respectively.

By expanding Eq.3.34, we get in the form of

$$f(T, P) = P - \alpha_1 - \alpha_2T + \alpha_3T^2 = 0 \quad (3.35)$$

where

$$\alpha_1 = P_c + \left(\frac{2b_{20}c_{40}}{c_{20}d}\right)T_c^2 \quad (3.36)$$

$$\alpha_2 = -\left(\frac{4b_{20}c_{40}}{c_{20}d}\right)T_c \quad (3.37)$$

$$\alpha_3 = \frac{2b_{20}c_{40}}{c_{20}d} \quad (3.38)$$

Then the coefficients α_1 , α_2 and α_3 were determined by fitting quadratic function (Eq.3.35) to the observed data [23] as given in Table 3.6. We plot in Fig.3.9 the calculated phase diagram according to Eq.3.34 with the observed data for the $\delta - \delta_{loc}$ transition in solid nitrogen. When we consider $\delta_{loc} - \epsilon$ transition of nitrogen, the free energy of the δ_{loc} and ϵ phases can be expressed based on the first order transition with the order parameter κ and ρ , respectively,

$$F_{\delta_{loc}} = b_2\kappa^2 + b_4\kappa^4 + b_6\kappa^6 \quad (3.39)$$

and

$$F_{\epsilon} = e_2\rho^2 + e_4\rho^4 + e_6\rho^6 \quad (3.40)$$

where b_2 , b_4 , b_6 and e_2 , e_4 , e_6 denote the pressure and temperature dependent coefficients. Due to the conditions for the first order $\delta_{loc} - \epsilon$ transition, we have $b_2 > 0$, $b_4 < 0$ and $b_6 > 0$ for $F_{\delta_{loc}}$, and $e_2 > 0$, $e_4 < 0$ and $e_6 > 0$ for F_{ϵ} . By using two boundary conditions which are the minimization of free energy with respect to the order parameter ($\frac{\partial F_{\delta_{loc}}}{\partial \kappa} = 0$ and $\frac{\partial F_{\epsilon}}{\partial \rho} = 0$) and equivalence of free energy of two phases ($F_{\delta_{loc}} = F_{\epsilon}$) at the transition region, we obtained phase line equation from Eqs.3.39 and 3.40 as

$$\frac{b_2^2}{b_4} \left(1 + \frac{b_2b_6}{2b_4^2}\right) = \frac{e_2^2}{e_4} \left(1 + \frac{e_2e_6}{2e_4^2}\right) \quad (3.41)$$

This phase line equation is valid under the ansatz $b_2b_6/b_4^2 \ll 1$ and $e_2e_6/e_4^2 \ll 1$. We assumed here temperature and pressure dependence of phase line coefficients as

$$b_2 = b_{20}(T - T_c) \quad (3.42)$$

$$b_4 = b_{40}(P - P_c) \quad (3.43)$$

$$b_6 = b_{60}(T - T_c)(P - P_c) \quad (3.44)$$

for the δ_{loc} phase and

$$e_2 = e_{20}(T - T_c) \quad (3.45)$$

$$e_4 = e_{40}(P - P_c) \quad (3.46)$$

$$e_6 = e_{60}(T - T_c)(P - P_c) \quad (3.47)$$

for the ϵ phase in N_2 . By using the same procedure as the $\delta - \delta_{loc}$ transition, functional form of the coefficients (Eqs.3.42- 3.47) was obtained and it was substituted into the phase line equation (Eq.3.41) to predict phase diagram of $\delta_{loc} - \epsilon$ transition of nitrogen.

$$\alpha_1 = P_c - T_c^2 \left(\frac{b_{20}^3 b_{60}}{2b_{40}^3} - \frac{e_{20}^3 e_{60}}{2be_{40}^3} \right) / \left(\frac{b_{20}^2}{b_{40}} - \frac{e_{20}^2}{e_{40}} \right) \quad (3.48)$$

$$\alpha_1 = 2T_c \left(\frac{b_{20}^3 b_{60}}{2b_{40}^3} - \frac{e_{20}^3 e_{60}}{2be_{40}^3} \right) / \left(\frac{b_{20}^2}{b_{40}} - \frac{e_{20}^2}{e_{40}} \right) \quad (3.49)$$

$$\alpha_1 = - \left(\frac{b_{20}^3 b_{60}}{2b_{40}^3} - \frac{e_{20}^3 e_{60}}{2be_{40}^3} \right) / \left(\frac{b_{20}^2}{b_{40}} - \frac{e_{20}^2}{e_{40}} \right) \quad (3.50)$$

Eqs. (3.48-3.50) are the definition of the coefficients of Eq.(3.35) for the $\delta_{loc} - \epsilon$ transition. Those values were predicted by Eq.3.30 to the experimental data [23] as given in Table 3.6. Fig.3.9 gives the T-P phase diagram for the $\delta_{loc} - \epsilon$ transition with the observed data [23] in nitrogen. For the $\delta - \delta_{loc} - \epsilon$ transitions, the T-P phase diagram was predicted by using the mean field model with the free energies, that was considered as of a second order transition for the $\delta - \delta_{loc}$ and a first order transition $\delta_{loc} - \epsilon$ separately in nitrogen [23]. The disordered δ phase undergoes the partially-ordered δ_{loc} phase at around 10.5 GPa and 300 K that is regarded as a second order due the change of the orientational behavior of molecular nitrogen from the free rotation to the localized mode. However, for the $\delta_{loc} - \epsilon$ transition, significant hysteresis prevents to specify the transition temperature as pointed earlier [23]. This uncertainty indicates metastability of one phase with respect to the other [23]. Both experimental [14, 22, 23, 51, 95] and theoretical calculations [25] stated that the ordered ϵ phase becomes stable in the pressure interval of 2-40 GPa. As a results, on the basis of

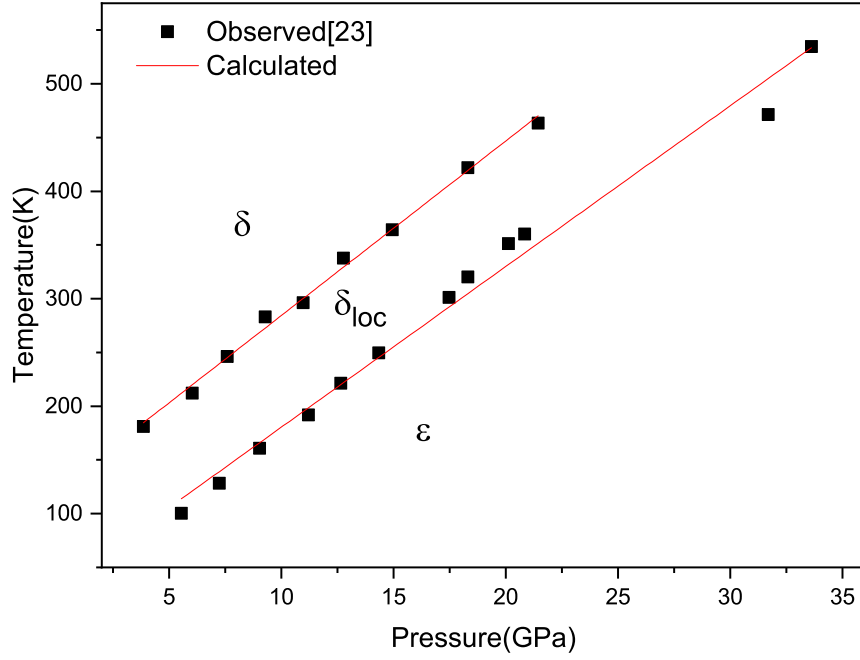


Figure 3.9: Calculated phase diagram of N_2 for the transitions of $\delta_{loc} - \epsilon$ and $\delta - \delta_{loc}$ according to Eq.3.35 using the experimental data [23].

these calculations, the analyzing of the T-P phase diagram by using mean field theory can also be used for the other molecular crystals.

3.3 "Calculation of the thermodynamic functions using a mean field model for the fluid-solid transition in nitrogen."

In our earlier studies, we calculated phase diagram of solid nitrogen by using the phase line equation derived from the free energy for the solid-fluid and, solid-solid transitions of the $\delta - \delta_{loc} - \epsilon$ in nitrogen [23, 55, 94] through the mean field models [58]. In this part, we predicted some thermodynamic quantities of solid nitrogen as a function of temperature near the melting temperature by applying same procedure as the previous study. We investigated those temperature dependences of the thermodynamic quantities such as order parameter, inverse susceptibility, thermal expansion, isothermal compressibility, specific heat etc. by using the measured melting temperature [56] and the observed T-P data [55].

First, we expanded free energy in terms of the order parameter ψ close to the solid-liquid transition according to the Landau phenomenological model with the cubic

term which leads to a first order solid-liquid transition as

$$F_s = a_2\psi^2 + a_3\psi^3 + a_4\psi^4 \quad (3.51)$$

where a_2 , a_3 and a_4 can generally depend on temperature and pressure. For this calculations, density is considered as an order parameter. By minimizing the free energy with respect to order parameter ($\partial F/\partial\psi = 0$) and using the first order condition according to which there is no ordering in the liquid phase ($F_S = F_L = 0$), we obtained the solution as

$$\psi = -\frac{2a_2}{a_3} = -\frac{a_3}{2a_4} \quad (3.52)$$

We then have the phase line equation from Eq.3.52

$$a_3^2 = 4a_2a_4 \quad (3.53)$$

We assumed the temperature and pressure dependence of the coefficient a_2 (Eq.3.53) as

$$a_2^3 = (P - P_t) - a_{20} - a_{21}(T - T_t) + a_{22}(T - T_t)^2 \quad (3.54)$$

Here, a_{20} , a_{21} and a_{22} are constants and we took the value of the a_2 as unity. To determine the value of the coefficients of Eq.3.54, we fitted the experimental data [55, 56] through functional form of phase line equation (Eq.3.54) as given in Table 3.8 with the transition temperature (T_t) and pressure (P_t) which have maximum values for the solid-liquid transition.

Table 3.8: Values of the coefficients a_2 , which were obtained by fitting Eq.(3.54) ($a_2=0$) to the experimental T-P data for the solid N_2 -liquid N_2 transition [54,53] within the temperature and pressure intervals indicated. Values of the transition temperature (T_t) and pressure (P_t) in Eq.(3.54), are also given here.

T_t (K)	P_t (GPa)	a_{20} (GPa)	$a_{21} \times 10^{-2}$ (GPa/K ²)	$a_{22} \times 10^{-5}$ (GPa/K ²)	Temperature Interval(K)	Pressure Interval(GPa)	Ref.
1769.4	74.3	-8.70	8.80	3.90	816.0<T<1769.4	15.9<P<74.2	23
1972.7	106.9	11.29	11.34	3.59	241.0<1972.7	1.5<P<106.9	54

First, we calculated the order parameter (ψ) as a function of temperature and pressure as plotted in Fig.3.10a and 3.10b, respectively, for the solid-liquid transition by using Eq.3.52. Calculated ψ decrease with the increment of the temperature and pressure

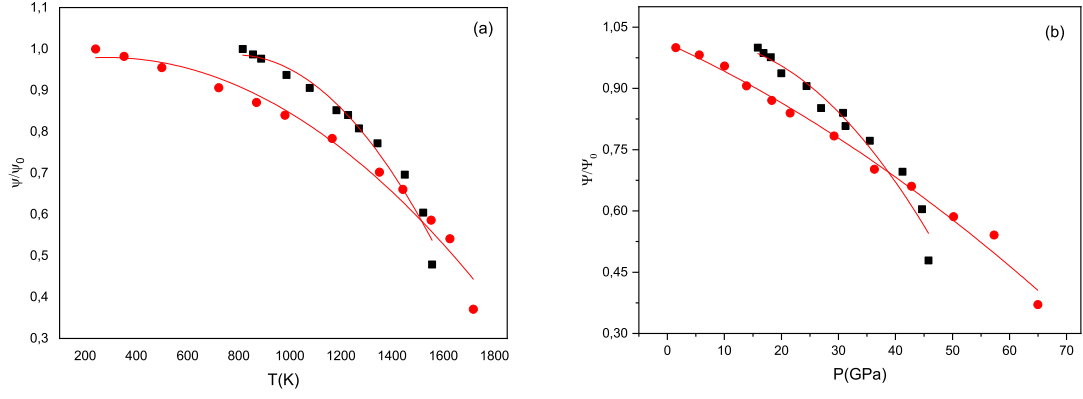


Figure 3.10: Variation of the order parameter ψ (normalized) with the temperature (a) and the pressure (b) at the transition pressures of $P_t = 74.3$ GPa and $P_t = 106.9$ GPa by using the observed T-P data (circles) [54] and (squares) [53], respectively, for the solid–liquid transition in N_2 according to Eq.3.52 through Eq.3.54.

as expected for two observed data taken from the literature [55, 56]. By using the definition of the inverse susceptibility (χ_ψ^{-1})

$$\chi_\psi^{-1} = \partial^2 F / \partial \psi^2 \quad (3.55)$$

and using the Eq.3.51, we predicted the inverse susceptibility χ_ψ^{-1} as a function of temperature and pressure. Figs.3.11a and 3.11b give the variation of the inverse susceptibility of the order parameter with the temperature and pressure, respectively. According to these figures, there is an almost linear decrease of the inverse susceptibility as the temperature and pressure increase.

The thermodynamic quantities of the entropy (S), heat capacity (C_P), thermal expansion (α_P) and isothermal compressibility (κ_T) were also calculated by using their definitions of $S = (\partial F / \partial T)_\nu$,

$$C_p = T(\partial S / \partial T)_\nu \quad (3.56)$$

$$\alpha_P = (1/V)(\partial V / \partial T)_P$$

and

$$\kappa_T = -(1/V)(\partial V / \partial P)_T$$

respectively, for the solid-liquid transition in N_2 .

We depicted the normalized entropy (S/S_0) as function of temperature (Fig.3.12)

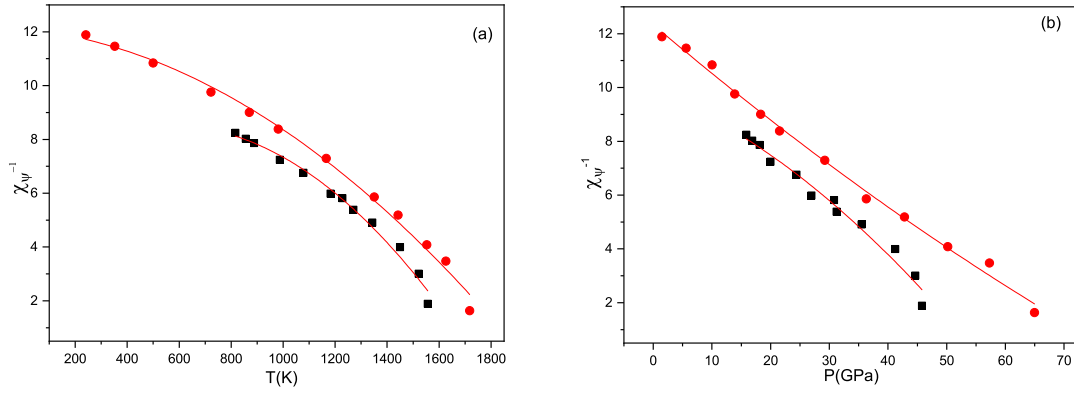


Figure 3.11: Inverse susceptibility χ_ψ^{-1} of the order parameter ψ as a function of temperature (a) and pressure (b) at the transition pressures of $P_t=74.3$ GPa and $P_t=106.9$ GPa by using the observed T-P data (circles) [54] and (squares) [53] respectively, for the solid –liquid transition in N_2 according to Eq.3.55.

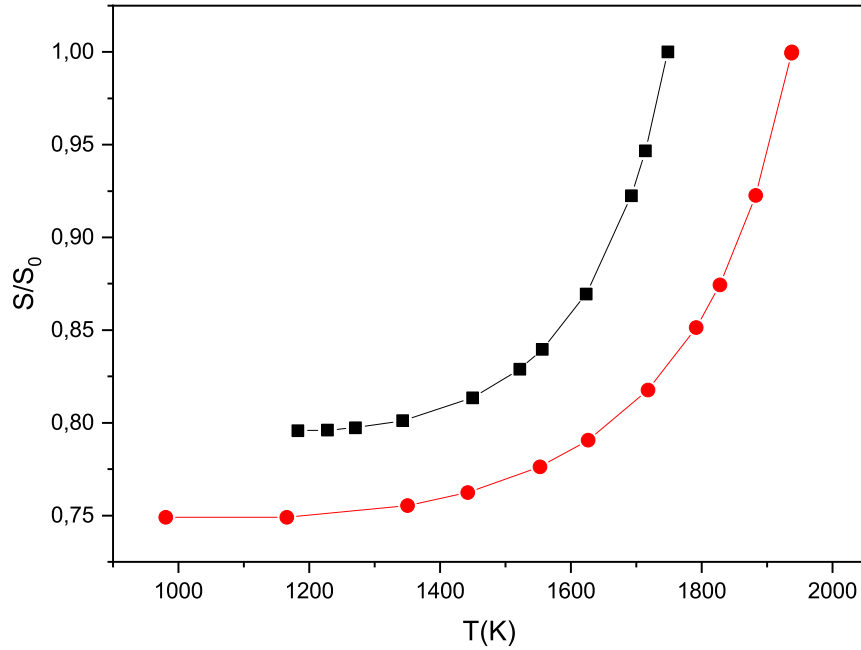


Figure 3.12: Entropy S (normalized) calculated from the free energy (Eq.11) as a function of temperature at the transition pressures of $P_t=74.3$ GPa and $P_t=106.9$ GPa by using the observed T-P data (circles) [54] and (squares) [53] respectively, for the solid –liquid transition in N_2 .

,the normalized heat capacity (C_V/C_{V0}) (Fig.3.13),the normalized thermal expansion (α_P/α_{P0}) (Fig.3.14) and the normalized isothermal compressibility (κ_T/κ_{T0}) (Fig.3.15) as a function of temperature at the transition pressure ($P=P_t$) for the solid

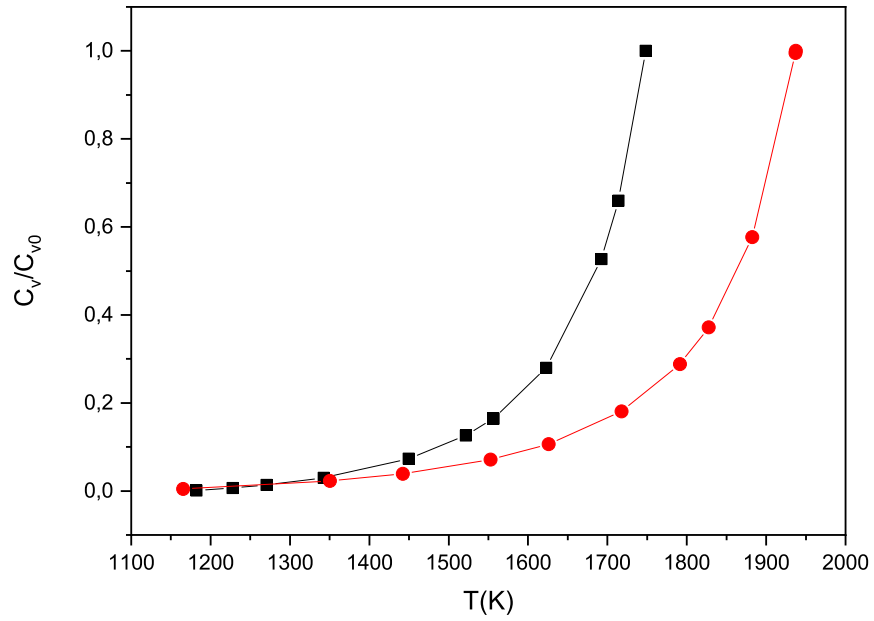


Figure 3.13: Heat capacity C_v (normalized) calculated from the free energy (Eq.3.56) as a function of temperature at the transition pressures of $P_t=74.3$ GPa and $P_t=106.9$ GPa by using the observed T-P data (circles) [54] and (squares) [53] respectively, for the solid –liquid transition in N_2 .

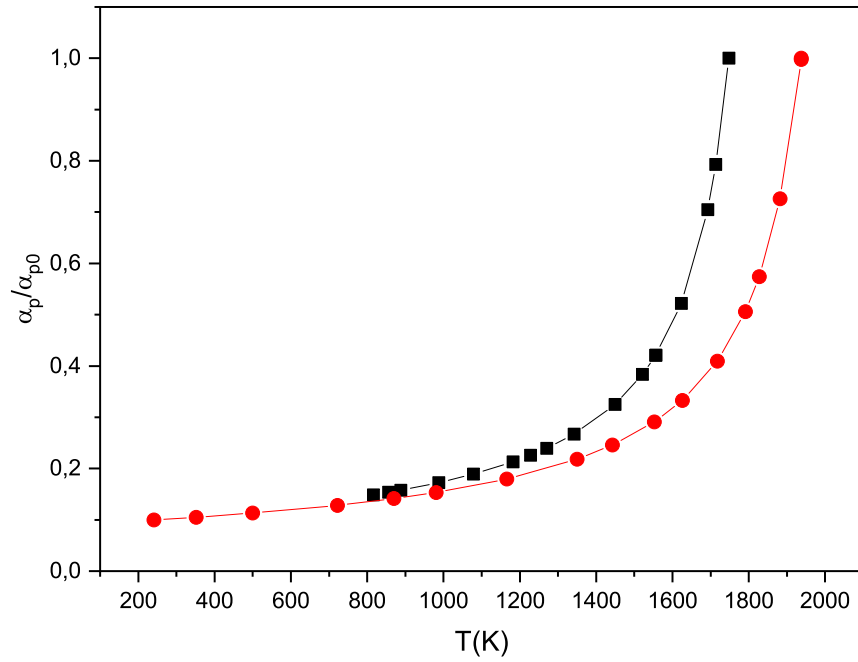


Figure 3.14: Thermal expansion α_p (normalized) as function of temperature at the transition pressures of $P_t=74.3$ GPa and $P_t=106.9$ GPa using the observed T-P data (circles) [54] and (squares) [53] respectively, for the solid –liquid transition in N_2 .

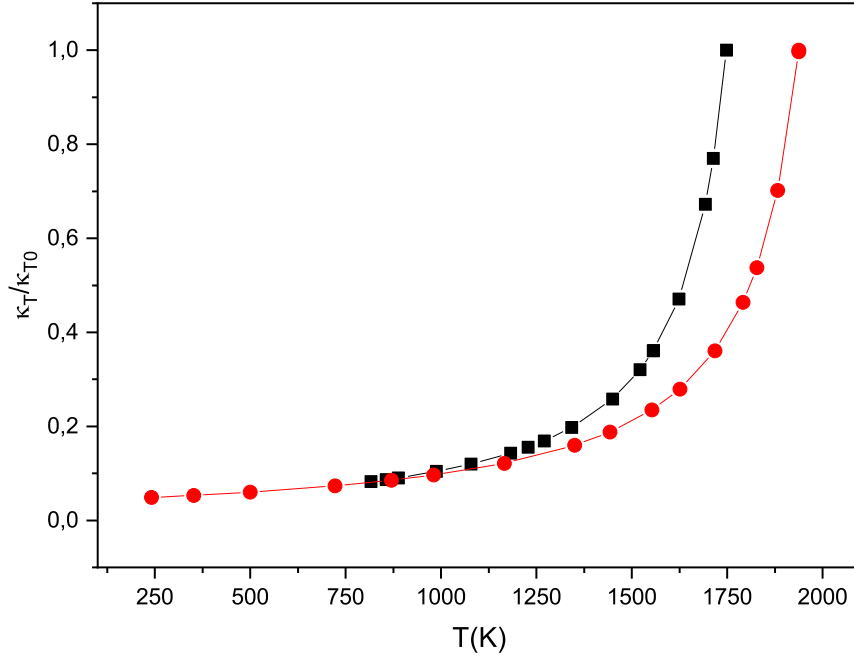


Figure 3.15: Isothermal compressibility κ_T (normalized) as a function of temperature at the transition pressures of $P_t=74.3$ GPa and $P_t=106.9$ GPa by using the T-P data (circles) [54] and (squares) [53] respectively, for the solid –liquid transition in N_2 .

liquid transition in N_2 . According to these figures (Figs. 3.12-3.15), they show the same behavior as a large increase especially close to the melting point. For C_v (Fig.3.13), α_P (Fig.3.14), and κ_T (3.15), we obtained nearly the same values by using two different observed data [55,56] as stated above. In the melting region, those thermodynamic quantities exhibit anomalous behavior due to the appearance of a liquid which is denser than the solid. Hence this critical behavior of them states that the mean field model with the cubic term is sufficient to analyze the first order liquid-solid transition in nitrogen.

3.4 "Raman bandwidths calculated for the librational (α -phase) and internal (ϵ , δ_{loc} and δ phases) modes in N_2 using pseudospin-phonon coupling (PS) and energy-fluctuation (EF) models"

The temperature dependence of Raman bandwidths was calculated by using the pseudospin-phonon coupling (PS), energy fluctuation models and Raman frequencies with respect to the order parameter was analyzed for the for the E_g librational mode in the α -phase

(P=0) and for the internal mode ν_1 in the phases of ϵ , δ_{loc} and δ at constant pressure (P=18 GPa) using the experimental data from the literature [23, 88]. In this context, the frequency difference of the internal modes ν_1 and ν_2 as a function of temperature was also analyzed at various pressures (13.2, 14.95, 18.5 and 21.2 GPa) using the experimental data [23]. Regarding to calculation of the Raman frequency, temperature dependence of the order parameter was studied in the molecular field theory [79, 96] as given by

$$s = 1 - \exp\left(-\frac{2T_c}{T}\right) \quad (3.57)$$

below the critical temperature (T_c). We calculated the order parameter (S) as a function of temperature at the P=0 for the E_g mode in the α phase and at the 18 GPa for the ν_1 mode in the ϵ , δ_{loc} and δ phases in nitrogen. In this calculation, normalized Raman frequency (ν/ν_0) was considered as an order parameter which varies from 0 (disordered phase) to 1 (ordered phase) and it was examined through Eq.3.58

$$\nu/\nu_0 = a_0 + a_1T + a_2T^2 \quad (3.58)$$

where ν_0 is the maximum frequency, the coefficients a_0 , a_1 and a_2 are constants. By the fact that we fitted experimental ν data for the E_g librational mode at P=0 [88] and for the internal mode ν_1 at P=18 GPa [23] in the solid nitrogen, the coefficients of Eq.3.58 (a_0 , a_1 and a_2) were determined as given in Table 3.9.

Table 3.9: Values of the coefficients a_0 , a_1 and a_2 (Eq.3.58) and, of the a, b and c (Eq.3.59) with the ν_0 and T_c values for the Raman modes of E_g for the transition of $\alpha - \beta$ [86] and ν_1 for the transition of $\epsilon - \delta_{loc} - \delta$ [23] at the pressures indicated within the temperature intervals in solid nitrogen.

P (GPa)	T_c (K)	Transition	Raman modes	a_0	$a_1 \times 10^{-3}$ (K ⁻¹)	$-a_2 \times 10^{-8}$ (K ⁻²)	ν_0 (cm ⁻¹)	a	b	c	Temperature Interval(K)
0	38.74	$\alpha - \beta$	E_g	0.99	2.4	9930	34.98	17.39	-35.88	19.56	4.88<T<38.74
18	413.87	$\delta_{loc} - \delta$	ν_1	0.99	0.0398	6.76	2388.35	8.95×10^5	-1.79×10^6	8.95×10^5	332.54<T<413.87
	323.34	$\epsilon - \delta_{loc}$		0.97	0.19	31.8	2389.57	-57.28	58.20	-	299.54<T<323.34

To analyze the correlation between order parameter S and the normalized Raman frequency (ν/ν_0), the quadratic expression

$$S = a + b(\nu/\nu_0) + c(\nu/\nu_0)^2 \quad (3.59)$$

was used. Values of coefficients a, b and c were obtained (Table 3.9) by means of fitting the order parameter calculated (Eq.3.57) to the normalized Raman frequency

(ν/ν_0) (Eq.3.59) for the E_g librational mode and ν_1 mode in the ϵ , δ_{loc} and δ phases in nitrogen. Fig.3.16 gives the temperature dependence of Raman frequency for the E_g librational mode in the α phase [88] calculated via Eq.3.59 with the observed data. The calculated Raman frequency of the ν_1 mode with the variation of temperature (P=18 GPa) according to Eq.3.59, was plotted in Fig.3.17 in the ϵ , δ_{loc} and δ phases [23] of solid nitrogen.

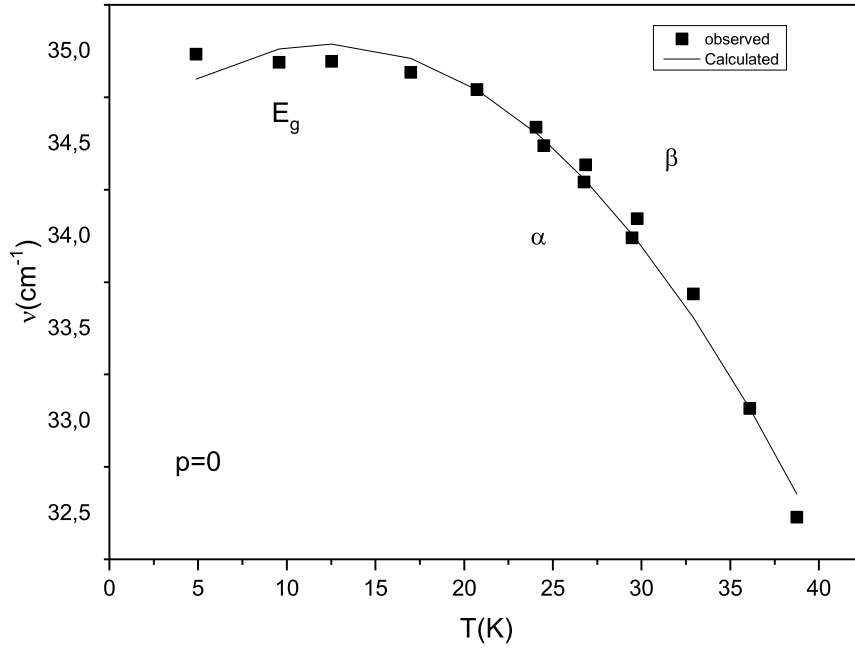


Figure 3.16: Raman frequency calculated for the Raman modes of E_g by using Eqs.(3.57) and (3.58) through Eq. (3.59) for the α phase (P=0) with the observed data [86] in solid nitrogen.

We also analyzed the difference between the Raman internal modes of ν_1 and ν_2 at constant pressures of 13.2, 14.95, 18.5 and 21.2 GPa for the ϵ , δ_{loc} and δ phases [23] of solid nitrogen. We obtained values of the coefficients of a_0 , a_1 and a_2 (Eq.3.58) by fitting observed frequency shift $(\nu_1 - \nu_2)$ [23] data through the Eq.3.58. Then we calculated the order parameter S by the molecular field theory and the values of coefficients of a, b and c (Eq.3.59) were determined from our analysis of $\nu_1 - \nu_2$ with respect to the temperature at constant pressures for the transitions of solid nitrogen as given in Table3.10 with the critical temperatures (T_c). We depicted the Raman frequencies calculated from Eq.3.59 for the frequency difference $\nu_1 - \nu_2$ as a function of temperature at constant pressures with the observed data in Fig.3.18

Damping constant was then calculated according to the pseudospin-phonon coupled

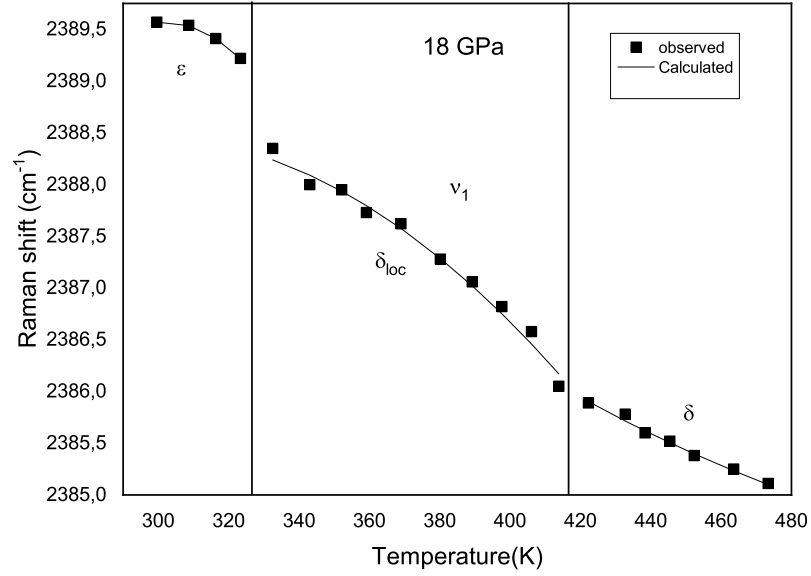


Figure 3.17: Raman frequency calculated for the internal mode of ν_1 by using Eqs.(3.57) and (3.58) through Eq. (3.59) for the ϵ , δ_{loc} and δ phases (P=18 GPa) with the observed data [23] in solid nitrogen.

Table 3.10: Values of the coefficients a_0 , a_1 and a_2 (Eq.3.57) and of the a,b and c (Eq.3.58) with the ν_0 and T_c values for the frequency difference ($\nu_1 - \nu_2$) of the ν_1 and ν_2 for the transition of $\epsilon - \delta_{loc} - \delta$ [23] at the pressures indicated within the temperature intervals in solid nitrogen.

P (GPa)	T_c (K)	Transitions	a_0	$a_1 \times 10^{-3}$ (K^{-1})	$-a_2 \times 10^{-5}$ (K^{-2})	ν_0 (cm^{-1})	a	-b	c	Temperature Interval(K)
13.2	336 ± 6	$\delta_{loc} - \delta$	-0.34	11.23	2.26	15.58	1.17	0.88	0.60	$300.88 < T < 333.23$
14.95	364 ± 6	$\delta_{loc} - \delta$	0.065	7.64	1.50	17.53	1.35	1.32	0.87	$304.56 < T < 358.97$
18.5	419 ± 9	$\delta_{loc} - \delta$	0.42	4.5	0.838	20.75	1.34	1.34	0.93	$321.47 < T < 425.15$
	329 ± 3	$\epsilon - \delta_{loc}$ (heating)	0.56	3.31	0.614	21.65	35.67	71.63	36.84	$300.15 < T < 323.68$
	312 ± 3	$\delta_{loc} - \epsilon$ (cooling)								
21.2	456 ± 12	$\delta_{loc} - \delta$	0.46	4.03	0.710	22.67	1.24	1.10	0.79	$352.35 < T < 451.62$
	372 ± 3	$\epsilon - \delta_{loc}$ (heating)	0.88	1.08	0.231	23.76	15.83	31.90	16.98	$302.35 < T < 371.47$
	351 ± 3	$\delta_{loc} - \epsilon$ (cooling)								

(PS) model (Eq.2.34) and the energy fluctuation (EF) model (Eq.2.36) by taking by Raman frequency as an order parameter (S). The values of the background damping

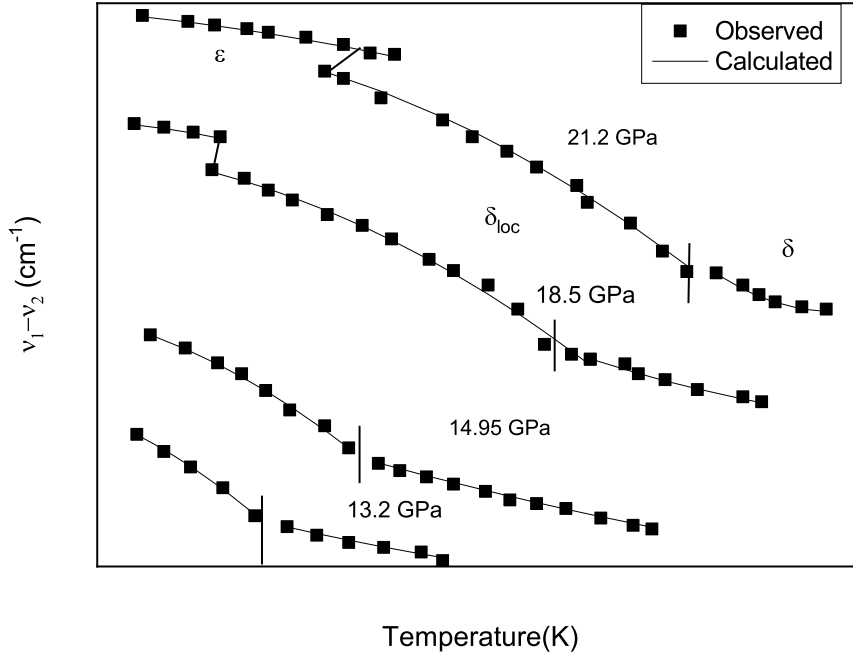


Figure 3.18: Raman frequency calculated for the frequency difference ($\nu_1 - \nu_2$) of the ν_1 and ν_2 by using Eqs.(3.57) and (3.58) through Eq. (3.59) for the ϵ , δ_{loc} and δ phases at constant pressures with the observed data [23] in solid nitrogen.

constant $\Gamma'_0(\Gamma_1)$ and the amplitude $A'(A)$ was obtained for the librational E_g mode in the α phase ($P=0$), the internal mode ν_1 ($P=18$ GPa) and for the frequency difference ($\nu_1 - \nu_2$) at constant pressures ($P=13.2, 14.95, 18.5$ and 21.2 GPa) in the phases of ϵ , δ_{loc} and δ as a function of temperature by fitting the experimental Raman linewidth (FWHM) data through Eqs.2.34 and 2.36 the E_g [88], ν_1 and ($\nu_1 - \nu_2$) [23] in solid nitrogen, as given in Tables 3.11,3.12 and 3.13, respectively. Then, we calculated damping constant Γ as a function of temperature by means of two models (PS and EF) using the values of order parameter S , the background damping constant $\Gamma'_0(\Gamma_1)$ and the amplitude $A'(A)$ for the E_g [88], ν_1 and ($\nu_1 - \nu_2$) [23] in solid nitrogen. Figs. 3.19-3.21 give our calculated temperature dependent damping constant (Γ) according to the PS (Eq.2.34) and EF (Eq.2.36) models for the librational mode E_g ($P=0$), the internal mode ν_1 ($P=18$ GPa) and the frequency difference ($\nu_1 - \nu_2$) at constant pressures (13.2, 14.95, 18.5 and 21.2 GPa) with the observed data.

For this study, as observed experimentally studies of Medina et.al. [88] and Tassini et al. [23], the librational E_g mode and the internal mode ν_1 were preferred because of their soft mode behaviors since their Raman frequencies decreases as the temperature

Table 3.11: Values of the coefficients calculated according to the Eqs.2.34 and 2.36 for the E_g librational mode of the α -phase (P=0) in solid nitrogen.

P (GPa)	Models	$\Gamma'_0(\Gamma_0)$ (cm^{-1})	$A'(A)$ (cm^{-1})	Temperature Interval(K)
0	PS	0.11	54.29	5.01<T<24.17
		-0.17	337.31	26.94<T<38.57
	EF	3.38×10^{-3}	7.62	5.01<T<20.99
		-3.36	22.92	24.17<T<38.56

Table 3.12: Values of the coefficients calculated according to the Eqs.2.34 and 2.36 for the ν_1 mode for the phases of ϵ , δ_{loc} and δ (P=18 GPa) in solid nitrogen.

P (GPa)	Phases	Models	$\Gamma'_0(\Gamma_0)$ (cm^{-1})	$A'(A)$ (cm^{-1})	Temperature Interval(K)
18	ϵ	PS	3.03	-33.32	298.92<T<325.47
		EF	0.23	1.06	
	δ_{loc}	PS	-3.77	72.59	338.40<T<418.38
		EF	-1.02	5.21	
	δ	PS	-2.36	59.56	423.06<T<443.46
		EF	0.07	3.89	

increase towards T_c (Figs.3.16 and 3.17). This decrease of the Raman frequency was also observed for the frequency difference ($\nu_1 - \nu_2$) with the increasing temperature at constant pressures (Fig.3.18). Related to the order parameter, there is a nonlinear relationship for the Raman frequency (Eq.3.59) i.e. $S \propto (\nu/\nu_0)^2$, as obtained for the E_g librational mode in the α phase at P=0 (Fig.3.16) and for the ν_1 internal mode in the phases ϵ , δ_{loc} and δ at P= 18 GPa (Fig.3.18) of solid nitrogen. Regarding to bandwidth of the librational E_g mode, the lines broaden as the temperature increases [97–99] (Fig.3.19). The combination of E_g with T_g librations in order to create

Table 3.13: Values of the coefficients calculated according to the Eqs. 2.34 and 2.36 for the frequency difference ($\nu_1-\nu_2$) for the phases of ϵ , δ_{loc} and δ at constant pressures in solid nitrogen.

P (GPa)	Phases	Models	$\Gamma'_0(\Gamma_0)$ (cm^{-1})	$A'(A)$ (cm^{-1})	Temperature Interval(K)
13.2	δ_{loc}	PS	-2.29	3.42	295.60<T<331.49
		EF	-0.79	6.95	
	δ	PS	0.06	0.42	340.85<T<386.10
		EF	0.29	0.52	
14.95	δ_{loc}	PS	-1.47	2.52	315.09<T<362.95
		EF	-0.37	5.16	
	δ	PS	-1.47	2.78	338.40<T<418.38
		EF	-0.29	5.93	
18.5	ϵ	PS	-0.28	0.49	298.92<T<325.47
		EF	-0.06	0.95	
	δ_{loc}	PS	-1.27	2.56	338.40<T<418.38
		EF	-0.22	5.72	
	δ	PS	-3.12	5.32	423.06<T<443.46
		EF	-1.15	13.66	
21.2	ϵ	PS	-0.03	0.23	302.81<T<361.26
		EF	0.08	0.49	
	δ_{loc}	PS	-0.38	1.32	365.34<T<431.23
		EF	0.16	2.98	
	δ	PS	-2.83	5.28	455.53<T<480.26
		EF	-0.45	10.38	

T_u phonon clarifies this behavior of the temperature dependence of the linewidth for E_g mode [88]. According to temperature dependence of damping constant (FWHM),

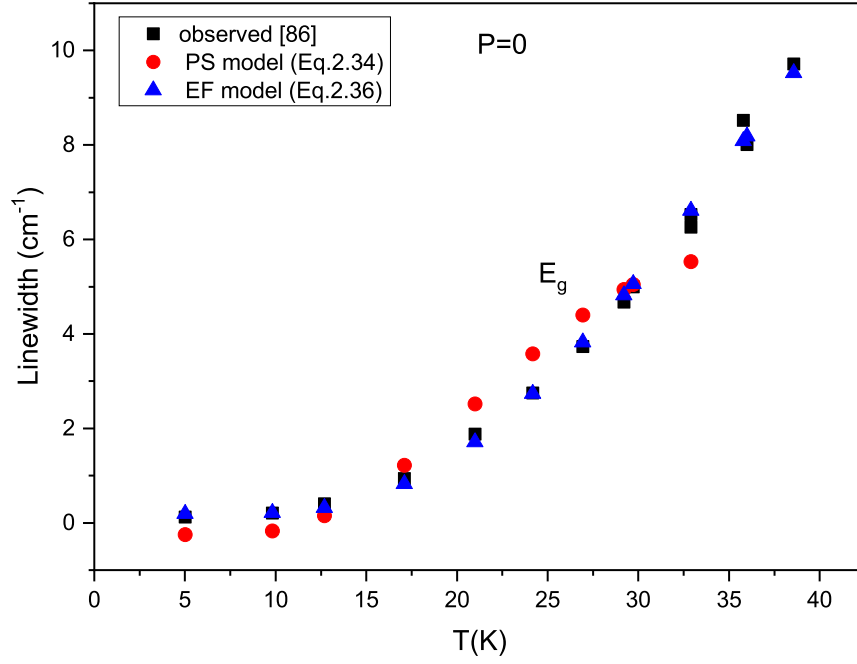


Figure 3.19: Damping constant (linewidth) calculated from Eqs.2.34 and 2.36 for the E_g mode for the α -phase ($P=0$) with the observed data[86] in solid nitrogen.

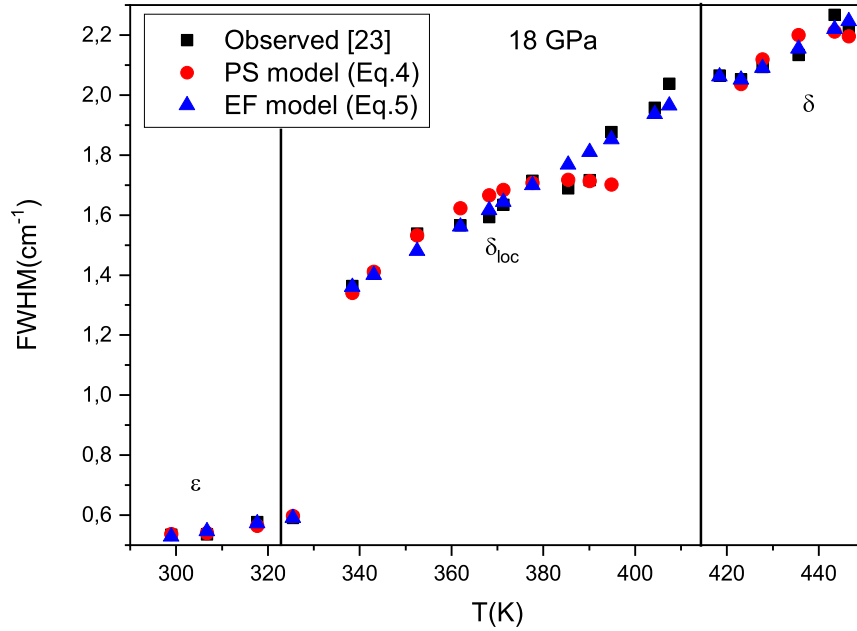


Figure 3.20: Damping constant (linewidth) calculated from Eqs.2.34 and 2.36 for the ν_1 mode of the ϵ , δ_{loc} and δ phases at constant pressures with the observed data [23] in solid nitrogen.

there is an abnormal jump for the phase transitions especially from ϵ to δ_{loc} for E_g and ν_1 modes as shown in Figs. 3.20 and 3.21. Although δ and δ_{loc} phases are disordered

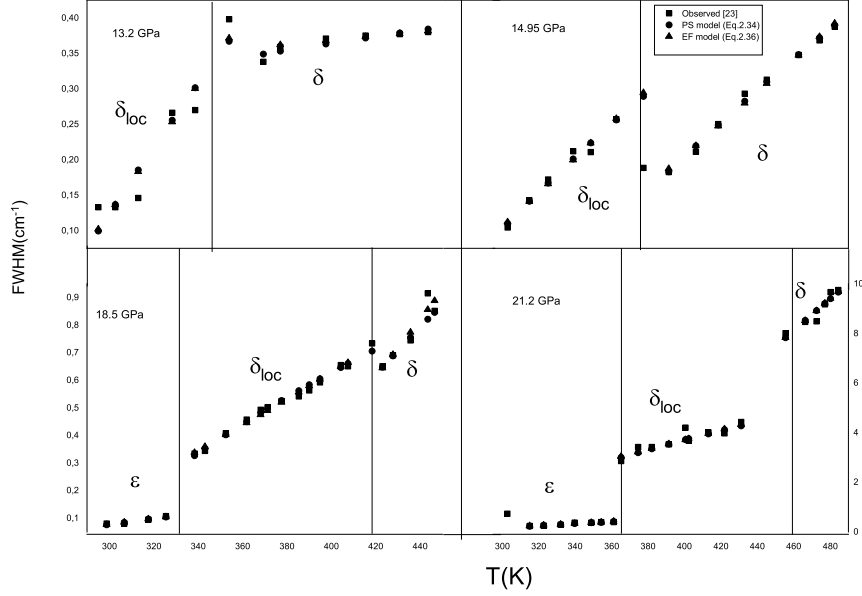


Figure 3.21: Damping constant (linewidth) calculated from Eqs.2.34 and 2.36 for the frequency difference ($\nu_1 - \nu_2$) for the phases of ϵ , δ_{loc} and δ at constant pressures with the observed data [23] in solid nitrogen.

, δ_{loc} phase becomes increasingly order with decreasing temperature [23]. In addition to that larger bandwidth value of the ν_1 mode (sphere) when compared to the ν_2 mode (disks) is the result of rising of the solid angle proped by the disk type molecules in the disordered δ phase [23].

3.5 "Calculation of the thermodynamic functions from the Raman frequency shifts close to the ϵ - δ_{loc} - δ phases transitions and Pippard relations in nitrogen."

In this part, we calculated the thermodynamic quantities of the thermal expansion (α_p), isothermal compressibility (κ_T) and the difference in the heat capacity ($C_p - C_v$) as a function of temperature close to the transitions of ϵ - δ_{loc} and δ_{loc} - δ by examining the experimental Raman frequency shifts of the internal modes ν_1 , ν_2 and ν_{22} in the solid nitrogen [23]. For this prediction, in addition to the observed Raman frequency shifts data, observed volume data as a function of various pressures from the literature were used for the ϵ - δ_{loc} - δ transitions [56, 94]. And also, the Pippard relations are analyzed for the ϵ - δ_{loc} and δ_{loc} - δ , fluid-solid transition and melting

curves in nitrogen.

Regarding the volume dependence of the vibrational frequency, the isobaric mode Grüneisen parameter was calculated by using the Eq.3.60

$$\gamma_P = -\frac{(1/\nu)(\partial\nu/\partial T)_P}{(1/V)(\partial V/\partial T)_P} \quad (3.60)$$

where ν is the vibrational frequency and V is the crystal volume. To calculate the thermal expansion with the definition $\alpha_P \equiv (1/V)(\partial V/\partial T)_P$, Eq.3.60 was arranged according to the frequency shifts of the Raman modes and their γ_P values expressed as

$$\alpha_P = -(1/\gamma_P)(1/\nu)(\partial V/\partial T)_P \quad (3.61)$$

In order to calculate the thermal expansion, observed Raman frequency was analyzed by using quadratic function as a function of temperature,

$$\nu(T) = a_0 + a_1T + a_2T^2 \quad (3.62)$$

In Eq.3.62, the values of coefficients a_0 , a_1 and a_2 were determined for ν_1 , ν_2 and ν_{22} in the ϵ , δ_{loc} and δ phases of solid nitrogen as given in Table 3.14 within the temperature intervals. For the calculation of thermal expansion (Eq.3.61), we used a constant γ_P value (-0.14) determined for the vibron ν_2 in the δ phase of solid nitrogen in an earlier study [100] for the ν_1 , ν_2 and ν_{22} in the ϵ , δ_{loc} and δ phases of solid nitrogen. After calculating the thermal expansion, we calculated the isothermal compressibility κ_T and the difference in the heat capacity $C_p - C_v$ as function of temperature by using Eqs.3.63 and 3.64, respectively,

$$\alpha_P/\kappa_T = dP/dT \quad (3.63)$$

and

$$C_p = C_v + TV\alpha_P^2/\kappa_T \quad (3.64)$$

For calculating the isothermal compressibility (Eq.3.63), we obtained dP/dT values from the observed T-P data [23] due to

$$P = a + bT + cT^2 \quad (3.65)$$

where a , b and c are constants and given in Table 3.15 for the δ - δ_{loc} and δ_{loc} - ϵ transitions in solid nitrogen [23]. Finally, we calculated the difference in the heat capacity

Table 3.14: Values of the coefficients calculated according to the Eq.3.62 for the vibrons indicated in solid nitrogen.

Raman modes	Phases	$a_0(cm^{-1})$	$a_1(cm^{-1}/K)$	$a_2(cm^{-1}/K^2)$	Temperature Interval(K)
ν_1	ϵ	2320.32	0.46	-7.61×10^{-4}	298.9<T<325.5
	δ_{loc}	2374.51	0.09	-7.6×10^{-4}	327.3<T<407.1
	δ	2402.93	-0.06	5.20×10^{-5}	423.1<T<477.5
ν_2	ϵ	2363.10	0.03	-5.32	301.3<T<323.6
	δ_{loc}	2377.73	-0.06	9.39	332.6<T<413.6
	δ	2366.06	0.01	-1.05	423.4<T<472.8
ν_{22}	ϵ	2372.90	-0.02	3.98	301.6<T<325.2
	δ_{loc}	2367.29	0.01	-1.20	331.3<T<411.78

per unit volume $(C_p - C_v)/V$ (Eq.3.64) with regard to the α_P and κ_T at 18 GPa for the phases of ϵ , δ_{loc} and δ in solid nitrogen.

Table 3.15: Values of the coefficients calculated according to the Eq.3.65 for the phase transitions indicated in solid nitrogen.

Transitions	$a(GPa)$	$b \times 10^{-2}(GPa/K)$	$c \times 10^{-5}(GPa/K^2)$
$\delta - \delta_{loc}$	-3.7	3.57	4.09
$\delta_{loc} - \epsilon$	0.51	4.56	3.40

Fig.3.22-3.24 represent the calculated thermal expansion α_P , the isothermal compressibility κ_T and the difference in the molar heat capacity $(C_p - C_v)/V$ in terms of temperature for the internal modes ν_1 , ν_2 and ν_{22} in the ϵ , δ_{loc} and δ phases of solid nitrogen. According to these figures, the α_P (Fig.3.22), κ_T (Fig.3.23) and $(C_p - C_v)/V$ (Fig.3.24) for the vibron ν_2 increase with increasing of temperature in the δ_{loc} phase while they decrease with temperature in the ϵ and δ phases. However, the calculated α_P , κ_T and $(C_p - C_v)/V$ for the ν_{22} mode decrease with increasing temperature in the ϵ and δ_{loc} phases.

Considering the linear variations between the calculated thermodynamic quantities α_P , κ_T and $(C_p - C_v)/V$, we examined Pippard relations according to

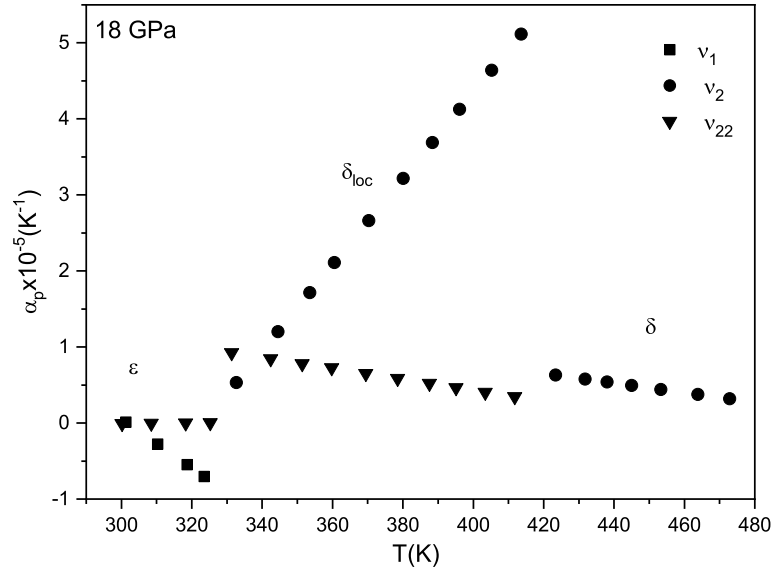


Figure 3.22: Temperature dependent thermal expansion calculated from Eq.3.61 for the Raman modes of ν_1 , ν_2 and ν_{22} for the phases of ϵ , δ_{loc} and δ in solid nitrogen.

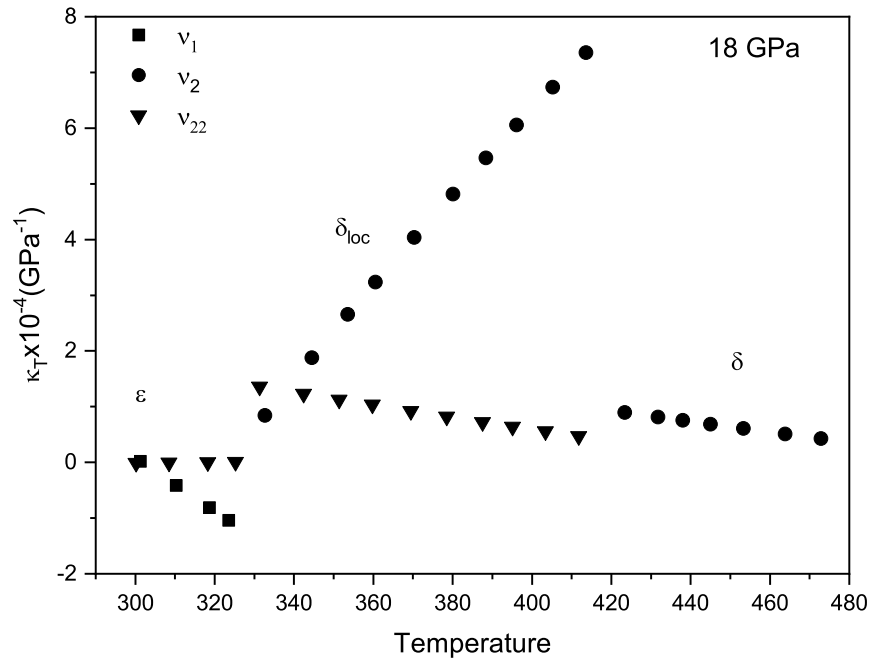


Figure 3.23: Temperature dependent isothermal compressibility calculated from Eq.3.63 for the Raman modes of ν_1 , ν_2 and ν_{22} for the phases of ϵ , δ_{loc} and δ in solid nitrogen.

$$C_p = TV\alpha_P(dP/dT)T + T(dS/dT) \quad (3.66)$$

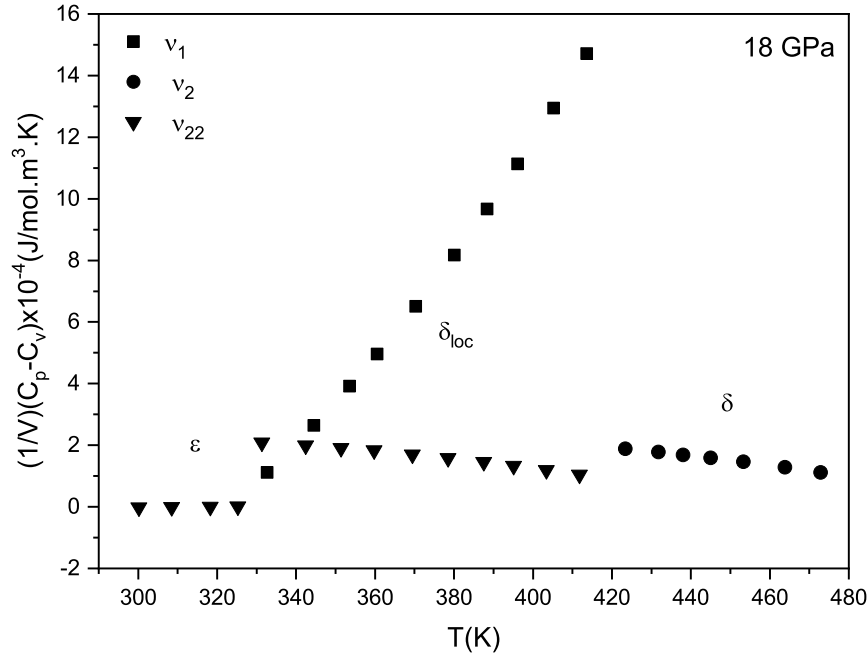


Figure 3.24: Difference in the heat capacity calculated from Eq.3.64 for the Raman modes of ν_1 , ν_2 and ν_{22} for the phases of ϵ , δ_{loc} and δ in solid nitrogen.

and

$$\alpha_P = \kappa_T(dP/dT)T + (1/V)(dV/dT) \quad (3.67)$$

We plotted $(C_p - C_v)/V$ versus $\alpha_P T$ (Fig.3.25) and α_P versus κ (Fig.3.26) and we obtained the slope values of dP/dT (Eqs.3.66 and 3.67) and the intercept $(1/V)(dV/dT)$ (Eq.3.67) as given in Table 3.16 at 18 GPa for the phases of ϵ , δ_{loc} and δ in solid nitrogen [23]. We also compared those dP/dT values with the values obtained from the Eq.3.65 using the coefficients in Table 3.15 for the δ - δ_{loc} [101] and δ_{loc} - ϵ [102] transitions.

Table 3.16: Calculated dP/dT values by using Eq.3.65 and the values of the slope dP/dT and the intercept of $(1/V)(dV/dT)$ (Eq.7) derived from the Pippard relations (Eqs.3.66 and 3.67) for the vibrons of solid nitrogen.

Transitions N_2	$T_c(K)$	$dP/dT \times 10^{-2}(GPa/K)$ Eq.(3.64)	$dP/dT \times 10^{-2}(GPa/K)$ Eqs.(3.66) and (3.67)	$(1/V)(dV/dT) \times 10^{-8}(K^{-1})$ Eq.(3.67)	Temperature Interval(K)
$\delta - \delta_{loc}$	419 ± 9	7.1 ± 0.1	6.8	4.86	$332.62 < T < 472.83$
$\epsilon - \delta_{loc}$ (heating)	329 ± 3	6.80 ± 0.02			$301.29 < T < 413.60$
$\epsilon - \delta_{loc}$ (cooling)	312 ± 3	6.68 ± 0.02			

From linear variation of $(C_p - C_v)/V$ with $\alpha_P T$ (Fig.3.25) and α_P with κ_T (Fig.3.26), we obtained the same slope value of dP/dT (Table 3.17) as pointed in Figs.3.25 and

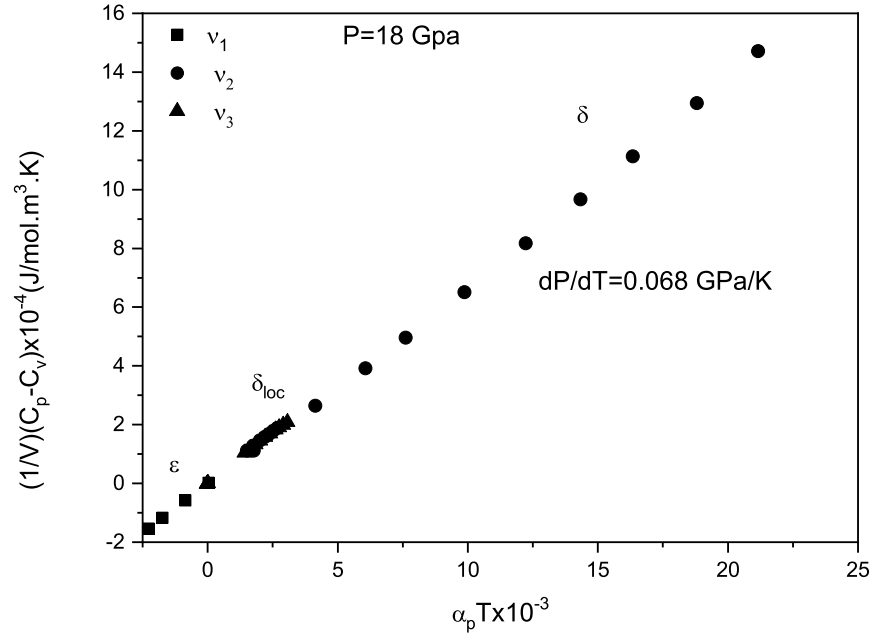


Figure 3.25: $(C_p - C_v)/V$ versus $\alpha_P T$ for the phases of ϵ , δ_{loc} and δ in solid nitrogen according to the Pippard relation (Eq.3.66).

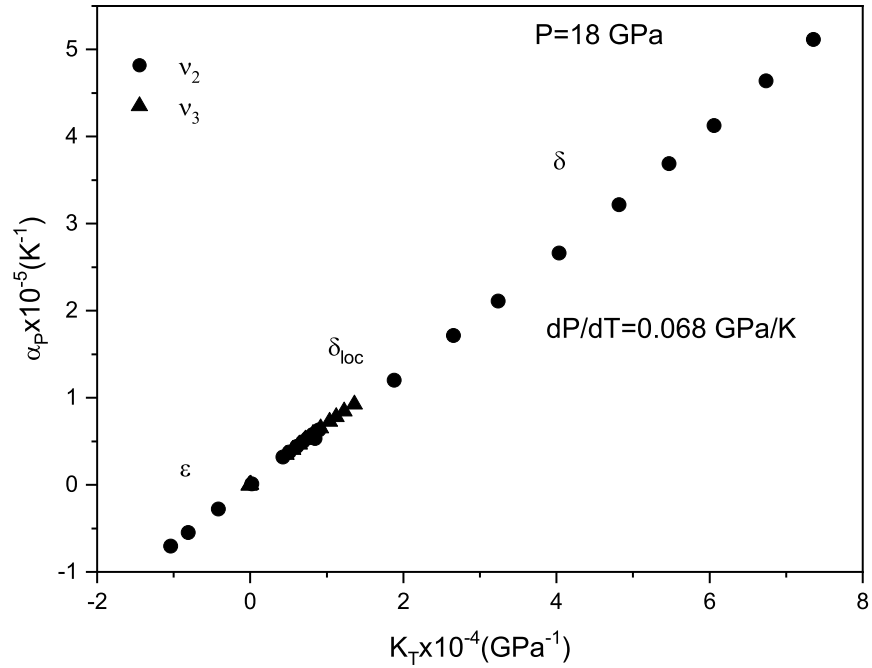


Figure 3.26: Thermal expansion (α_P) versus the isothermal compressibility (κ_T) for the phases of ϵ , δ_{loc} and δ in solid nitrogen according to the Pippard relation (Eq.3.67).

3.26 for the vibrons ν_1 , ν_2 and ν_{22} in the ϵ , δ_{loc} and δ phases of solid nitrogen. By means of the pressure dependence of the isothermal compressibility κ_T , thermal expansion α_P and heat capacity C_p which were calculated, we examined the Pippard

relations (Eqs.3.66 and 3.67) for the fluid-solid transitions [55] and melting curves [94] in nitrogen. First of all, we analyzed the pressure dependence volume data to calculate the isothermal compressibility as a function of pressure

$$V = b_0 + b_1P + b_2P^2 \quad (3.68)$$

Here, the values of coefficients b_0 , b_1 and b_2 were obtained by fitting Eq.3.68 to the observed volume data [56] as given in Table 3.17. Then, we calculated the isothermal

Table 3.17: Values of the fitted parameters according to Eq.3.68 for the fluid-solid transition[53] in nitrogen.

V-P	$b_0 \text{\AA}^3/\text{atom}$	$b_1 \text{\AA}^3/(\text{atom.GPa})$	$b_2 \times 10^{-4}(\text{\AA}^3/\text{atom.GPa}^2)$	Pressure range (GPa)
Eq.3.68	12.41	-0.105	5.29	18.63<P<80.23

compressibility with the definition

$$\kappa_T = -\frac{1}{V} \frac{\partial V}{\partial P_T} \quad (3.69)$$

close to the fluid-solid phase transition in nitrogen. Fig.3.27 represents the isothermal compressibility as a function of pressure for the two different observed V-P data [55, 56] for solid nitrogen. The thermal expansion α_P was calculated via the calculated isothermal compressibility κ_T through Eq.3.63. In this relation, the value of dP/dT was obtained from the observed P-T phase diagrams [55, 94] for nitrogen.

We analyzed the P-T phase diagrams by the quadratic functions expressed as

$$f(T, P) = T - \alpha_1 + \alpha_2P + \alpha_3P^2 = 0 \quad (3.70)$$

Table 3.18: Values of the fitted parameters according to Eq.3.70 for the fluid-solid transition[53] and melting curve[92] in nitrogen.

f(T,P)	$\alpha_1(K)$	$\alpha_2 \times 10^{-2}(K/GPa)$	$\alpha_3 \times 10^{-5}(K/GPa^2)$	Pressure Interval(GPa)
Fluid-Solid transition	265.12	39.99	-0.27	15.9<P<74.3
Melting curve	200.98	3599.0	-	0.2<P<49.7

where α_1 , α_2 and α_3 are constants. By fitting this equation to the two observed T-P data [55, 94], the values of coefficients α_1 , α_2 and α_3 were obtained for the fluid solid transition as given in Table 3.18. For melting curves in nitrogen, because of the

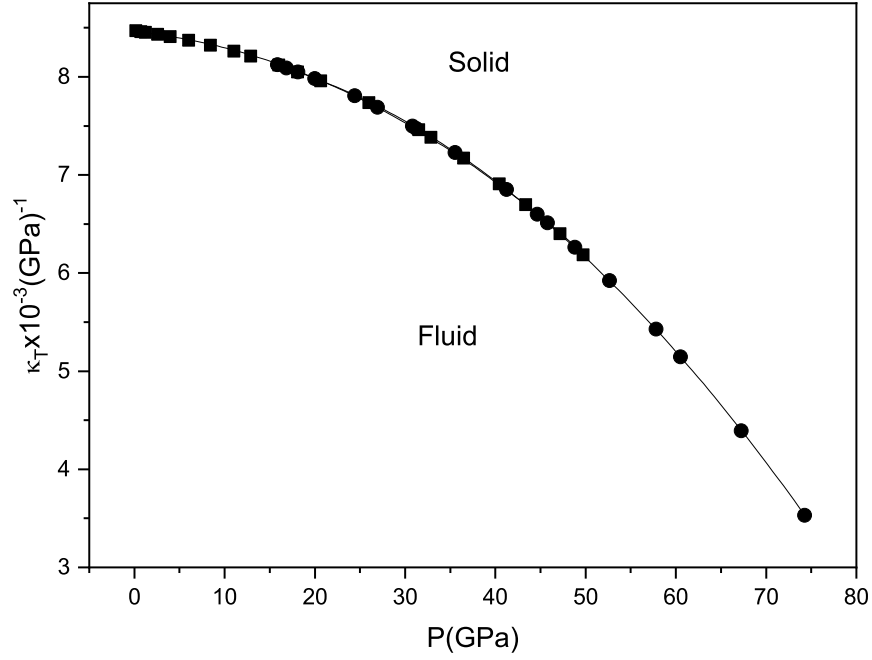


Figure 3.27: Isothermal compressibility (κ_T) at various pressures calculated according to Eq.3.69 for the two different observed V-P data (circle[53] and square[54]).

Table 3.19: Values of the dP/dT and the $(1/V)(dV/dT)$ according to the Pippard relations (Eqs.3.66 and 3.67) for the fluid-solid transition in nitrogen.

Transitions N_2	$dP/dT \times 10^{-3} (\text{GPa}/\text{K})$ Eq.(3.63)	Pressure Interval (GPa)	$dP/dT \times 10^{-3} (\text{GPa}/\text{K})$ Eq.(3.67)	$(1/V)(dV/dT) \times 10^{-4} (\text{K}^{-1})$ Eq.(3.67)	Pressure Interval (GPa)
Fluid-Solid (Calculated)	36	15.85<P<74.26	18	-19.0	24.3<P<48.79
			34	-1.18	52.64<P<74.26
Melting curve (Observed[2])	28.6	0.17<P<49.72	36	0	0.17<P<49.72

linear relationship between temperature and pressure, we found α_3 as zero when we calculated dP/dT value as pointed in Table 3.18. We depicted pressure dependence of thermal expansion α_P according to Eq.3.63 by using observed T-P data of the fluid-solid transition [55] and melting curve [94] in Fig.3.28. Then by using Eq.3.64, we predicted the difference in the heat capacity $C_p - C_v$ as a function of pressure for the fluid-solid transition as given in Fig.3.29. when the κ (Fig.3.27), α_P (Fig.3.28) and $C_p - C_v$ (Fig.3.29). We find that they decrease with increasing pressure. As obtained above, we also obtained linear variation $(C_p - C_v)/V$ with $\alpha_P T$ (Fig.3.30) and α_P with κ_T (Fig.3.31) for the fluid-solid transition. Table 3.19 gives the values of dP/dT obtained from Pippard relations (Figs.3.30 and 3.31) and the experimental values for the fluid-solid transition [94]. When our calculated slope values were compared (

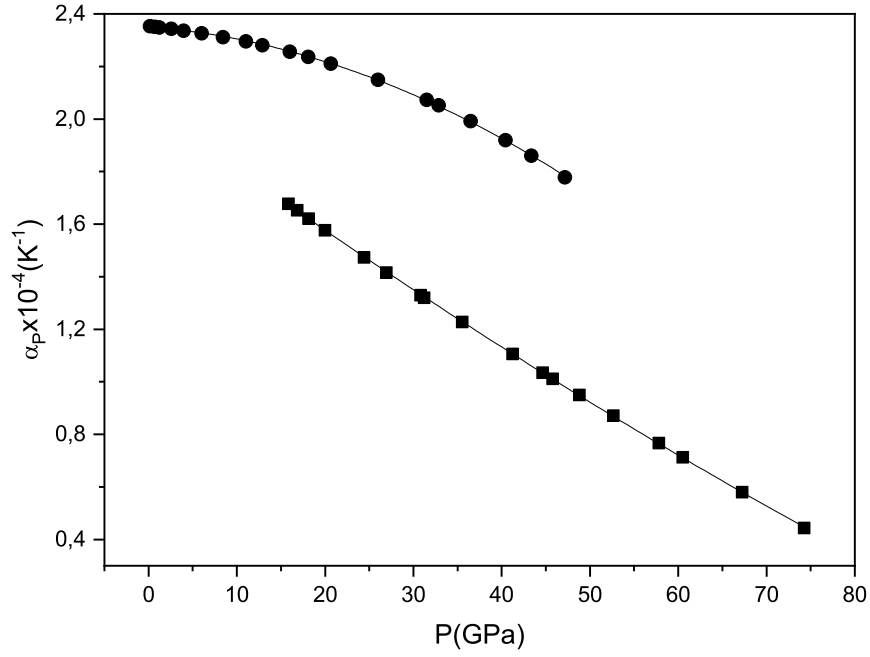


Figure 3.28: Thermal expansion (α_P) at various pressures calculated according to Eq.3.63 for the two different observed T-P data (circle[92] and square[53]).

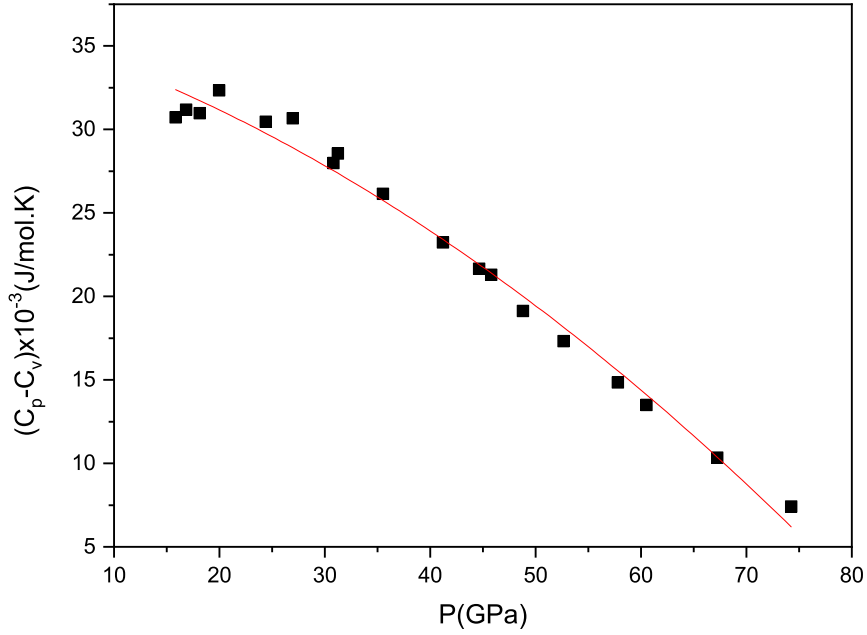


Figure 3.29: Difference in the heat capacity at various pressures calculated according to Eq.(3.64) for the fluid-solid transition in nitrogen.

$36 \times 10^{-3} \text{ GPa/K}$) with the experimental data ($34 \times 10^{-2} \text{ GPa/K}$) ($52.64 < P < 74.26$), we nearly obtained the same value for the fluid-solid transition [55]. For the melting curve, it can also be compared with the observed value of 28.6 GPa/K in the

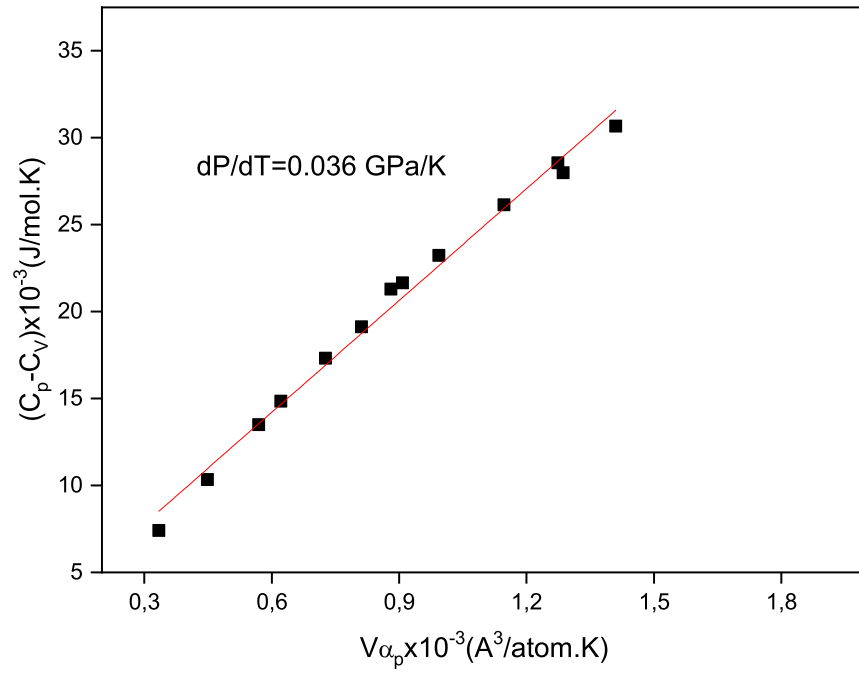


Figure 3.30: $(C_p - C_v)$ versus $V\alpha_P$ as a function of pressures according to the Pippard relation (Eq.3.66).

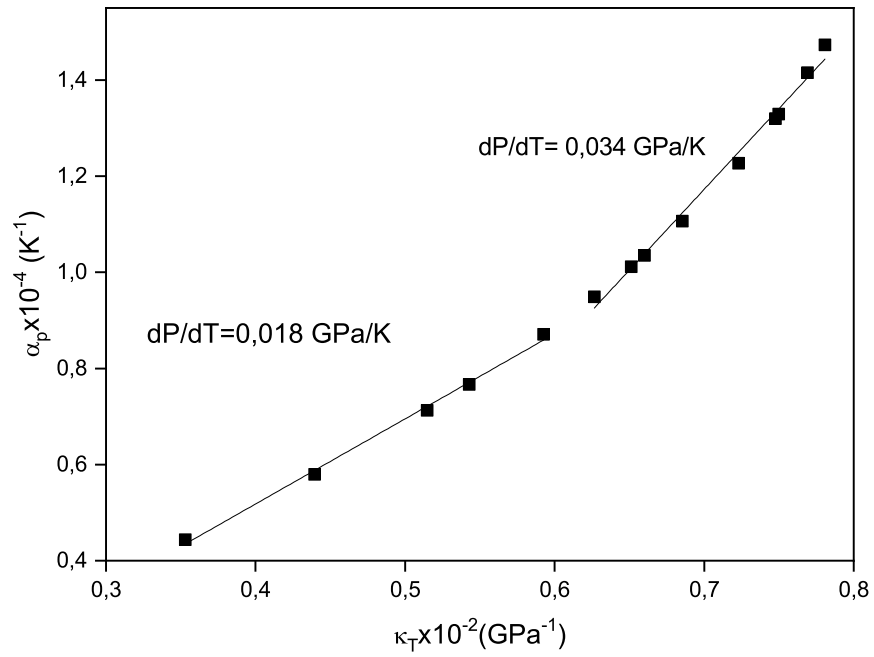


Figure 3.31: Thermal expansion (α_P) versus isothermal compressibility (κ_T) as a function of pressures according to the Pippard relation (Eq.3.67) at two different pressure interval.

pressure interval of $0 < P < 50$ GPa [94]. In the pressure interval $49.72 < P < 71$ GPa, the slope is negative that can be explained with the denser liquid phase than the under-

lying solid [94]. This sharp change of the slope can be evidence of a first order liquid-liquid polymer transition and transition of molecular nitrogen into a chainlike polymeric form [94].

3.6 "Calculation of the Raman frequency and linewidth of vibrons using anharmonic self energy model for the ϵ - δ_{loc} - δ phases in nitrogen."

In this study, we analyzed the Raman frequency shifts and linewidth (FWHM) of the vibrons ν_1, ν_2 and ν_{22} with respect to temperature (P=18 GPa) and also frequency difference ($\nu_1 - \nu_2$) at constant pressures of 13.2, 14.95, 18.5 and 21.2 GPa by the anharmonic self energy model in the ϵ , δ_{loc} (localized δ) and δ phases of solid nitrogen. According to anharmonic self energy, energy shifts can be expressed as a complex , as pointed out in Chapter 2

$$\hbar\Delta\omega(\lambda) = \hbar\Delta(\lambda) - i\hbar\Gamma(\lambda) \quad (3.71)$$

for a mode λ with a particular wavevector and polarization [87,88]. So that the temperature dependence of frequency shift and linewidth of vibrons can be calculated close the phase transitions by using this expression (Eq.3.71). Regarding to Raman frequencies of vibrons ν_1, ν_2 and ν_{22} , Eq.2.46 was fitted to experimental data [23], for the ν_1 , ν_2 and ν_{22} at various temperatures (P=18 GPa) and also the frequency difference ($\nu_1 - \nu_2$) at constant pressures indicated above for the phases of ϵ , δ_{loc} and δ in solid nitrogen. We plot temperature dependence of Raman shift calculated for the vibrons ν_1 (Fig.3.32) and ν_2 and ν_{22} (Fig.3.33) with the observed data [23]. Fig.3.34 gives the frequency shifts ($\nu_1 - \nu_2$) of the Raman vibrons as a function of temperature for the ν_1 and ν_2 in Fig.(3.34) for the phases of ϵ , δ_{loc} and δ at constant pressures (13.2, 14.95, 18.5 and 21.2). Table 3.20 and Table 3.21 represent the fitted parameters of Eq.2.46 (ω_0 , ω_1 and ω_2) for the vibrons ν_1 , ν_2 , ν_{22} and for the frequency difference ($\nu_1 - \nu_2$), respectively, in the phases of ϵ , δ_{loc} and δ in solid nitrogen.

As observed experimentally [23], we found decrease of the Raman frequency of vibron ν_1 with increasing temperature at 18.5 GPa in the phases of ϵ , δ_{loc} and δ (Fig.3.32). The Raman frequency of vibrons ν_2 and ν_{22} increase with the increas-

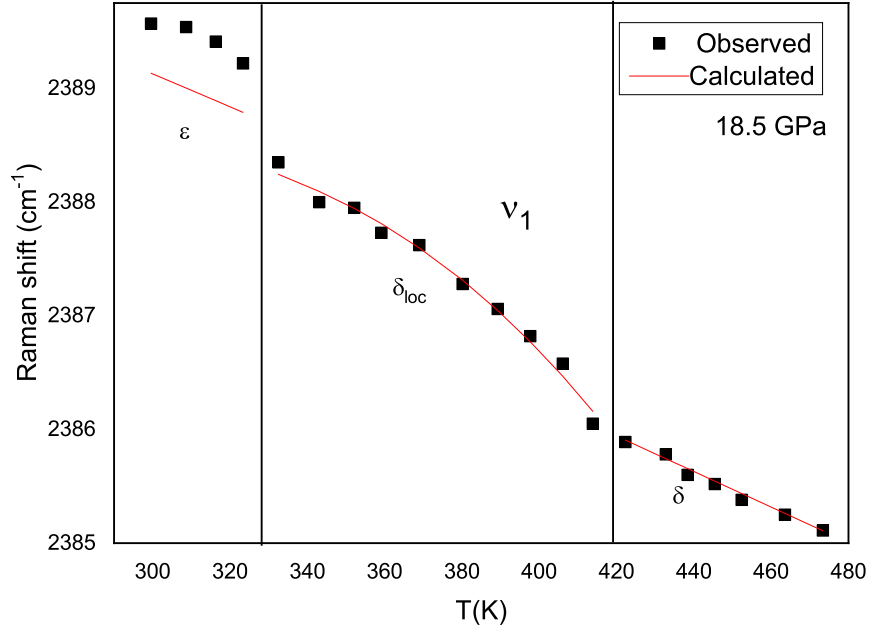


Figure 3.32: Temperature dependence of the Raman frequency for the vibron ν_1 as a function of temperature ($P=18.5$ GPa) according to Eq.2.46 which was fitted to the experimental data [23] for the phases of ϵ , δ_{loc} and δ in the solid nitrogen.

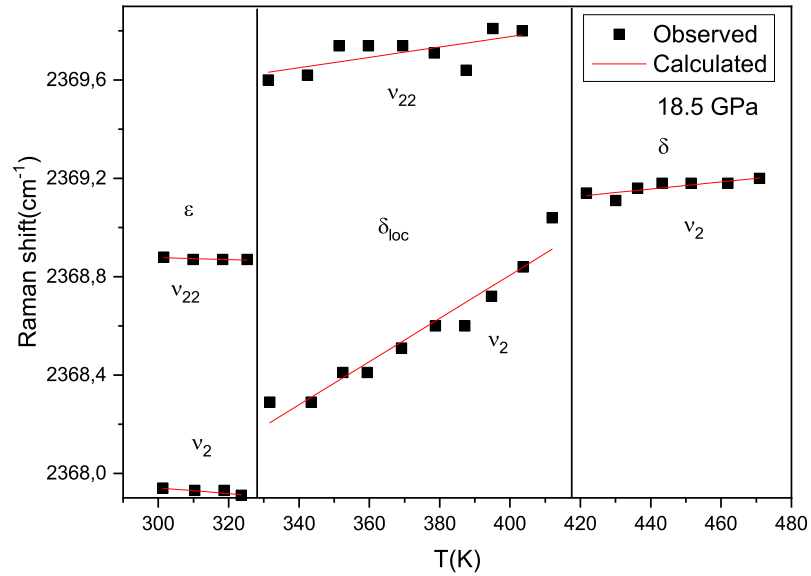


Figure 3.33: Temperature dependence of the Raman frequency for the vibrons ν_2 and ν_{22} as a function of temperature ($P=18.5$ GPa) according to Eq.2.46 which was fitted to the experimental data [23] for the phases of ϵ , δ_{loc} and δ in the solid nitrogen.

ing temperature in the δ phase while they are independent of the temperature in the ϵ phase as shown in Fig.3.33. Similar behavior of decreasing ν_1 with increasing tem-

Table 3.20: Values of the parameters for the Raman frequencies of the vibrons ν_1 , ν_2 and ν_{22} according to Eq.2.46 by using the observed data [23] within the temperature intervals indicated for the phases of ϵ , δ_{loc} and δ (P=18 GPa) in solid nitrogen.

Vibron modes	Phases	$\omega_1(cm^{-1})$	$\omega_2(cm^{-1})$	$\omega_0(cm^{-1})$	Temperature Interval(K)
ν_1	ϵ	2393.61	-0.80	55.03	298.9<T<325.5
	δ_{loc}	2388.76	-1912.74	2732.47	327.3<T<407.1
	δ	2392.48	-0.05	3.20	423.1<T<477.5
ν_2	ϵ	2367.99	-18.62	1777.37	301.3<T<323.6
	δ_{loc}	2365.35	0.13	15.05	332.6<T<413.6
	δ	2368.52	0.003	1.95	423.4<T<472.8
ν_{22}	ϵ	2368.99	-0.01	25.6	301.6<T<325.2
	δ_{loc}	2368.97	0.04	17.57	331.3<T<411.78

Table 3.21: Values of the parameters for the frequency difference ($\nu_1-\nu_2$) of the Raman internal modes ν_1 and ν_2 according to Eq.2.46 by using the observed data [23] within the temperature intervals at constant pressures indicated for the phases of ϵ , δ_{loc} and δ in the solid nitrogen.

Pressures	Phases	$\omega_1(cm^{-1})$	$-\omega_2(cm^{-1})$	$\omega_0(cm^{-1})$	Temperature Interval(K)
13.2	δ	18.56	0.04	2.88	342.06<T<384.71
	δ_{loc}	30.08	0.10	2.08	300.88<T<333.24
14.95	δ	21.09	0.08	4.83	367.06<T<442.06
	δ_{loc}	30.03	0.08	1.98	304.56<T<358.97
18.5	δ	24.70	0.08	4.13	425.15<T<472.20
	δ_{loc}	32.74	0.08	2.20	321.47<T<425.15
	ϵ	21.91	4282.16	2919.59	300.15<T<323.68
21.2	δ	29.66	0.09	3.70	459.71<T<489.85
	δ_{loc}	36.18	0.09	2.42	352.35<T<451.62
	ϵ	24.14	142.20	1790.64	302.35<T<371.47

perature, was observed in the frequency difference ($\nu_1-\nu_2$) at constant pressures (13.2, 14.95, 18.5 and 21.2 GPa) (Fig.3.34) since frequency of the vibron ν_2 is constant in the phases of ϵ and δ in solid nitrogen. It has been indicated that when the pressure increases in the ϵ , δ_{loc} and δ phases of solid nitrogen, the magnitude of the frequency difference ($\nu_1-\nu_2$) increases with increasing temperature (Fig.3.34). As a second or-

der transition associated with changes in the orientational behavior of N_2 molecules from a free rotation into orientationally located mode, it has been stated that an abnormal behavior of the vibration frequency shift occurs with decreasing temperature in the δ phase of nitrogen [23]. This anomalous behavior can give softening of some of the intermolecular vibrations [49, 92] that can be either caused by the weakening of intramolecular bonding or increased vibrational coupling [41]. On the basis of increasing intermolecular interactions, vibrational splitting can occur as observed for the internal mode ν_2 which splits into a ν_{22} internal mode in the ϵ and δ_{loc} phases of solid nitrogen (Fig.3.33). Our calculations for the temperature dependent Raman frequencies follow the same trend as observed values except the change of Raman frequencies of the ν_1 vibron between the δ_{loc} and ϵ phases at 18.5 GPa (Fig.3.32). The nitrogen molecules are orientated in the ordered ϵ phase when compared to the partially ordered δ_{loc} and disordered δ phases. Hence, this unexpected behavior of the ν_1 vibron between the δ_{loc} and ϵ phases at 18.5 GPa may occur due to the orientation-vibron coupling. On this basis, the anharmonic self energy model is insufficient with strong orientation-vibron coupling for the ν_1 internal mode in the ϵ phase in N_2 . By using anharmonic self energy model, the temperature dependence of linewidths (FWHM) $\Gamma(\lambda)$ was calculated for the ν_1 , ν_2 and ν_{22} vibrons and also for the ν_1 - ν_2 of the modes ν_1 and ν_2 of the phases ϵ , δ_{loc} and δ in N_2 . For this calculation, Eq.2.47 was fitted to the experimental FWHM data taken from the literature [23]. The value of coefficients ($\Gamma_1(\lambda)$, $\Gamma_2(\lambda)$ and ω') (Eq.2.47) are represented for the ν_1 , ν_2 and ν_{22} vibrons at 18 GPa and frequency difference (ν_1 - ν_2) at constant pressures (13.2, 14.95, 18.5 and 21.2 GPa) in Table3.22 and Table3.23, respectively, within the temperature intervals.

We give our calculated FWHM values as a function of temperature according to Eq.2.47 in Fig.3.35 for the vibrons ν_1 , ν_2 and ν_{22} (P=18.5GPa) and in Fig.3.36 for the frequency difference (ν_1 - ν_2) (P= 13.2, 14.95, 18.5 and 21.2 GPa) with the observed data [23] for the phases of ϵ , δ_{loc} and δ in solid nitrogen. FWHM of the ν_1 internal mode increases as the temperature increase in the phases of ϵ , δ_{loc} and δ and also the same behavior is observed for the ν_1 vibron in ϵ , δ_{loc} phases except the ν_2 in the δ phase where the FWHM decreases with the increasing temperature as shown in Fig.3.35. In the case of the ν_{22} , its FWHM increases in δ_{loc} while it remains nearly constant in the ϵ phase of solid nitrogen. As shown in Fig.3.36, we obtained the same

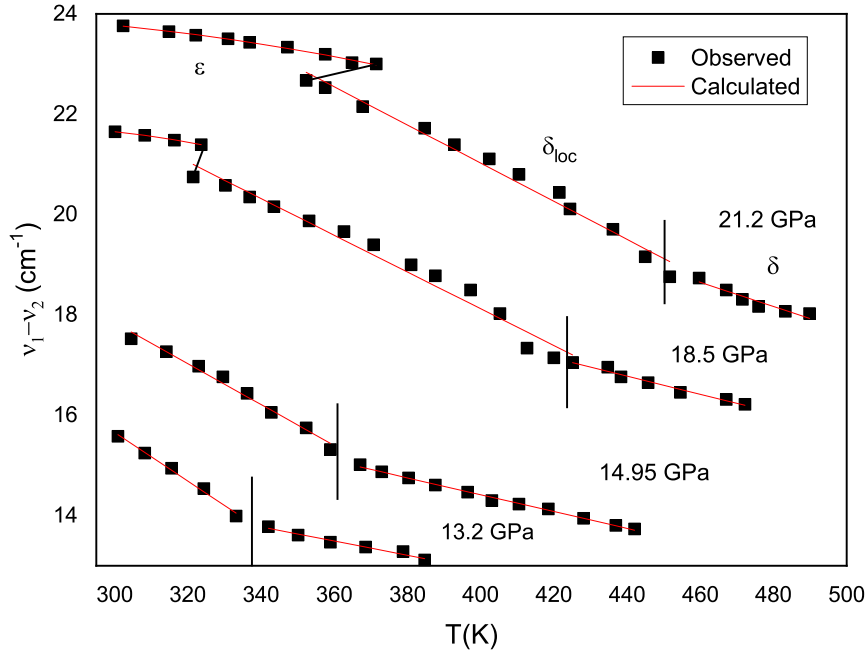


Figure 3.34: Temperature dependence of the Raman frequency shifts ($\nu_1-\nu_2$) for the Raman internal modes ν_1 and ν_2 as a function of temperature at constant pressures according to Eq.2.46 which was fitted to the experimental data [23] for the phases of ϵ , δ_{loc} and δ in the solid nitrogen.

Table 3.22: Values of the parameters for the linewidths, of the vibrons ν_1 , ν_2 and ν_{22} according to Eq.2.47 by using the observed data [23] within the temperature intervals indicated for the phases of ϵ , δ_{loc} and δ (P= 18 GPa) in solid nitrogen.

Vibron modes	Phases	$\Gamma_1(\lambda)(cm^{-1})$	$\Gamma_2(\lambda)(cm^{-1})$	$\omega'(cm^{-1})$	Temperature Interval(K)
ν_1	ϵ	-0.17	0.01	4.33	298.9<T<325.5
	δ_{loc}	-1.61	0.01	1.06	327.3<T<407.1
	δ	-1.41	0.08	9.38	423.1<T<477.5
ν_2	ϵ	-0.26	0.01	2.43	301.3<T<323.6
	δ_{loc}	-0.32	0.01	2.43	332.6<T<413.6
	δ	1.83	-0.03	23.59	423.4<T<472.8
ν_{22}	ϵ	0.62	-0.01	10.10	301.6<T<325.2
	δ_{loc}	-	-	-	-
	δ	-	-	-	-

picture for the FWHM of the ν_1 mode for the FWHM of the frequency difference ($\nu_1-\nu_2$) of the ν_1 and ν_2 at constant pressures in the ϵ , δ_{loc} and δ phases. Its magnitude increases as the pressure increases. There is a good agreement between our fits and

Table 3.23: Values of the parameters for the linewidths, of the frequency difference ($\nu_1 - \nu_2$) of the Raman internal modes ν_1 and ν_2 according to Eq.2.47 by using the observed data [23] within the temperature intervals at constant pressures indicated for the phases of ϵ , δ_{loc} and δ in the solid nitrogen.

Pressures	Phases	$\Gamma_1(\lambda)(cm^{-1})$	$\Gamma_2(\lambda)(cm^{-1})$	$\omega'(cm^{-1})$	Temperature Interval(K)
13.2	δ	0.12	2.38×10^{-3}	3.11	342.06<T<384.71
	δ_{loc}	-2.02	3.35×10^{-3}	0.47	300.88<T<333.24
14.95	δ	-1.40	0.013	2.35	367.06<T<442.06
	δ_{loc}	-1.10	1.92	226.1	304.56<T<358.97
18.5	δ	0.07	4.57×10^{-5}	526.0	425.15<T<472.20
	δ_{loc}	-2.21	-2.04	-1538.94	321.47<T<425.15
	ϵ	-2.09	16.92	423.73	300.15<T<323.68
21.2	δ	0.66	0.94	729.2	459.71<T<489.85
	δ_{loc}	-0.24	0.92	477.68	352.35<T<451.62
	ϵ	-0.24	1.57×10^{-5}	0.01	302.35<T<371.47

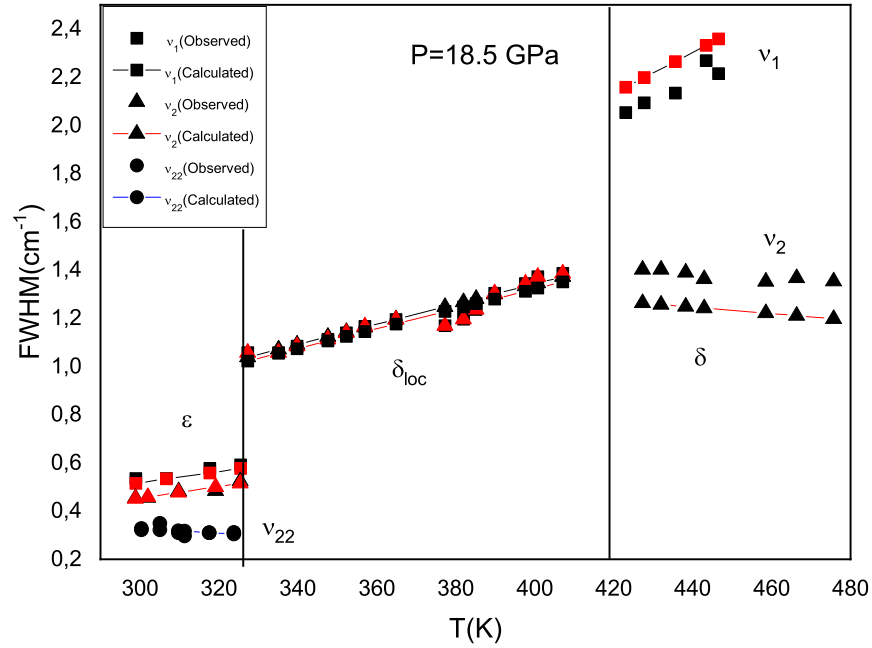


Figure 3.35: Temperature dependence of the linewidths for vibrons ν_1 , ν_2 and ν_{22} as a function of temperature (P=18.5 GPa) according to Eq.2.47 which was fitted to the experimental data [23] for the phases of ϵ , δ_{loc} and δ in the solid nitrogen.

the experimental linewidth at constant pressures [23]. However, in Figs.3.35 and 3.36, our fits were not compatible for the difference in FWHM of the corresponding fre-

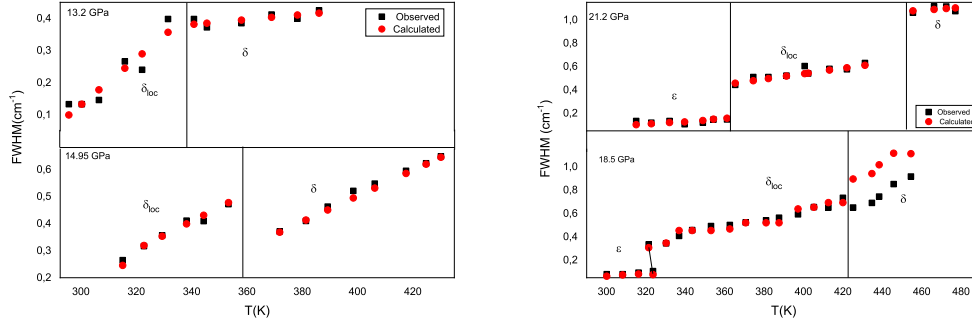


Figure 3.36: Temperature dependence of the difference in the linewidths for the corresponding to the frequency difference ($\nu_1 - \nu_2$) of vibrons ν_1 and ν_2 as a function of temperature at four constant pressures indicated according to Eq.2.47 which was fitted to experimental data [23] for the phases of ϵ , δ_{loc} and δ in the solid nitrogen.

quency difference ($\nu_1 - \nu_2$) of the ν_1 and ν_2 internal modes at 18.5 GPa in the δ phase of solid nitrogen.

3.7 "Calculation of the inverse relaxation time and the activation energy as a function of temperature for the Raman modes close to the phase transitions in solid nitrogen."

The inverse relaxation time τ^{-1} as a function of temperature was calculated for the α - β transition ($P=0$) and ϵ - δ_{loc} - δ transitions at constant pressures in solid nitrogen. On that basis, we used the observed data from the literature for the Raman frequencies and linewidths for the E_g librational mode (α - β) [88] and the ν_1 and ν_2 vibrons (ϵ - δ_{loc} - δ) in the nitrogen [23]. The inverse relaxation time was able to be calculated via the Eq.3.72 expressed as

$$\tau^{-1} = \nu^2 / \Gamma \quad (3.72)$$

where ν is the frequency and Γ is the linewidths of a vibrational mode. Fig.3.37 and Fig.3.38 gives the inverse relaxation time as a function of temperature for the librational E_g mode ($P=0$) in the α phase and the internal modes ν_1 and ν_2 ($P=18$ GPa) in the phases of ϵ , δ_{loc} and δ , respectively. We also predicted also activation energy E_a by using calculated relaxation time for the E_g librational mode [88] and the ν_1 and ν_2 vibrons [23] in solid nitrogen. For this calculation, the relaxation time

was investigated through the Arrhenious law (in the logarithmic form) defined as

$$\ln\tau = \ln\tau_0 - E_a/k_B T \quad (3.73)$$

Here, τ_0 is the attempt relaxation time and k_B is the Boltzmann constant. We extracted the values of the activation energy from Eq.3.73 by taking the linear fit of the $-\ln\tau$ vs. $1/T$ for the E_g mode in the α phase (Fig.3.39) and for the Raman modes ν_1 and ν_2 (P=18GPa) (Fig.3.40) in the phases of ϵ , δ_{loc} and δ . The values of the attempt relaxation time τ_0 and k_B are given in Table3.24 for the E_g mode and Table 3.25 for the internal modes ν_1 and ν_2 in solid nitrogen. We also predicted inverse relaxation time (τ^{-1}) by using observed Raman frequency and damping constant (linewidth) via the Eq.3.72 for the frequency difference ($\nu_1 - \nu_2$) of the internal modes ν_1 and ν_2 at constant pressures (13.2, 14.95 and 21.2 GPa) in solid nitrogen [28]. We gave the inverse relaxation time as a function of temperature for the frequency differences $\nu_1 - \nu_2$ in Figs.3.41(a) (P=13.2 GPa) ,3.41(b) (P=14.95 GPa) and 3.41(c)(P=21.2 GPa) in the phases of ϵ , δ_{loc} and δ in solid nitrogen. As before, the time dependent activation energy E_a was obtained by the means of Eq.3.73 for the $\nu_1 - \nu_2$ within the temperature interval. The values of E_a and τ_0 (attempt relaxation time) due to the $\nu_1 - \nu_2$ of the internal modes ν_1 and ν_2 which were obtained from the linear fit of the $-\ln\tau$ vs ($1/T$) (Fig.3.42) are given in Table 3.26. The inverse relaxation time τ^{-1} decreases in a smooth manner with the temperature for the E_g mode in the α phase at P=0 (Fig.1) however, there is a sharp decrease in τ^{-1} towards ϵ phase to δ_{loc} phase at 18 GPa for the internal modes ν_1 and ν_2 (Fig.3.38) which represents the order-disorder transition in N_2 . From Fig.3.38, this sharp decrease softens in the δ_{loc} phase even in δ phase and the τ^{-1} is nearly independent of the temperature at P=18 GPa. In the case of τ^{-1} of the frequency differences ($\nu_1 - \nu_2$), while at 13.2 GPa and 14.95 GPa, it decreases with the increasing temperature for δ_{loc} and δ phases, in the ϵ phase the τ^{-1} increases with the temperature, then remains almost constant in the phases of δ_{loc} and δ phases at 21.2 GPa (Fig.3.41) in solid nitrogen.

We are able to approximate damping constant (FWHM) as a function of temperature by

$$\Gamma(FWHM) = A + BT + Cexp(-E_a/k_B T) \quad (3.74)$$

where A,B and C are the coefficients. The coefficient A depends on the structural and compositional defects, the linear BT term represents the influence of phonon-phonon

Table 3.24: Values of the activation energy (E_a) and the attempt relaxation time (τ_0), which were extracted from Eq.3.73 for the E_g librational mode [86] in the solid nitrogen (P=0).

Raman mode	$\tau_0(s)$	$E_a \times 10^{-21}(J/mol)$	$E_a \times 10^{-4}(eV/mol)$	Temperature Interval(K)
E_g	5.61	1.03	64.4	5.01<P<38.57

Table 3.25: Values of the activation energy (E_a) and the attempt relaxation time (τ_0), which were extracted from Eq.3.73 for the internal modes of ν_1 , ν_2 and ν_{22} in the solid nitrogen (P=18 GPa).

Raman modes	Phases	$\tau_0(s)$	$E_a \times 10^{-21}(J/mol)$	$E_a \times 10^{-4}(eV/mol)$	Temperature Interval(K)
ν_1	ϵ	3.62	5.65	353.1	298.92<T<325.47
	δ_{loc}	16.2	8.89	555.6	338.40<T<418.38
	δ	14.8	8.26	516.2	423.06<T<443.06
ν_2	ϵ	2.50	4.63	289.4	298.87<T<325.44
	δ_{loc}	4.47	4.04	252.5	327.30<T<407.07
	δ	1.36	-3.56	-222.5	427.36<T<475.70
ν_{22}	ϵ	0.025	-0.14	-8.75	300.35<T<323.75

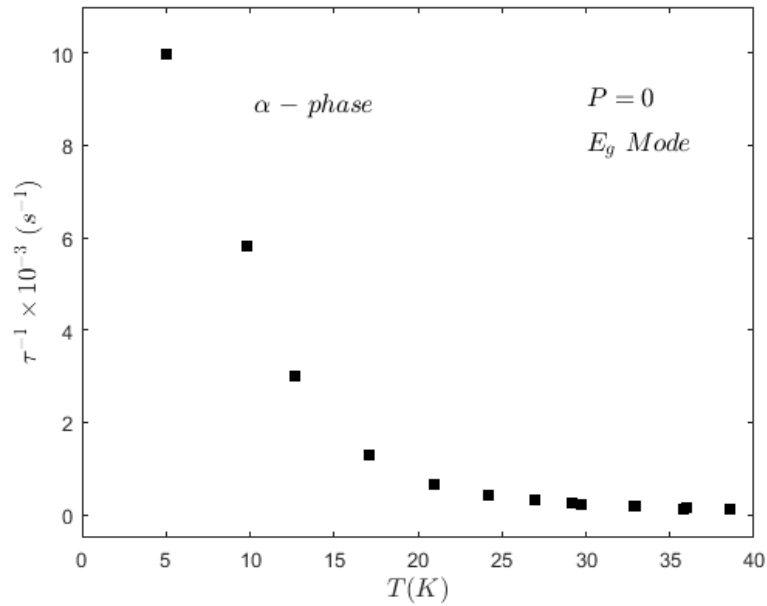


Figure 3.37: Temperature dependence of the inverse relaxation time (τ^{-1}) calculated according to Eq.3.72 for the E_g mode of solid nitrogen (α phase, P=0) by using the observed data [86].

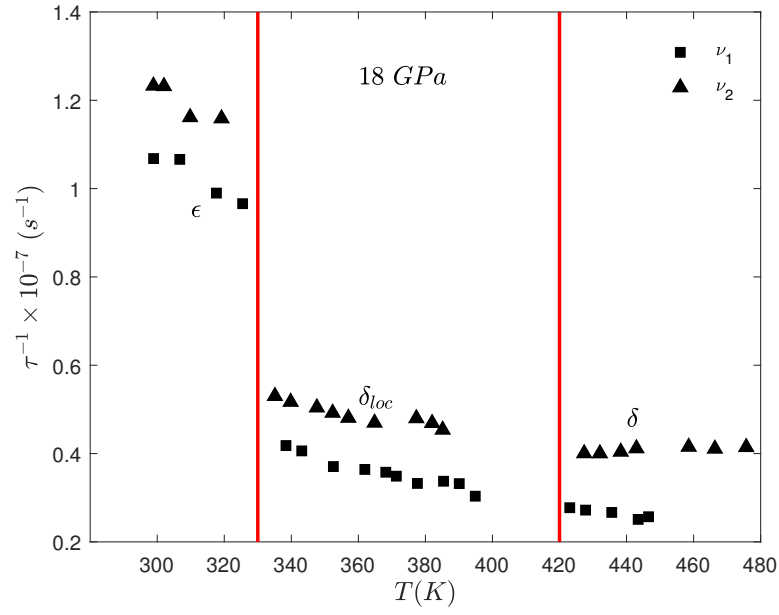


Figure 3.38: The temperature dependence of the inverse relaxation time (τ^{-1}) calculated according to Eq.3.72 for the ν_1 and ν_2 modes for the ϵ , δ_{loc} and δ phases in N_2 (P=18 GPa) by using the observed data [23]. Vertical lines denote the phase boundaries (at T_c) between the two phases.

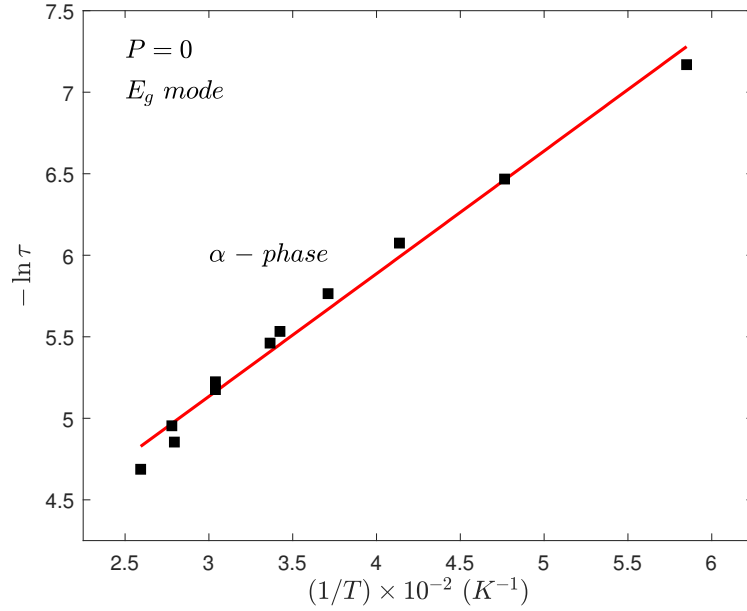


Figure 3.39: Relaxation time (logarithmic) as a function of the inverse temperature for the E_g mode according to Eq.3.73 in the solid nitrogen (α phase, P=0). Solid line represents the best fit (Eq.3.73) to the values given.

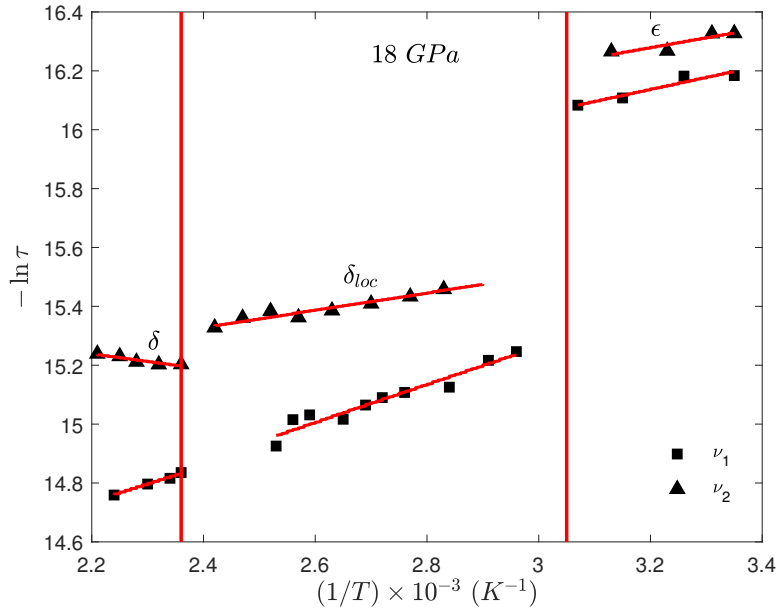


Figure 3.40: Relaxation time (logarithmic) as a function of the inverse temperature for the ν_1 and ν_2 modes according to Eq.3.73 in the N_2 (ϵ , δ_{loc} and δ phases, $P=18$ GPa). Vertical lines denote the phase boundaries (at T_c) between the two phases.

anharmonic interactions and the exponential term with the coefficient C describes the thermally activated reorientational processes. We predicted the coefficient A, B, C and the activation energy E_a by fitting Eq.(3.74) to the observed data for the E_g mode [88] in the α phase and ν_1 , ν_2 and ν_{22} modes (18 GPa) in the ϵ , δ_{loc} and δ phases [23] in the solid nitrogen. Table 3.27 gives the estimated values of A, B, C and the E_a within the temperature intervals indicated in solid nitrogen. The values of A, B, C and the E_a are given in Table 3.28 for the $(\nu_1 - \nu_2)$ at constant pressures (13.2, 14.95 and 21.2 GPa) in the ϵ , δ_{loc} and δ phases in N_2 . We plot the linewidth data with respect to temperatures through Eq.3.74 for the E_g mode at $P=0$ (Fig.3.43), for the ν_1 , ν_2 and ν_{22} vibrons at 18 GPa (Fig.3.44) and for the frequency differences $(\nu_1 - \nu_2)$ at the pressures of 13.2, 14.95 and 21.2 GPa (Fig.3.45) in solid nitrogen.

Corresponding to the temperature dependent damping constant (linewidth), as expected, calculated linewidth Γ increases as the temperature increases for the E_g mode in the α phase (Fig.3.43), for the ν_1 and ν_2 modes $P=18$ GPa and for the $\nu_1 - \nu_2$ at the pressures of 13.2, 14.95 and 21.2 GPa with the exception of the ν_2 mode at 18 GPa (Fig.3.44) and the frequency difference $\nu_1 - \nu_2$ at 21.2 GPa (Fig.3.45) in the δ phase. Linewidths decrease with temperature in solid nitrogen

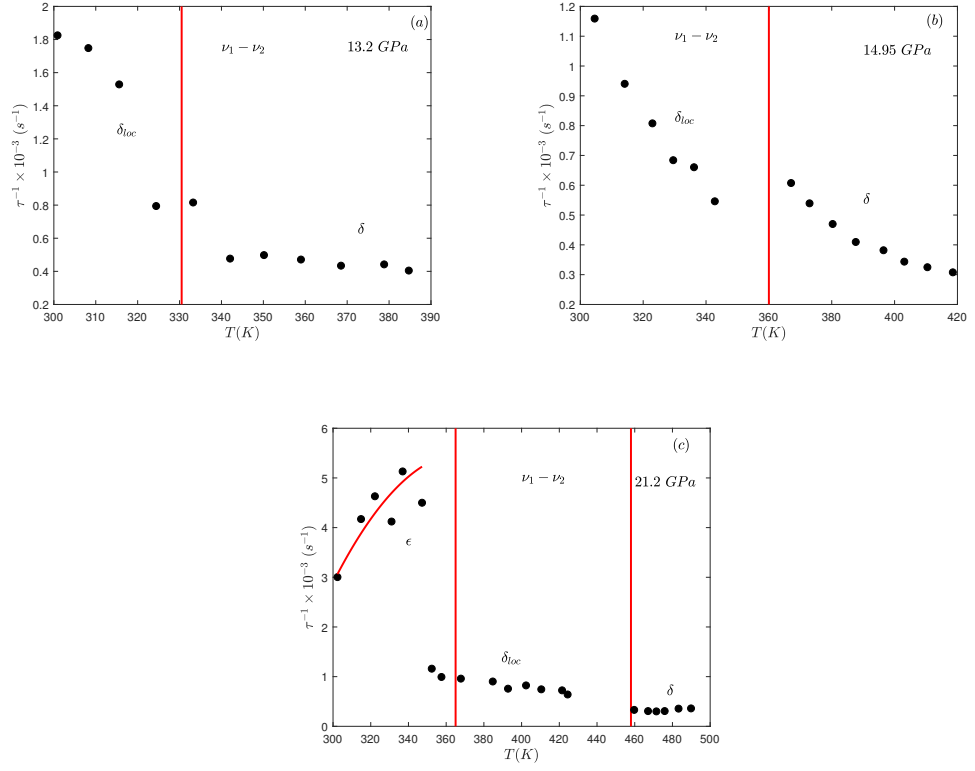


Figure 3.41: Temperature dependence of the inverse relaxation time (τ^{-1}) calculated according to Eq. (3.73) for the frequency shifts $\nu_1 - \nu_2$ of the internal modes ν_1 and ν_2 by using the observed Raman frequency and FWHM data[23] at constant pressures indicated in the solid nitrogen. In the ϵ phase (c), solid line is the best fit (Eq.3.72) to the τ^{-1} values. Vertical lines denote the phase boundaries (at T_c) between the two phases.

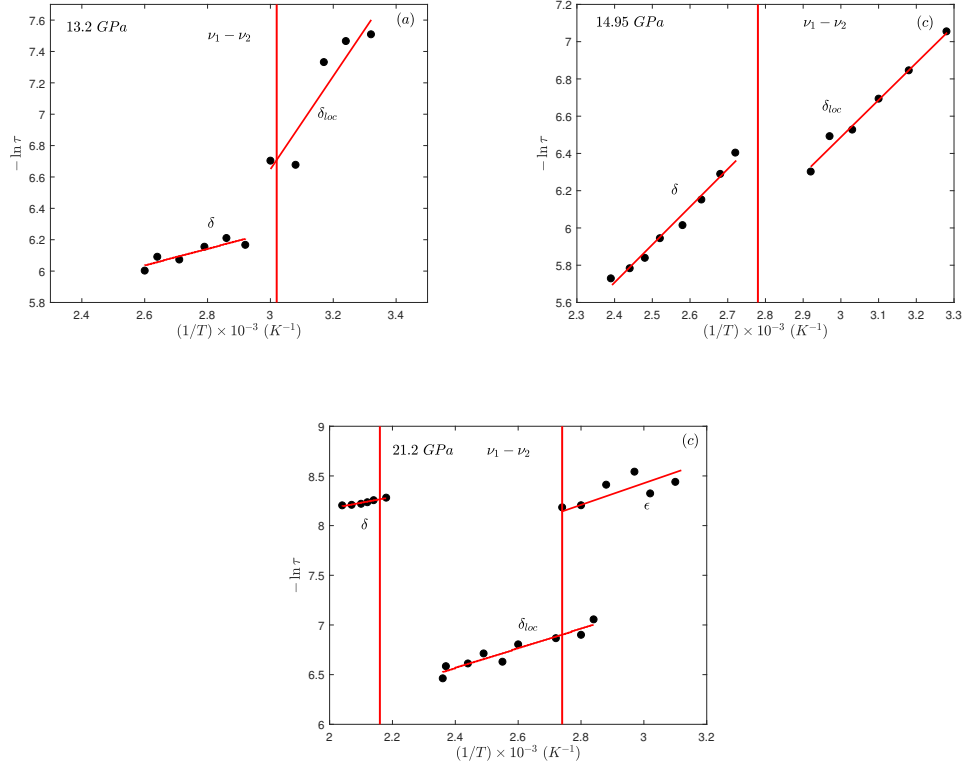


Figure 3.42: Relaxation time (logarithmic) as a function of the inverse temperature for the difference in the frequency shifts ($\nu_1 - \nu_2$) of the internal modes ν_1 and ν_2 by using the observed Raman frequency and FWHM data [23] according to Eq.(3.73) at constant pressures indicated in the solid nitrogen. Solid lines represent the best fit (Eq.3.74) to the values. Vertical lines denote the phase boundaries (at T_c) between the two phases.

Table 3.26: Values of the activation energy (E_a) and the attempt relaxation time (τ_0), which were extracted from Eq.3.74 for the difference in the frequency shifts ($\nu_1 - \nu_2$) of the Raman internal modes ν_1 and ν_2 within the temperature intervals for the phases at constant pressures indicated in N_2 by using the observed frequency and linewidth data [23].

Pressures	$(\nu_1 - \nu_2)$	$\tau_0 \times 10^{-3} (s)$	$E_a \times 10^{-21} (J/mol)$	$E_a \times 10^{-4} (eV/mol)$	Temperature Interval(K)
13.2	δ_{loc}	10170	0.41	25.6	295.60<T<331.49
	δ	9.4	7.28	455.0	340.85<T<386.10
14.95	δ_{loc}	570	0.27	16.9	315.09<T<362.95
	δ	440	0.37	23.1	371.86<T<430.13
21.2	ϵ	1.93	9.94	621.2	315.13<T<361.26
	δ_{loc}	15.1	0.14	8.75	365.34<T<431.23
	δ	0.93	8.19	511.9	455.53<T<480.26

Table 3.27: Values of the activation energy (E_a) with the coefficients A,B and C which were extracted by fitting (Eq.3.74) to the observed FWHM for the E_g mode at P=0 [86] and for the internal modes of ν_1 , ν_2 and ν_{22} at P=18 GPa [23] within the temperature intervals indicated in the solid nitrogen.

Raman modes	Pressures (GPa)	Phases	A (cm^{-1})	B $\times 10^{-2}$ (cm^{-1}/K)	C (cm^{-1})	$E_a \times 10^{-21}$ (J/mol)	$E_a \times 10^{-4}$ (eV/mol)	Temperature Interval(K)
E_g	0	α	-0.27	6.0	121.58	1.46	91.2	5.01<T<38.57
ν_1	18	ϵ	-0.65	-4.0	34.21	4.15	259.4	298.92<T<325.47
		δ_{loc}	-1.04	0.3	6.22	6.93	433.1	338.40<T<418.38
		δ	-1.40	1.0	1.28	6.68	417.5	423.06<T<443.06
ν_2	18	ϵ	0.04	-2.0	15.89	4.38	273.2	298.87<T<325.44
		δ_{loc}	1.41	2.0	-13.53	3.70	237.2	327.30<T<407.07
		δ	0.18	-0.4	5.27	-3.05	-190.6	427.36<T<475.70
ν_{22}	18	ϵ	3.03	-0.06	-2.62	-0.18	-11.2	300.35<T<323.75

similar anomalous decreasing of τ^{-1} (Fig.3.38), FWHM increases drastically for the for the ν_1 and ν_2 internal modes at 18 GPa (Fig.3.44) from the ϵ to the δ_{loc} phase in nitrogen. As stated above, we deduced activation energy E_a by using Eq.3.73 for the E_g mode (Table 3.24), for the ν_1 and ν_2 vibrons (Table 3.25) and by using Eq.3.74 as given in Table 3.27. When compared the these two E_a values, there is a inconsistent between the two results as expected, and the E_a values extracted from Eq.3.74 is more reliable because there is a phonon-phonon anharmonic interactions (BT term) on the basis of Eq.3.74 and it also depends on the structural and compositional defects (A

Table 3.28: Values of the activation energy E_a with the coefficients A,B and C which were extracted from Eq.3.74 by fitting to the observed FWHM data [23] for the difference in the frequency shifts ($\nu_1 - \nu_2$) of the Raman internal modes ν_1 and ν_2 at constant pressures within the temperature intervals indicated in the solid nitrogen.

Pressures (GPa)	Phases	A (cm^{-1})	B $\times 10^{-2}$ (cm^{-1}/K)	C (cm^{-1})	$E_a \times 10^{-21}$ (J/mol)	$E_a \times 10^{-4}$ (eV/mol)	Temperature Interval(K)
13.2	δ_{loc}	27.10	4.0	-55.28	1.27	79.4	295.60<T<331.49
	δ	0.82	-0.5	6.27	7.51	469.4	340.85<T<386.10
14.95	δ_{loc}	2.22	0.5	-3.59	0.24	15.0	315.09<T<362.95
	δ	2.58	0.6	-4.54	0.36	22.5	371.86<T<430.13
21.2	ϵ	18.80	-12.0	139.74	8.85	553.1	315.13<T<361.26
	δ_{loc}	2.42	0.2	-2.96	0.12	7.5	365.34<T<431.23
	δ	8.73	-7.0	81.31	8.06	503.7	455.53<T<480.26

term) as pointed out above. Similarly, Table 3.26 and Table 3.28 gave the estimated E_a values via the Eqs.3.73 and 3.74, respectively, for the frequency difference $\nu_1 - \nu_2$ at constant pressures within the temperature intervals in the ϵ , δ_{loc} and δ phases of N_2 . When we examined the values of the activation energy E_a in the phase transition, E_a values of the ν_1 (ν_2) increase (decrease) at the transitions from the ordered to the disordered phases (ϵ - δ_{loc} - δ) for the internal modes ν_1 and ν_2 even E_a of the ν_2 gets negative value in the δ phase (Table 3.25 and 3.27). Also the E_a values of the frequency difference $\nu_1 - \nu_2$ for the transitions of δ_{loc} - δ increase at 13.2 and 14.95 GPa except the order-disorder transition at 21.2 GPa (Table 3.26). This is correlated with the behavior of the inverse relaxation time τ^{-1} that decreases for the ν_1 and ν_2 modes as the temperature increases at 18 GPa (Fig.3.38) and also for the $\nu_1 - \nu_2$ at the pressures of 13.2 and 14.95 GPa (for the δ_{loc} - δ transition) except the ϵ phase at 21.2 GPa (Fig.3.41). For the E_g mode, increasing damping constant (FWHM) is accompanied with the decreasing of the τ^{-1} in the α phase of solid nitrogen.

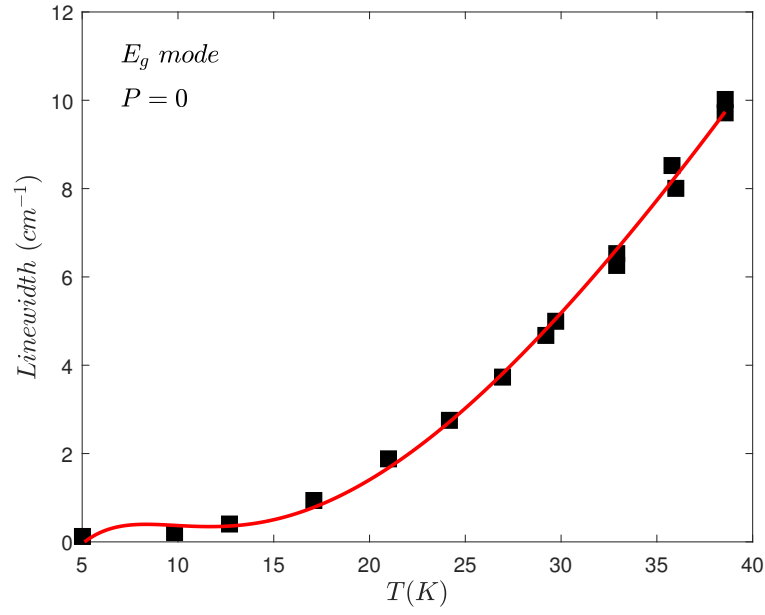


Figure 3.43: Temperature dependence of the linewidth of the E_g line of the α phase ($P=0$) in N_2 . Solid line represents best fit (Eq.3.74) to the experimental data [86].

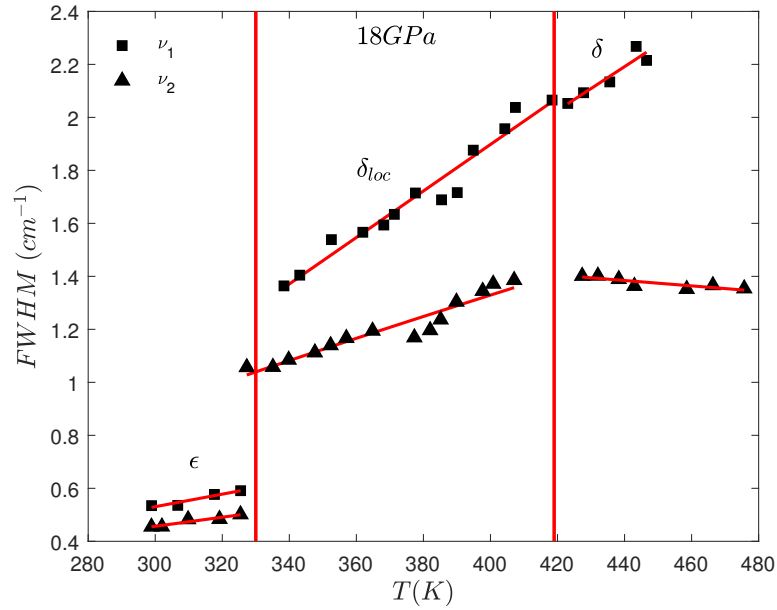


Figure 3.44: Temperature dependence of the FWHM of the internal modes of the ν_1 and ν_2 for the phases of ϵ , δ_{loc} and δ ($P=18$ GPa) in N_2 . Solid lines represent best fit (Eq.3.74) to the observed FWHM data [23]. Vertical lines denote the phase boundaries (at T_c) between the two phases.

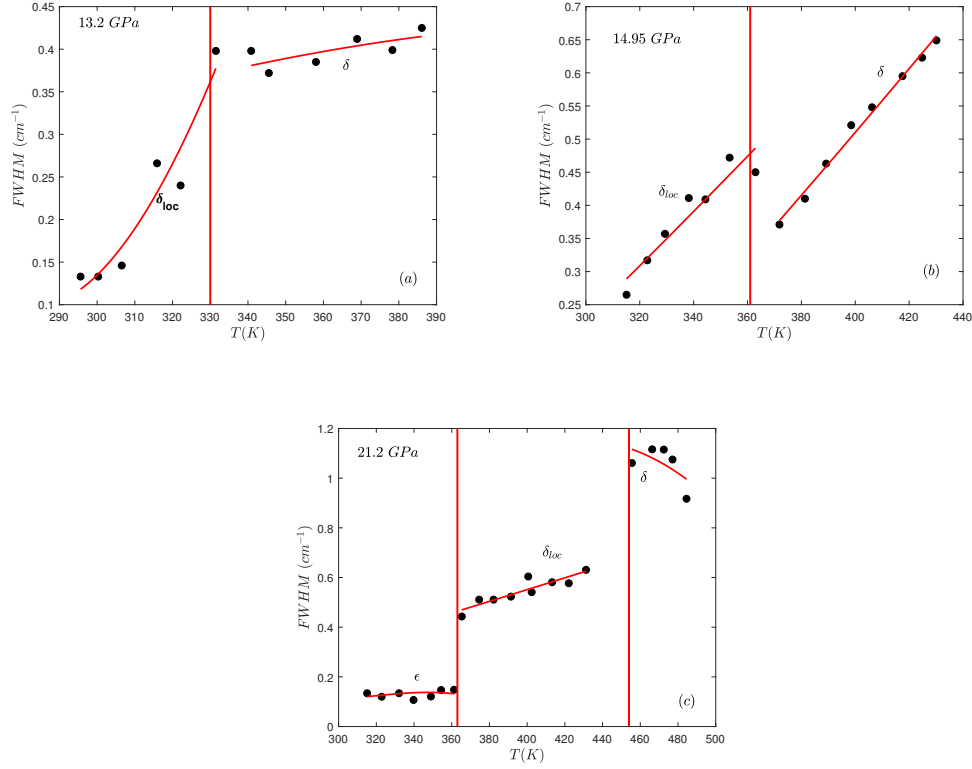


Figure 3.45: Temperature dependence of the FWHM of the $\nu_1 - \nu_2$ of the internal modes of the ν_1 and ν_2 for the phases of ϵ , δ_{loc} and δ at constant pressures indicated in N_2 . Solid lines represent best fit (Eq.3.74) to the observed FWHM data [23]. Vertical lines denote the phase boundaries (at T_c) between the two phases.

3.8 "Calculations of the temperature and pressure dependence of the thermodynamic quantities and analysis of the dielectric properties by using the Raman frequencies of cubic gauche nitrogen."

In this study, the pressure and temperature dependence of the thermodynamic quantities of cubic gauche nitrogen (cg-N) that is a kind of polymeric nitrogen, was predicted by using the observed volume [48, 103] and thermodynamic data [28] from the literature. In this part of study, we also investigated the vibrational frequencies, dielectric and elastic properties of cubic gauche solid nitrogen. We started to calculate the temperature dependence of the thermodynamic quantities with the thermal expansion α_P through its definition given by

$$\alpha_P = (1/V)(\partial V/\partial T)_P \quad (3.75)$$

For this calculation, assuming the variation of volume with the temperature quadratically, we fitted the observed volume data (P=0) according to Eq.3.76 expressed as

$$V(T) = V_0 + \alpha T + \beta T^2 \quad (3.76)$$

The values of fitted parameters of Eq.3.76 are given in Table 3.29. We then analyzed the bulk modulus B that is the inverse isothermal compressibility κ_T ($=1/B$) as a function of temperature by using

$$B(T) = \kappa_0 + \alpha' T + \beta' T^2 \quad (3.77)$$

where $\kappa_0, \alpha', \beta'$ are constant and determined as given in Table 3.30 in the cg-N phase. We also analyzed the $C_V(T)$ data [28] at P=0 according to Eq.3.78

Table 3.29: Values of the coefficients V_0 , α and β (Eq.3.75) at the pressures indicated for the cubic gauche solid nitrogen.

V(T)	$-V_0(\text{\AA}^3)$	$\alpha \times 10^{-6}(\text{\AA}^3/K)$	$-\beta \times 10^{-7}(\text{\AA}^3/K^2)$
Eq.	52.47	4.73	7.63

We also analyzed the $C_V(T)$ data [28] at P=0 according to Eq.3.78

$$C_V(T) = e_0 + e_1 T + e_2 T^2 \quad (3.78)$$

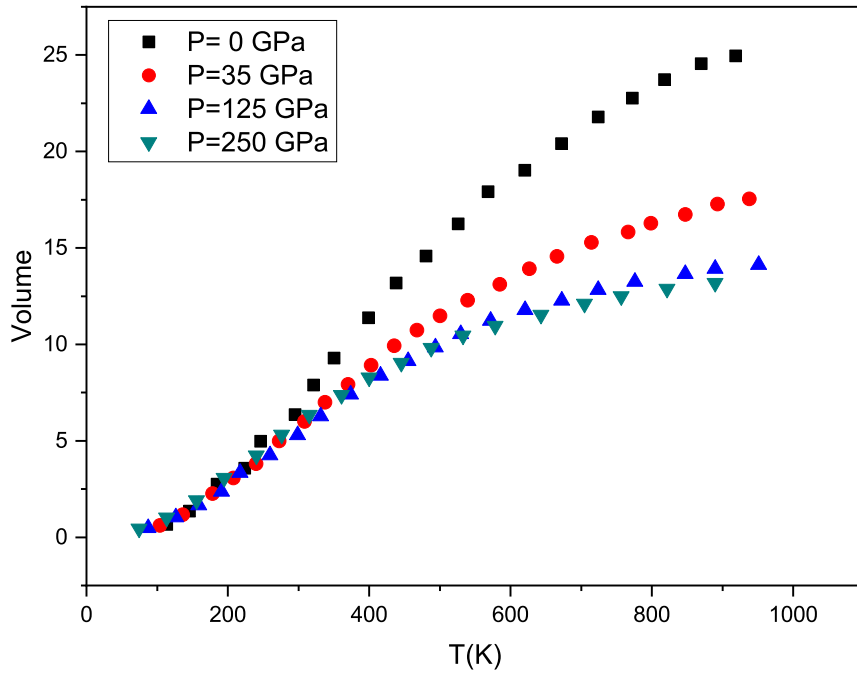


Figure 3.46: Temperature dependence of volume at various pressures (0,35,125 and 250 GPa) for the cubic gauche solid nitrogen.

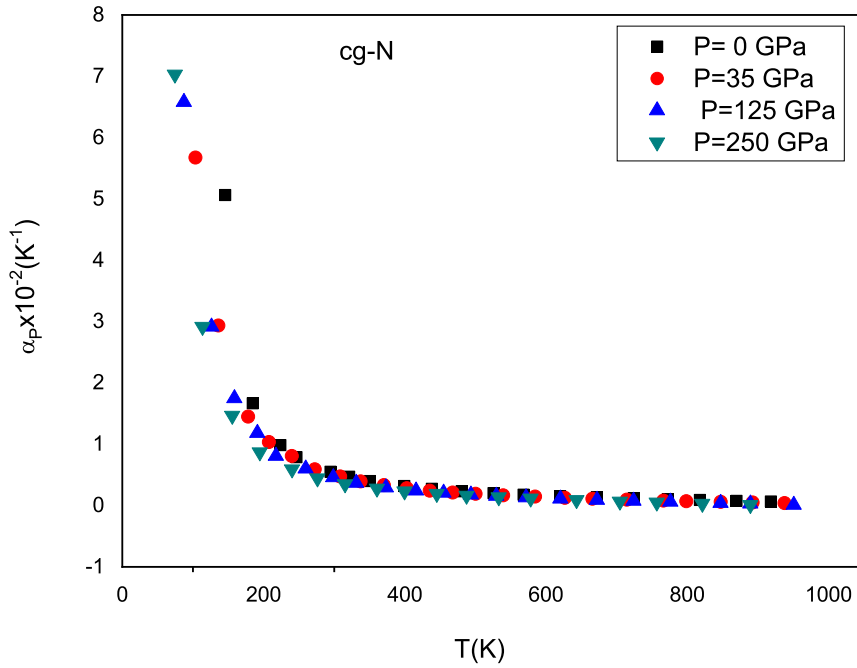


Figure 3.47: Time dependence thermal expansion (α_P) calculated through Eq.3.75 at various pressures for the cg-N.

where e_0, e_1, e_2 are constants. Values of coefficients of 3.78 are given in Table 3.31 at constant pressures in the cg-N phase by fitting Eq. 3.78 to the observed data [28]. There is a linear relation between isothermal compressibility and thermal ex-

pansion with the slope of P-T phase diagram (dP/dT) defined as

$$dP/dT = \alpha_P / \kappa_T \quad (3.79)$$

This provided us to determine the slope value of dP/dT in the P-T phase diagram of the cg-N phase by using the values of α_P and B at P=0, T=295 K. The values of the thermal expansion α_P , bulk modulus B and the dP/dT value at T=295 K (P=0) are given in 3.30.

Table 3.30: Values of the fitted parameters for the the temperature dependence of the isothermal compressibility $\kappa_T=(1/B)$ (Eq.3.77) with the thermal expansion α_P at 295 K and the slope dP/dT of the transition line in the P-T phase diagram for the cubic gauche nitrogen.

B(T) (GPa)	κ_0 (GPa)	$-\alpha' \times 10^{-3}$ (GPa/K)	$-\beta' \times 10^{-5}$ (GPa/K ²)	cg-N	$\alpha_P \times 10^{-5}$ (K ⁻¹)	B (GPa)	$(dP/dT) \times 10^{-3}$ (GPa/K)	γ
Eq.3.77	298.28	9.1	1.3	T=295K	0.81	294.46	2.385	3.35

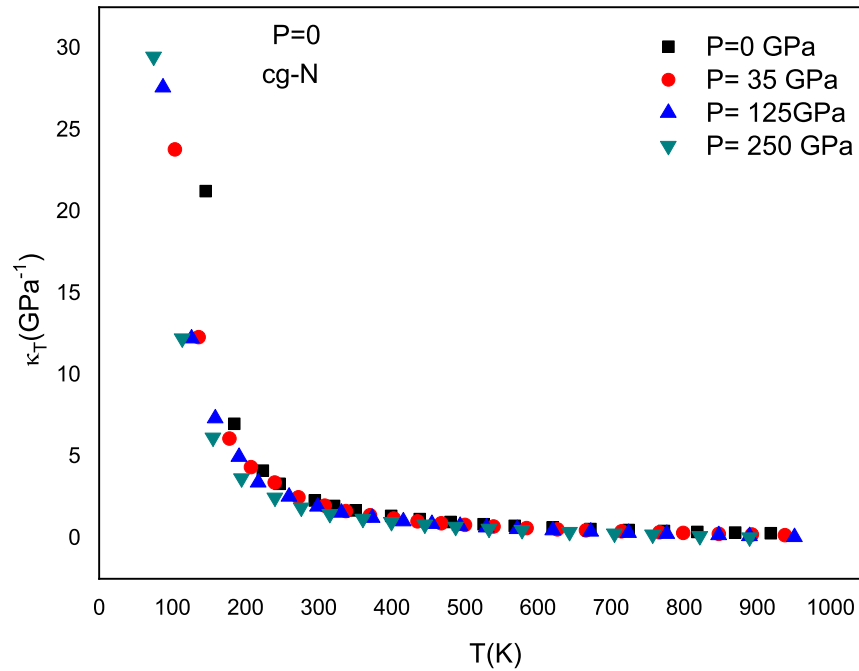


Figure 3.48: Temperature dependence of the isothermal compressibility κ_T calculated (3.79) at the pressures indicated for the cubic gauche nitrogen.

By using the dP/dT value at 295 K (P=0) with the temperature dependence of $V(T)$ (Eq.3.77) and the $C_v(T)$ data analyzed through the Eq.3.78 (Table 3.31), we obtained

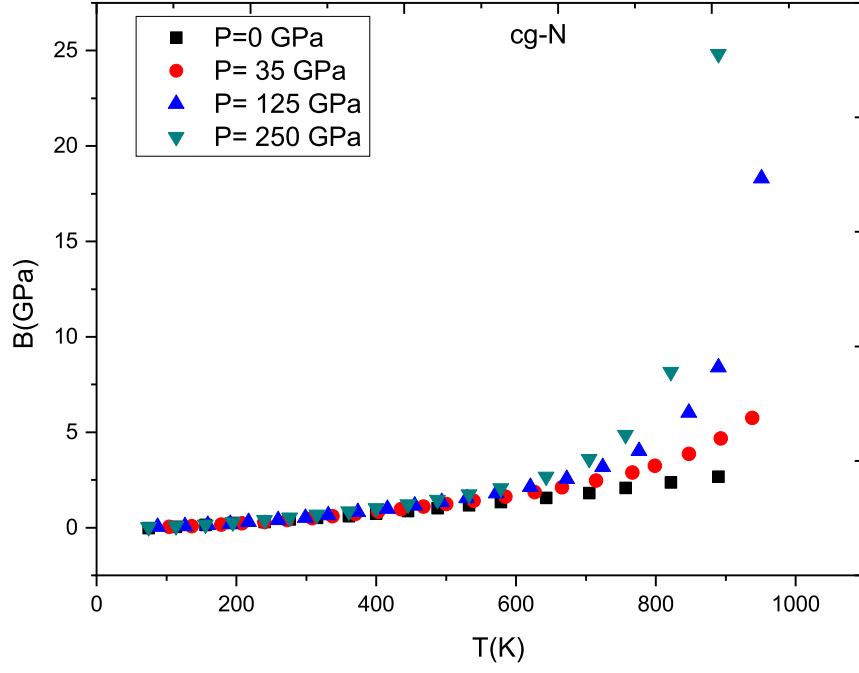


Figure 3.49: Temperature dependence of the bulk modulus $B(T)$ according to $B(T)=1/\kappa_T$ (Eq.3.79) at the pressures indicated for the cubic gauche nitrogen.

Table 3.31: Values of the coefficients e_0, e_1, e_2 at constant pressures indicated (Eq.3.78) for cubic gauche solid nitrogen.

P(GPa)	$-e_0(J/mol.K)$	$e_1(J/mol.K^2)$	$-e_2 \times 10^{-5}(J/mol.K^3)$
0	18.72	0.16	5.77
35	18.41	0.18	7.72
125	19.06	0.21	10.3
250	16.59	0.22	11.9

the macroscopic Grüneisen parameter γ defined as

$$\gamma = (V/C_v)(\alpha_P/\kappa_T) \quad (3.80)$$

as a functions of temperature at $P=0$ in the cubic gauche phase. We analyzed here the volume at various pressures according to relation

$$V(P) = b_0 + b_1P + b_2P^2 \quad (3.81)$$

where b_0, b_1 and b_2 are constants, as given in Table 3.32. At constant pressures of 35, 125 and 250 GPa, we were also able to evaluate the γ values (Eq.3.80) by using the

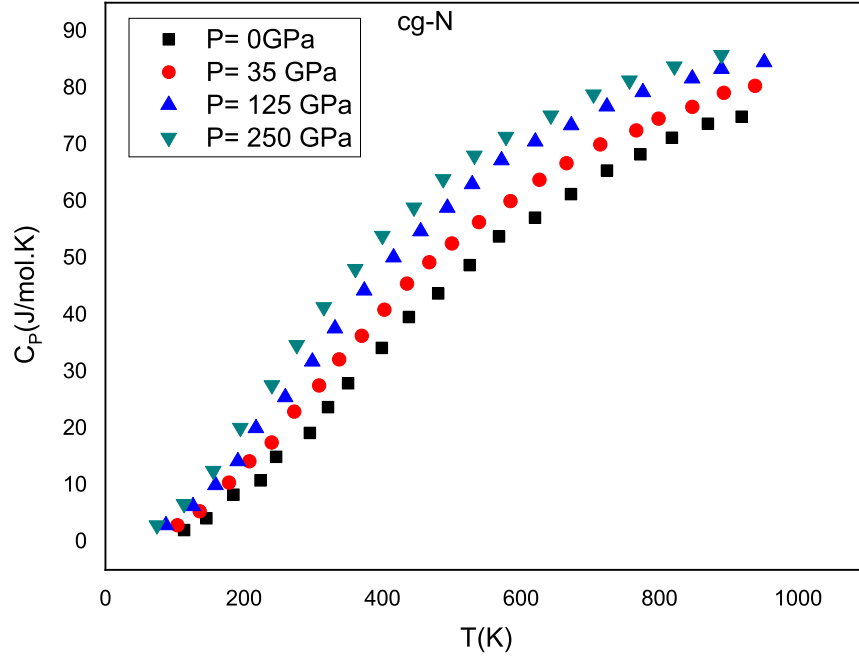


Figure 3.50: Heat capacity (C_P) as a function of temperature by using the calculated $V(T)$ and C_v data[28] through Eq.3.82 at the pressures indicated for the cubic gauche nitrogen.

$V(P)$ [48] and the C_V data [28] with a constant dP/dT value (Table 3.30). For this calculation, we analyzed the C_V data [28] according to Eq.(3.78) for the pressures considered with the coefficients of e_0, e_1 and e_2 determined, as given in Table 3.31. By means of the γ values determined, we then calculated the temperature dependence of the volume $V(T)$ using the C_V data [28] with the constant dP/dT (Table 3.30) at the pressures of 0, 35, 125 and 250 GPa, as plotted in Fig.3.46. Values of the coefficients for $V(T)$ for constant pressures studied according to Eq.(3.76), are given in Table 3.33

Table 3.32: Values of the coefficients b_0 , b_1 and b_2 (Eq.3.81) and b'_0 , b'_1 and b'_2 (Eq.3.83) for various pressures for the cubic gauche solid nitrogen.

κ_T (GPa^{-1})	b'_0 (GPa^{-1})	$-b'_1 \times 10^{-4}$ (GPa^{-2})	$b'_2 \times 10^{-6}$ (GPa^{-3})	$V(P)$	b_0 (\AA^3)	$-b_1 \times 10^{-2}$ ($\text{\AA}^3/GPa$)	$b_2 \times 10^{-5}$ ($\text{\AA}^3/GPa^{-1}$)
Eq.3.83	0.99	7.4	1.06	Eq.3.81	6.76	2.21	7.35

Then, by using the coefficients of b_0, b_1 and b_2 at constant pressures, (Table 3.33), we obtained the thermal expansion as a function of temperature at constant pressures as illustrated in Fig.3.47. As seen in Fig.3.47, there is a sharp drop up to about 400

Table 3.33: Values of the coefficients V_0 , α and β (Eq.3.75) at the pressures indicated for the cubic gauche solid nitrogen.

P(GPa)	$-V_0(\text{\AA})$	$\alpha \times 10^{-2}(\text{\AA}^3/K)$	$-\beta \times 10^{-5}(\text{\AA}^3/K^2)$
0	6.28	5.21	1.90
35	4.01	3.89	1.68
125	3.18	3.46	1.72
250	2.54	3.28	1.83

GPa and α_P shows temperature independent behavior for the cubic gauche solid nitrogen. This also gave us the temperature dependence of the isothermal compressibility κ_T (3.79) where dP/dT value (Table 3.30) was used, and the bulk modulus $B(T)$ ($=1/\kappa_T$) at constant pressures considered as plotted in Figs. 3.48 and 3.49 respectively. The isothermal compressibility represents same behaviour for the cubic gauche nitrogen. Since we have the values of V , α_P , κ_T and specific heat C_v , we calculated the heat capacity C_P via the thermodynamic relation,

$$C_P = C_v + TV(\alpha_P^2/\kappa_T) \quad (3.82)$$

Fig. 3.50 gives the variation of heat capacity with the temperature at constant pressures ($P=0, 35, 125$ and 250 GPa). Unlike isothermal expansion, the heat capacity increases with increasing temperature (3.50). Regarding the pressure dependence of the thermodynamic quantities for the cubic gauche nitrogen, we calculated the pressure dependence of the thermal expansion α_P by analyzing the compressibility (κ_T) of the cubic gauche structure by using the a/a_0 lattice parameter data [28] at 295 K by means of the expression,

$$\kappa_T/\kappa_0 = b'_0 + b'_1 P + b'_2 P^2 \quad (3.83)$$

where b'_0 , b'_1 and b'_2 are constants. The values of coefficients of Eq. 3.83 are given in Table 3.32 as also given in our previous work [104]. In Figs. 3.51 and 3.52, we plot the κ_T/κ_0 and the thermal expansion α_P as a function of pressure (Eq. 3.79) with the definition of $\kappa_T \equiv ((-1)/V)(\partial V)/(\partial P)_T$ at 295 K and the constant dP/dT value (3.30) for cg-N, respectively. As expected, α_P decreases almost linearly with the increasing

pressure (Fig.3.52) and κ_T exhibits similar critical behavior for the cubic gauche nitrogen. By having $V(P)$, α_P and $\kappa_T(P)$ at $T=295$ K, the heat capacity C_P was also evaluated as a function of pressure according to Eq.(3.82) for cg-N. For this calculation, values of V (Eq.3.81), κ_T [28] and α_P (Eq.3.79) through the dP/dT value (Table 3.30) at constant pressures of $P=0, 35, 125$ and 250 GPa were determined and by using the C_v data at those pressures [28]. We were then able to calculate C_P (Eq.3.82) and γ (Eq. 3.80) at $T=295$ K in the cg-N phase, as plotted in Figs. (3.53) and (3.54), respectively. Owing to the inverse relation between thermal expansion α_P (Eq.3.79), C_P increases as the pressure increases (Fig.3.52) at 295 K.

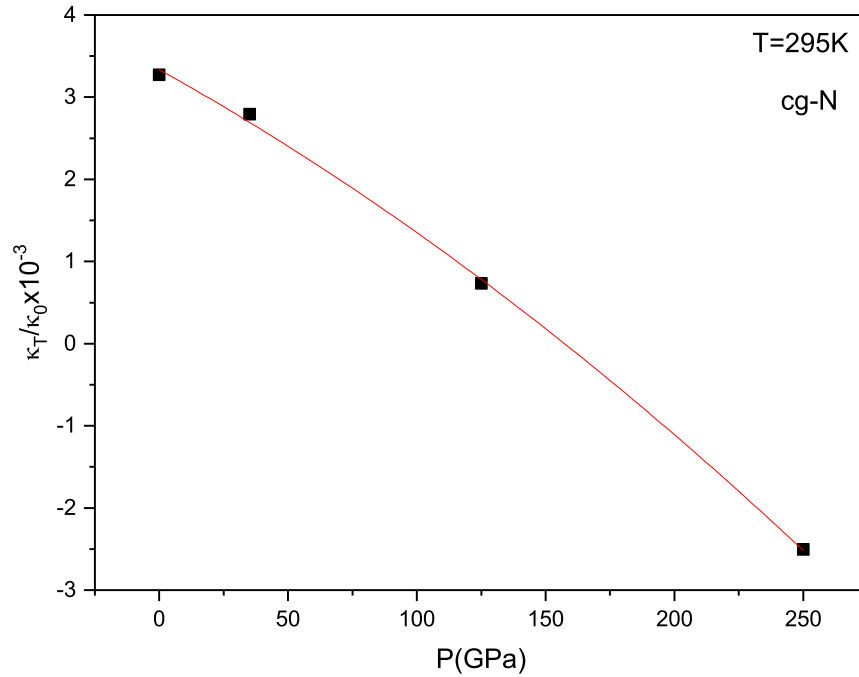


Figure 3.51: Thermal expansion κ_T/κ_0 as a function of pressure ($T=295$ K), which was calculated according to Eq.3.79 for cubic gauche solid nitrogen.

In this part, the vibrational frequencies were estimated with the volume change through the mode Grüneisen parameter. For this calculation, we used the isothermal mode Grüneisen parameter (Eq.3.84) to analyze the relation between the Raman frequency shift and the volume change in the cubic gauche nitrogen,

$$\gamma_T(P) = \frac{V(P)(\partial\nu/\partial P)_T}{\nu(P)(\partial V/\partial P)_T} \quad (3.84)$$

In order to analyze the Raman frequencies of various modes and the volume as a function of pressure, expressions,

$$\nu_T(P) = a_0 + a_1P + b_2a^2 \quad (3.85)$$

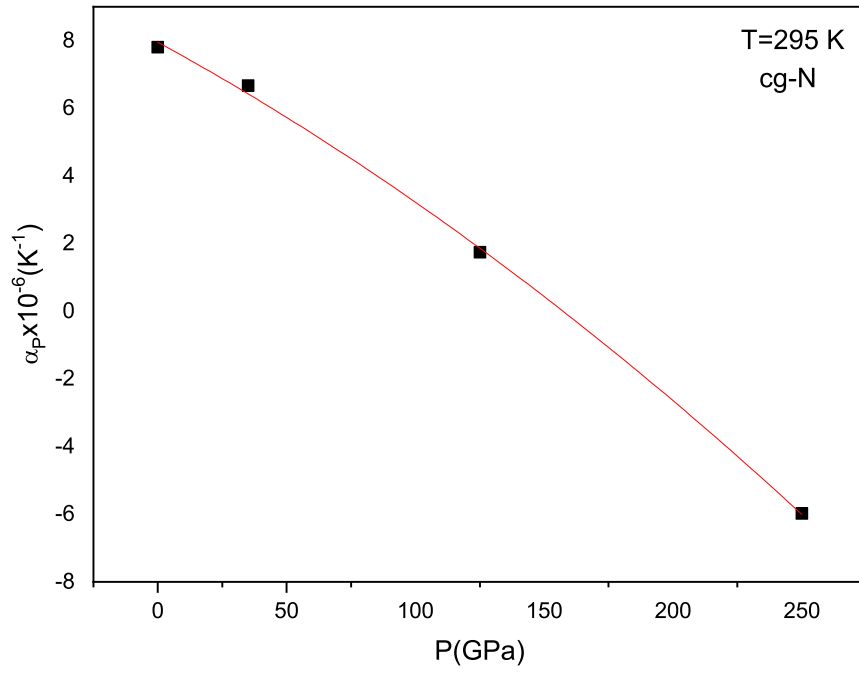


Figure 3.52: Thermal expansion α_P as a function of pressure ($T=295$ K), which was calculated according to Eq.3.79 for cubic gauche solid nitrogen.

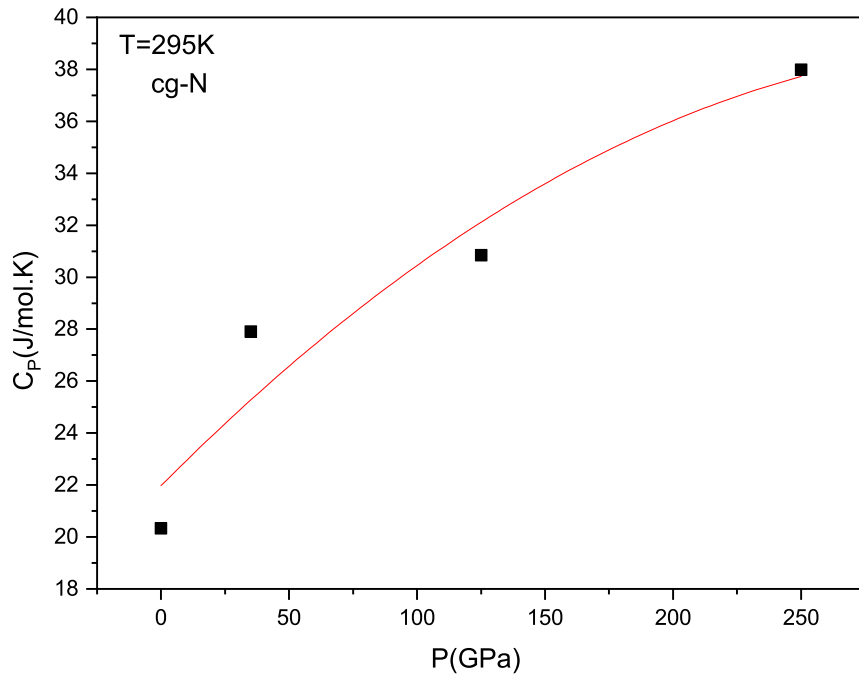


Figure 3.53: Heat capacity as a function of pressure ($T=295$ K) which was calculated according to Eq.3.82 for cg-N.

and

$$V_T(P) = b_0 + b_1P + b_2P^2 \quad (3.86)$$

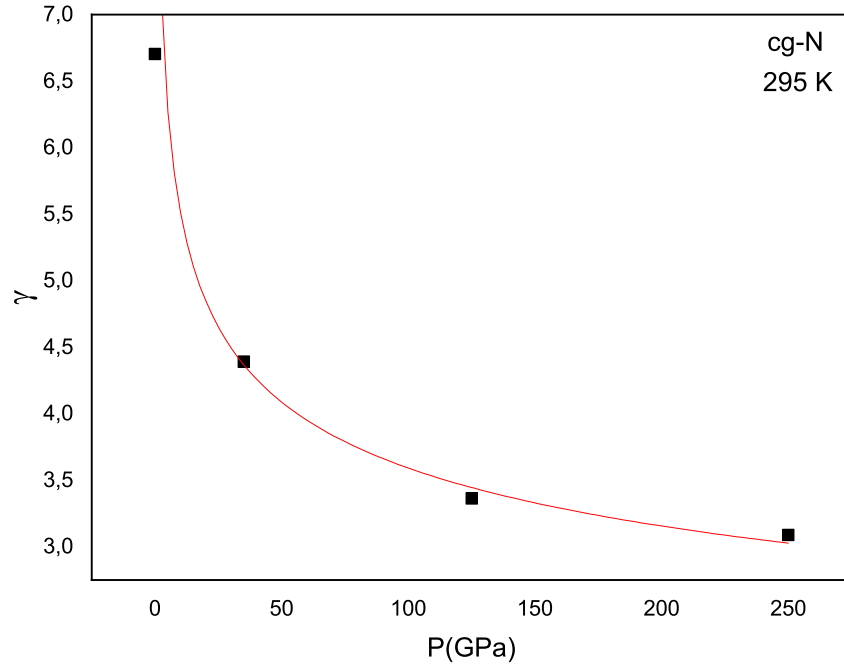


Figure 3.54: Grüneisen parameter γ as a function of pressure, which was calculated according to Eq.3.80 for the cubic gauche solid nitrogen.

were used, where a_0 , a_1 , a_2 and b_0 , b_1 , b_2 are constants. We fitted the Eqs.3.85 and 3.86 to the observed Raman and infrared frequency data for the optic modes of A, E and the translational modes of T(TO) and T(LO) at the center (Γ point) [28] with volume data within the 0-140 GPa pressure interval (295 K) [48] for the structure of cubic gauche nitrogen. The values of fitted parameters (a_0 , a_1 , a_2 and b_0 , b_1 , b_2) are given in Table 3.34 for the optical (A,E) and the translational (T(TO), T(LO)) modes [28] and in Table 3.35 for the observed V-P data at 295 K [48]. Then, with the isothermal mode Grüneisen parameter determined by using the constants (Table 3.34 and Table 3.35) through Eq.3.84, we obtained the pressure dependence Raman frequency for the cg-N phase via

$$\nu_T(P) = A(P) + \nu_0 \exp[-\gamma_T(P) \ln \left(\frac{V_T(P)}{V_0} \right)] \quad (3.87)$$

In Eq.3.87, ν_0 and V_0 are the frequency and volume values at ambient conditions ($P=0$, $T=295$ K), respectively. $A(P)$ is the additional term and it was determined by fitting Eq.3.87 to the observed frequency data for the cg-N with the relation

$$A(P) = c_0 + c_1 P + c_2 P^2 \quad (3.88)$$

where c_0 , c_1 and c_2 are constants and their values are given in Table 3.34. Figs.3.55 and 3.56 give the pressure dependence of isothermal mode Grüneisen parameter (γ_T)

(Eq.3.84) and calculated frequencies of the Raman and optic modes (Eq.3.87) indicated [28, 44] with the observed A mode only [47], respectively. There is a good relation between the calculated frequency values for the optical modes in the zone center of cg-N structure [28, 44]. As stated by Caracas [28], when the pressure increases, all the modes harden with a nonlinear behavior (Fig.3.56).

Table 3.34: Values of coefficients a_0 , a_1 , a_2 for the Raman and infrared modes in the phases indicated according to Eq.(3.85) and the coefficients of the additional term $A(P)$ which were determined by fitting Eq.(3.88) to the observed frequency data[28] for the cubic gauche solid nitrogen.

Raman and IR modes	$a_0(= \nu_0)$ (cm^{-1})	a_1 (cm^{-1}/GPa)	$-a_2 \times 10^{-2}$ (cm^{-1}/GPa^2)	$-C_0$ (cm^{-1})	C_1 (cm^{-1}/GPa)	$-C_2$ (cm^{-1}/GPa^2)
A	628.01	2.29	2.99	1031.17	30.72	0.21
T(LO)	806.98	1.72	2.65	573.74	17.18	0.12
T(TO)	842.41	1.59	2.45	523.54	15.68	0.11
E	985.58	3.52	5.04	1438.59	42.91	0.29
T(LO)	1257.35	2.19	2.55	891.43	26.67	0.19

Table 3.35: Values of the coefficients b_0 , b_1 and b_2 by using the volume-pressure (V-P) data [46] according to Eq.(3.86) within the pressure range indicated for cubic gauche solid nitrogen.

$V(\text{\AA}^3)$	$b_0(= V_0)(\text{\AA}^3)$	$-b_1 \times 10^{-2}(\text{\AA}^3/GPa)$	$b_2 \times 10^{-5}(\text{\AA}^3/GPa^2)$	Pressure Interval(GPa)
$Cg - N_2$	6.67	2.21	7.35	$0 < P < 140$

Table 3.36: Values of coefficients a_0 , a_1 , a_2 for the frequencies of zone-center phonon modes according to Eq.(3.85) by using the observed data [42].

Raman and IR modes	$a_0(cm^{-1})$	$a_1(cm^{-1}/GPa)$	$-a_2 \times 10^{-3}(cm^{-1}/GPa^2)$
$600\text{ }cm^{-1}$ (1xRaman)	586.54	2.03	2.28
$900\text{ }cm^{-1}$ (2xRaman)	941.94	3.53	4.19
$900\text{ }cm^{-1}$ (3xRaman)	802.19	1.52	1.91
$1200\text{ }cm^{-1}$ (3xRaman)	1234.46	2.40	2.68

In an another analysis, we used the Raman frequencies (1xRaman, 2xRaman and

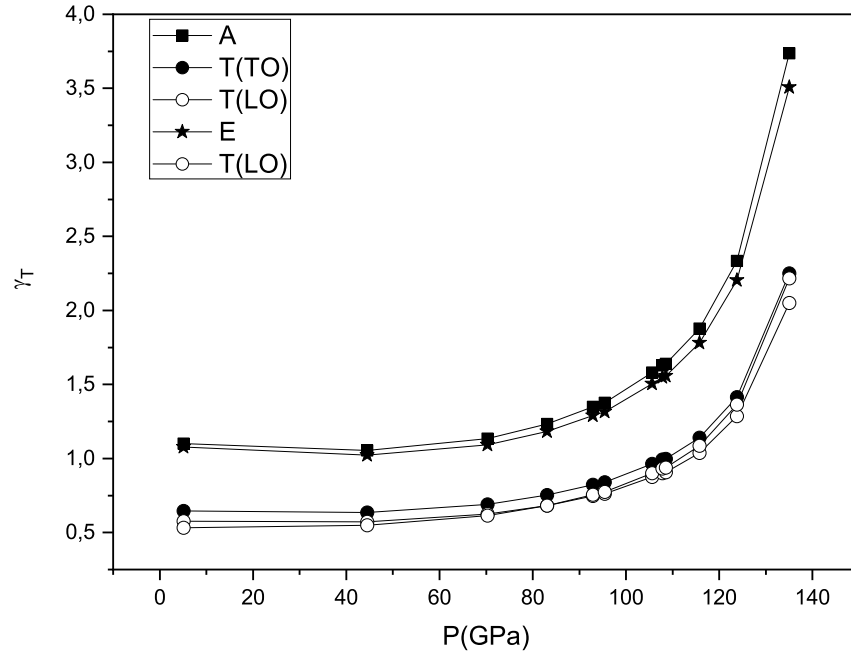


Figure 3.55: Isothermal mode Grüneisen parameter γ_T as a function of pressure which was calculated using Eq.3.84 for the optic modes indicated in cg-N.

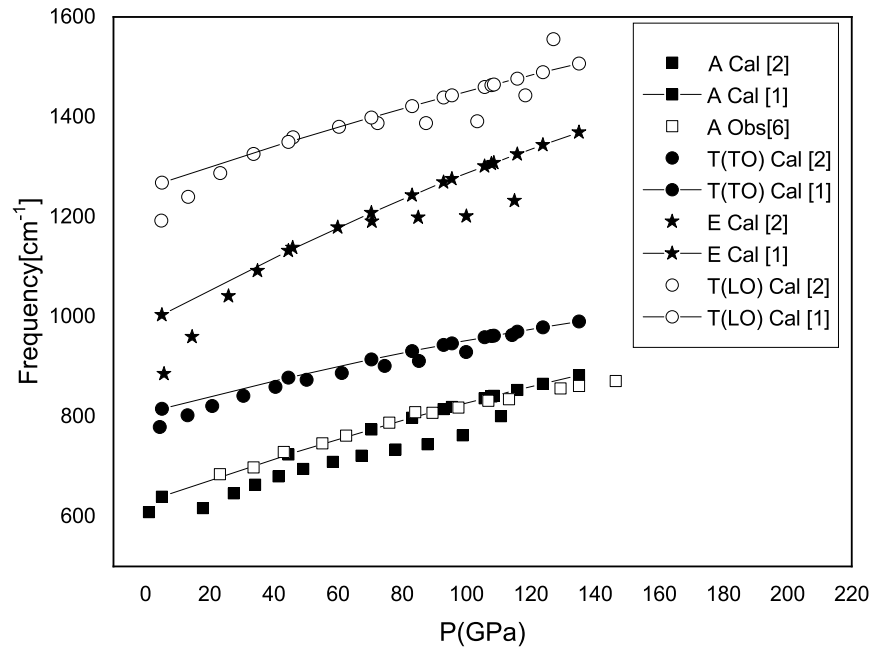


Figure 3.56: Calculated frequencies of the optic modes as a function of pressure through Eq.3.87 with the observed data only [45] for the cg-N.

3xRaman) which were obtained by density functional theory [44] within the $0 < P < 360$ GPa pressure interval. Then, we investigated the Raman frequencies for the phases of zone center phonon modes for cg-N according to Eq.3.85 and V-P data [103] in

Table 3.37: Values of the coefficients b_0 , b_1 and b_2 using the volume-pressure (V-P) data [101] according to Eq.(3.86) with V_0 within the pressure range indicated for cubic gauche solid nitrogen.

$V_0(\text{\AA})$	$b_0(\text{\AA})$	$b_1 \times 10^{-2}(\text{\AA}^3/GPa)$	$b_2 \times 10^{-5}(\text{\AA}^3/GPa^2)$	Pressure Interval(GPa)
<i>cg - N</i>	6.86	-2.22	7.93	0<P<100

the pressure interval of 0-100 GPa according to Eq.3.86. The values of the coefficients of Eq.3.85 (a_0 , a_1 and a_2) (Table 3.36) and of Eq.3.86 (b_0 , b_1 and b_2) (Table 3.37) were determined. By the correlation of the Raman frequency and volume data, we predicted the isothermal mode Grüneisen parameter as a function of pressure through Eq.3.84 as plotted in Fig.3.57 for the Raman modes of the zone-center phonon modes [44] in cubic gauche nitrogen. According to Fig.3.57, γ_T remains nearly constant first in the pressure interval 0 to 40 GPa, then it increases with the pressure increase, as expected. In order to understand the anharmonic properties

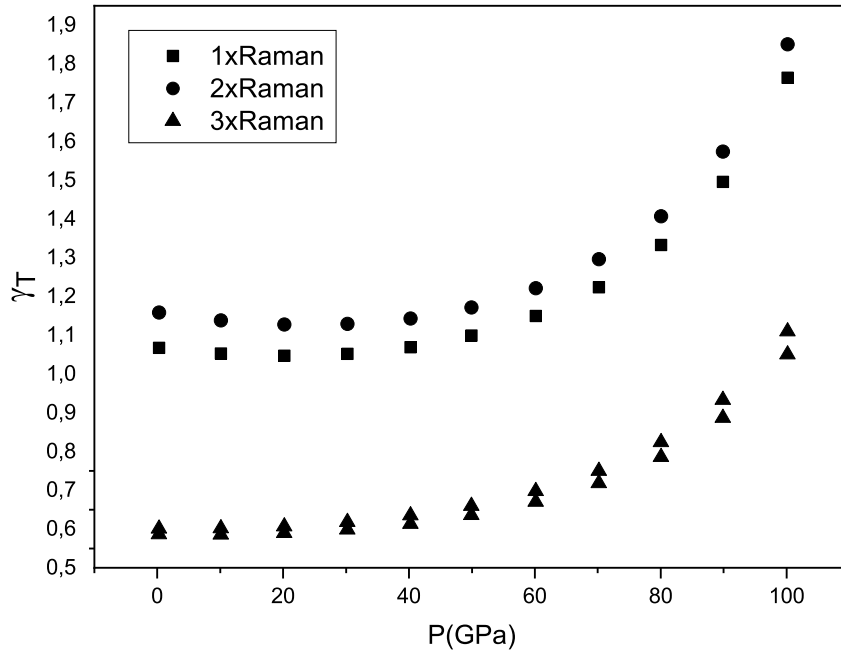


Figure 3.57: Static frequency dielectric constant as a function of frequency for the pressure dependent optic modes [28] in the cg-N.

of the cg-N, we analyzed the relation between the vibrational frequency (ν) and the elastic modulus (c_{ij}) which can be expressed as

$$\nu^2 = a + bc_{ij} \quad (3.89)$$

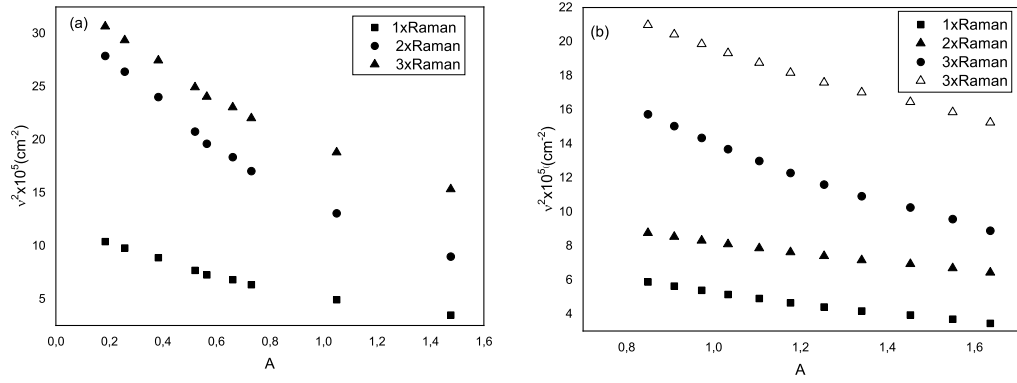


Figure 3.58: The Raman frequencies (ν^2) [45] as a function of the elastic anisotropy(A) [12] due to the elastic constant c_{11} , c_{12} and c_{44} in the pressure range of 0-360 GPa (a) and 0-100 GPa (b).

where a and b are constants. The variation of Raman frequency(squared) with the elastic constants (c_{ij}) was examined by using the pressure dependence of the Raman frequencies [44] and the elastic constants (c_{11} , c_{12} and c_{44}) within the pressure interval of 0-360 GPa [105]. We plot the Raman frequencies (ν^2) against the elastic anisotropy (A) which is the ratio of the two shear moduli c_{44} and $(c_{11} - c_{12})/2$ [12] in (3.58a). We also obtained Raman frequencies (ν^2) [44] with the pressure dependence of elastic constants c_{11} , c_{12} and c_{44} in the range of 0-100 GPa [12] in Fig.(3.58b). As seen in Figs.(3.58a) and (3.58b), ν^2 decreases as the pressure increases and there is a good agreement between the variation of the Raman frequency (ν^2) with the elastic anisotropy (A) in the two pressure intervals of 0-360 GPa (3.58a) [105] and 0-100 GPa (3.58b) [12]. According to the elastic constants, the cg phase is the most stable one among the polymeric phases of nitrogen [105] which agrees with the other studies up to 170 GPa [27, 106, 107]. Regarding the investigation of the relation between the Raman frequency and the elastic moduli (c_{ij}), we plot the Raman frequency shifts $(1/\nu)(\partial\nu/\partial P)$ against the elastic anisotropy (A) in Fig.3.59. We obtained nearly increasing trend for the Raman frequency shift as a function of the elastic anisotropy as shown in Fig.3.59.

We also investigated dielectric properties of cubic gauche solid nitrogen by using the real and imaginary parts of the complex dielectric permittivity. Materials contain permanent dipoles and they are randomly oriented in polar materials. When the electric field is applied, these dipoles reoriented towards the direction of electromagnetic

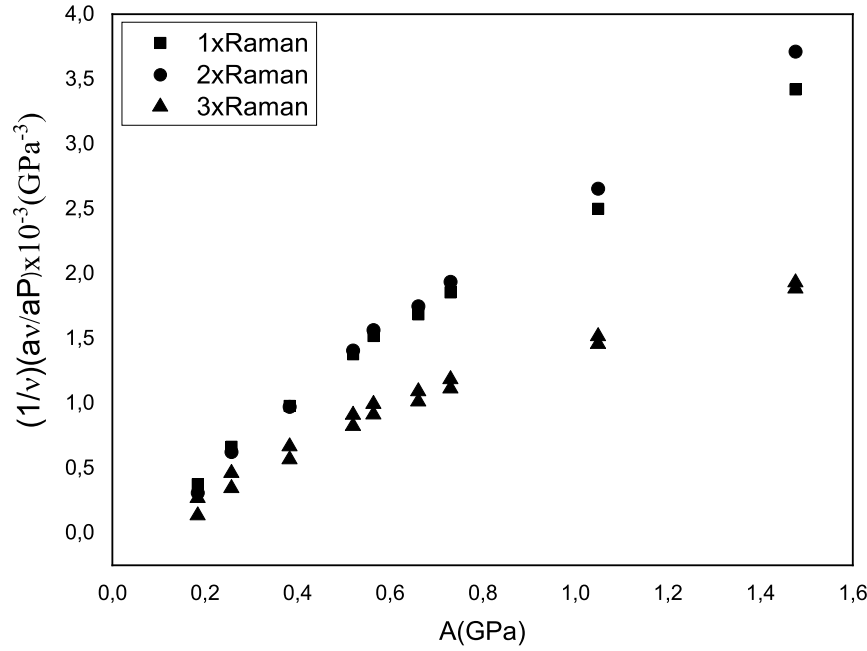


Figure 3.59: Static frequency dielectric constant as a function of Variation of the frequency shifts $(1/\nu)(\partial\nu/\partial P)$ as derived from the Raman frequencies as a function of elastic anisotropy (A) for the Raman frequencies of the zone-center phonon modes in cubic gauche nitrogen. for the pressure dependent optic modes [28] in the cg-N.

field. And when electric field is turned off, the time is required in order to turn back to a random distribution dipoles and the delay occurs on molecular polarization that is called dielectric relaxation. When the electric field is exerted to a polar dielectric, the polarization builds up expressed as

$$P(t) = P_{\infty} \left(1 - e^{-\frac{t}{\tau}} \right) \quad (3.90)$$

$P(t)$ is polarization at time t , τ is relaxation time and is a function of temperature [108]. By taking the derivation of Eq.3.90, the rate of polarization building is obtained as

$$\frac{dP(t)}{dt} = \frac{-P_{\infty} e^{-\frac{t}{\tau}}}{\tau} \quad (3.91)$$

Then, by putting Eq.3.90 into Eq.3.91 and assuming the total polarization due to dipoles expressed as

$$\frac{dP(t)}{dt} \cong \frac{P_{\mu} - P(t)}{\tau} \quad (3.92)$$

where P_{μ} is the orientational polarization. By neglecting atomic polarization, the total polarization $P_T(t)$ is got

$$P_T(t) = P_{\mu}(t) + P_e \quad (3.93)$$

with

$$P_T = \epsilon_0(\epsilon_s - 1)E \quad (3.94)$$

and

$$P_e = \epsilon_0(\epsilon_\infty - 1)E \quad (3.95)$$

where ϵ_s and ϵ_∞ are the electric constants under voltage and at infinity frequency respectively and E is the electric field. Then by substituting Eqs.3.94 and 3.95 in Eq.3.93 and simplifying it, we obtain

$$P_\mu = \epsilon_0(\epsilon_s - \epsilon_\infty)E \quad (3.96)$$

we get Eq.3.97 by solving Eq.3.92 via the solution of first-order differential equation with the alternating electric field ($E = E_{max}e^{i\omega t}$) as

$$P(t) = \epsilon_0 \frac{(\epsilon_s - \epsilon_\infty)E_m e^{i\omega t}}{(1 + i\omega\tau)} \quad (3.97)$$

We get total polarization by using Eq.3.96 and Eq.3.97

$$P(t) = \left[\epsilon_\infty - 1 + \frac{(\epsilon_s - \epsilon_\infty)}{1 + i\omega\tau} \right] \epsilon_0 E_m e^{i\omega t} \quad (3.98)$$

The value of flux density can be defined as

$$D(t) = \epsilon_0 \epsilon^* E_m e^{i\omega t} \quad (3.99)$$

and

$$D(t) = \epsilon_0 E_m e^{i\omega t} + P(t) \quad (3.100)$$

Hence, by equating these two flux density functions (Eqs.(3.99, 3.100) to each other, we get

$$(\epsilon' - i\epsilon'') = 1 + \left[\epsilon_\infty - 1 + \frac{(\epsilon_s - \epsilon_\infty)}{1 + i\omega\tau} \right] \quad (3.101)$$

The imaginary and real parts of permittivity are obtained as

$$\epsilon'(\omega) = \frac{\epsilon_0 - \epsilon_\infty}{1 + \omega^2\tau^2} + \epsilon_\infty \quad (3.102)$$

and

$$\epsilon''(\omega) = -\frac{\omega\tau(\epsilon_0 - \epsilon_\infty)}{1 + \omega^2\tau^2} \quad (3.103)$$

where ϵ_0 and ϵ_∞ are the static and high-frequency dielectric constants respectively [108]. The frequency dependence of $\epsilon'(\omega)$ and $\epsilon''(\omega)$ was predicted according to

Eqs.3.102 and 3.103 by using the pressure dependence of optical modes A,E,T(TO) and T(LO) in the zone center of cubic gauche structure with the values of ϵ_0 and ϵ_∞ at the pressures of 35,75, 125,175 and 250 GPa as taken from literature [28].The predicted values of the frequency dependence of real $\epsilon'(\omega)$ and imaginary parts $\epsilon''(\omega)$ of the complex dielectric permittivity, are given in Figs.3.60 and 3.61 respectively for the optic modes studied at various pressures [28]. Finally, we gave the relation between the $\epsilon'(\omega)$ and the dielectric loss $\epsilon''(\omega)$ in terms of the cole- cole plot for the optic modes of A,E, T(TO) and T(LO) at various pressures for the cg-N as shown in Fig.3.62.

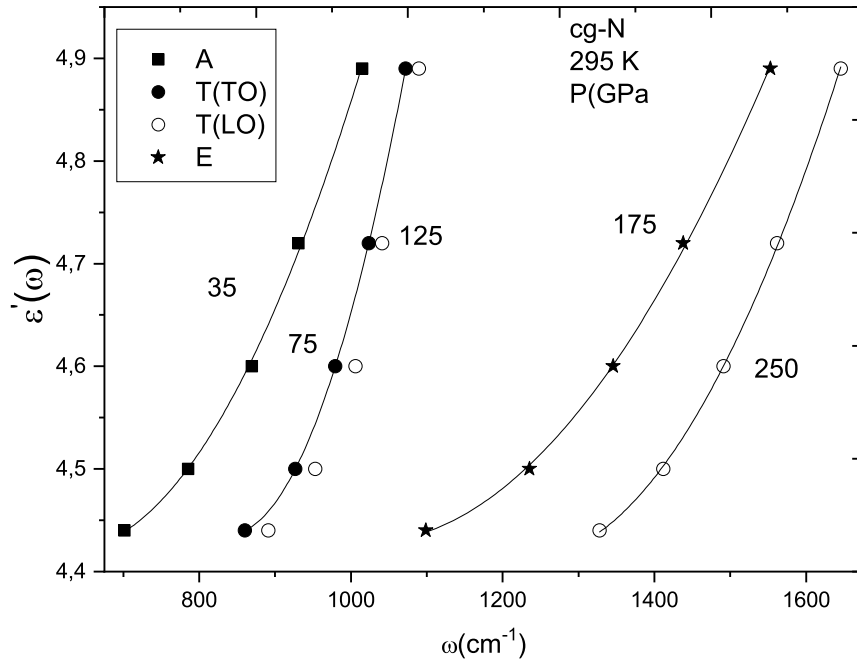


Figure 3.60: Static frequency dielectric constant as a function of the frequency for the pressure dependent optic modes [28] in the cg-N.Solid lines represent the best fits to the values given.

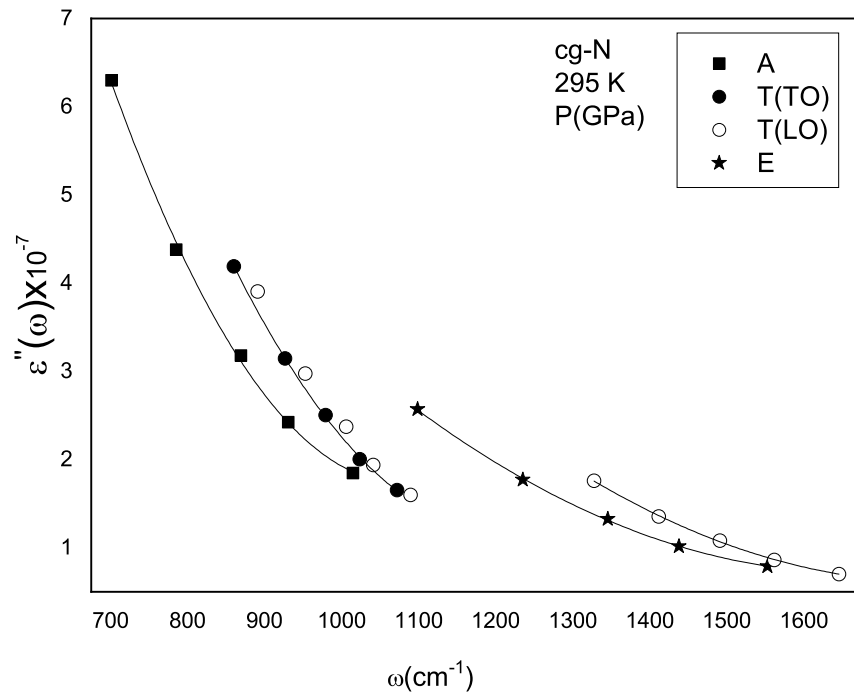


Figure 3.61: High frequency dielectric constant as a function of the frequency for the pressure dependent optic modes [28] in the cg-N. Solid lines represent the best fits to the values given.

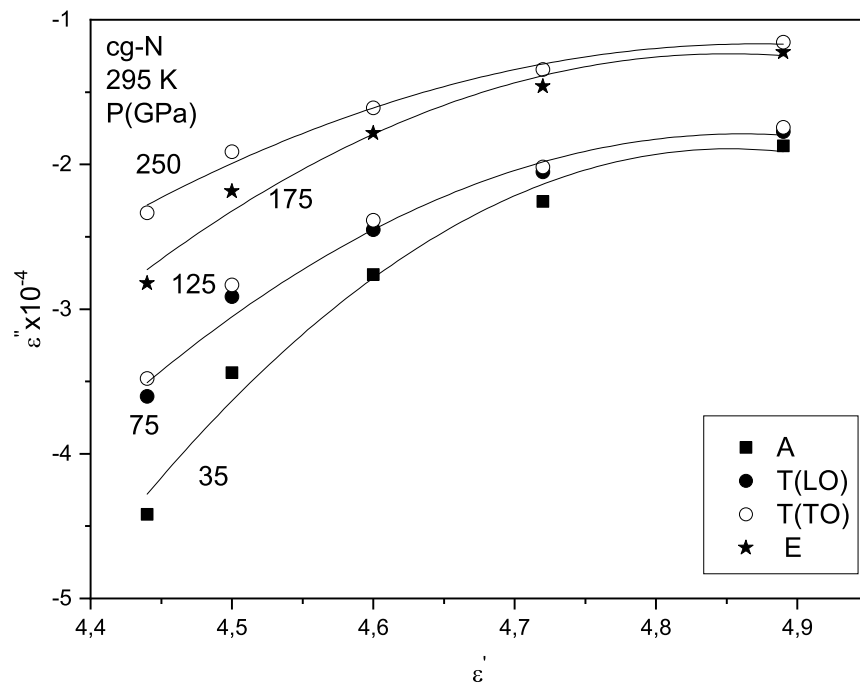


Figure 3.62: Cole-Cole plot of the optic modes at various pressures [28] for the cg-N. Solid lines represent the best fits to the values given.

CHAPTER 4

CONCLUSIONS

In this thesis, the thermodynamic and the spectroscopic properties of solid nitrogen in the vicinity of the phase transitions was investigated. By means of using various models and methods, we analyzed the experimental and theoretical data which were taken from the literature in order to explain the observed behavior of thermodynamical quantities and dynamical properties of solid nitrogen at high temperatures and pressures. The dynamical properties of solid nitrogen were studied by using the Raman frequencies that vary with the pressures and temperatures close to the phase transitions and solid nitrogen is one of the most convenient molecular structures to analyze these properties since it has a fundamental pressure and temperature induced phase transitions. The pressure dependence of the Raman and IR frequencies of solid nitrogen was predicted by using observed volume and frequency data up to 160 GPa at the room temperatures. For this calculation, the isothermal mode Grüneisen parameter as a function of pressure was calculated for the lattice and internal modes of the solid nitrogen and then it was used to predict the Raman and IR frequencies of Raman modes studied at high pressures for solid nitrogen. Our calculated the Raman and IR frequencies are in good agreement with the observed frequency data for the vibrons and lattice modes of solid nitrogen as expected that they increase as the pressure increases except the vibron ν_2 that decreases with the increasing pressure at the 80-160 GPa pressure interval. Hence, our results shows that this methods is adequate the calculate Raman frequencies of solid nitrogen and it can be used for other molecular crystals. The phase diagram of nitrogen was calculated for the fluid-solid and solid- solid (ϵ - δ_{loc} - δ) by using the mean field model at high pressures. By using the free energy expanded in terms of order parameter, the phase line equation was derived and it was fitted the observed data. Temperature and pressure dependent

coefficients of free energy were determined and used to calculate the phase diagram of solid nitrogen for the fluid-solid, the δ - δ_{loc} and the δ_{loc} - ϵ transitions. Also, by using free energy, we predicted thermodynamic quantities of the order parameter, inverse susceptibility, entropy, heat capacity thermal expansion and the isothermal compressibility as a function of temperature. Again, observed P-T data was used to calculate thermodynamic quantities. According to our results, while order parameter and inverse susceptibility decrease with increasing temperature and pressure, the entropy, heat capacity, thermal expansion and isothermal compressibility increase as the temperature increasing and they represent abnormal behavior near the phase transition region. The mean field model can be an applicable model to calculate phase diagram (P-T or X-T) and thermodynamic quantities of molecular crystals close to the phase transitions. As an another calculation, the temperature dependence of the Raman bandwidths (linewidths) of Eg librational mode (P=0) and the internal modes of ν_1 and ν_2 (P=18 GPa) was calculated by using pseudospin-phonon coupling (PS) and energy fluctuation (EF) models. First of all, the temperature dependence of the Raman frequency as assumed the order parameter was calculated from the molecular field theory by analyzing the experimental frequency data from the literature. By using these calculated frequencies, Linewidth (FWHM) was predicted at various temperature via the PS and EF models for the Eg mode, ν_1 and ν_2 internal modes and the difference in the frequency (ν_1 - ν_2) at constant pressures. As observed experimentally, our calculated linewidth values increase as the temperature increases at constant pressures. Hence, Our results indicate that pseudospin-phonon coupling and energy fluctuation model can be used to describe the observed behavior of the Raman bandwidth of the molecular crystals. Regarding to thermodynamic properties of solid nitrogen, we calculated the thermodynamic functions of the isothermal compressibility, the difference of heat capacity and the thermal expansion in terms of temperature and pressure from the Raman frequency of the internal modes ν_1 , ν_2 and ν_{22} close to the phase transition of ϵ , δ_{loc} and δ in solid nitrogen. The observed volume data was also used to predict the thermodynamic functions. After calculations of the thermodynamic functions, the Pippard relations were employed in order to investigate linear relations between the heat capacity with the thermal expansion and the isothermal compressibility with the thermal expansion. By using this linear relation, we obtained dP/dT values for the fluid solid and ϵ - δ_{loc} - δ transitions for solid nitrogen

and compared the previous values obtained by Mukherjee et al. for melting curve of solid nitrogen [94]. The method of calculating thermodynamic functions from the Raman frequency shift and volume data can be applicable for the other molecular crystals as shown in our results. We calculated in section 3.6 the Raman frequency and Raman bandwidth by means of the anharmonic self energy model at various temperature for the vibrons ν_1 , ν_2 in the phases of ϵ, δ_{loc} and δ (P=18.5 GPa) of solid nitrogen. The anharmonic self energy model was also carried out for the calculation of the Raman frequency and linewidth of the $\nu_1 - \nu_2$ as a function of temperature at constant pressure (P= 13.2, 14.95, 18.5 and 21.2 GPa). when compared our results to the observed values, there is some inconsistency between them, as expected since the anharmonic self energy model does not work well at high temperatures. Values of the inverse relaxation time and activation energy was obtained by consulting the power law formula for the librational E_g mode ($\alpha - \beta$), the vibrons ν_1 , ν_2 ($\epsilon - \delta_{loc} - \delta$) and also the frequency difference ($\nu_1 - \nu_2$) in the nitrogen. The activation energy were derived from the temperature dependence of inverse relaxation time close the phase transitions studied. The inverse relaxation time decreases when the temperature increase as we expected from the mechanism of the order-disorder transition ($\alpha - \beta$ and ($\epsilon - \delta_{loc} - \delta$) in the solid nitrogen. As stated in our results, the values of activation energy are too large compared to those obtained for some other molecular solids. As a last part of this thesis work, we investigated the thermodynamic functions at various temperatures and pressures and analyzed the dielectric properties of cubic gauche solid nitrogen (cg-N). By analyzing temperature dependence of volume, we obtained the thermal expansion and the isothermal compressibility as a function of temperature. The values of heat capacity were also predicted by using the observed volume data, calculated thermal expansion and the isothermal compressibility for cubic gauche nitrogen. The pressure dependence of thermodynamic functions was also calculated with the observed volume data as a function of pressure. The vibrational frequencies of cg-N were predicted by applying the correlation between the Raman frequency and volume change established by the mode Grüneisen parameter. These predictions of the vibrational frequencies were used to investigate the dielectric and elastic properties of solid nitrogen and also the anharmonic properties of cg-N.

REFERENCES

- [1] P. Papon, J. Leblond, and P. Meijer, *The physics of phase transitions: Concepts and applications*. Springer, 01 2006.
- [2] D. Hohl, V. Natoli, D. M. Ceperley, and R. M. Martin, “Molecular dynamics in dense hydrogen,” *Phys. Rev. Lett.*, vol. 71, pp. 541–544, Jul 1993.
- [3] K. Takemura, K. Sato, H. Fujihisa, and M. Onoda, “Structural phase transitions in iodine under high pressure,” *Zeitschrift Fur Kristallographie - Z KRISTALLOGR*, vol. 219, pp. 749–754, 11 2004.
- [4] S. Buchsbaum, R. L. Mills, and D. Schiferl, “Phase diagram of nitrogen determined by Raman spectroscopy from 15 to 300 K at pressures to 52 GPa,” *The Journal of Physical Chemistry*, vol. 88, no. 12, pp. 2522–2525, 1984.
- [5] E. Butter, “Chemistry of the elements. pergamon press oxford 1984, 1542 seiten, 7 anhänge preis: Us \$ 34.95. isbn 0–08–022057–6,” *Crystal Research and Technology*, vol. 20, no. 5, pp. 662–662, 1985.
- [6] R. M. Martin and R. J. Needs, “Theoretical study of the molecular-to-nonmolecular transformation of nitrogen at high pressures,” *Phys. Rev. B*, vol. 34, pp. 5082–5092, Oct 1986.
- [7] A. K. McMahan and R. LeSar, “Pressure dissociation of solid nitrogen under 1 Mbar,” *Phys. Rev. Lett.*, vol. 54, pp. 1929–1932, Apr 1985.
- [8] A. K. McMahan, “New materials at high pressure,” *International Journal of Quantum Chemistry*, vol. 30, no. S20, pp. 393–408, 1986.
- [9] Y. Ma, A. R. Oganov, Z. Li, Y. Xie, and J. Kotakoski, “Novel high pressure structures of polymeric nitrogen,” *Phys. Rev. Lett.*, vol. 102, p. 065501, Feb 2009.

- [10] K. Nordlund, A. Krashennnikov, N. Juslin, J. Nord, and K. Albe, “Structure and stability of non-molecular nitrogen at ambient pressure,” *Europhysics Letters EPL*, vol. 65, pp. 400–406, feb 2004.
- [11] T. Zhang, S. Zhang, Q. Chen, and L.-M. Peng, “Metastability of single-bonded cubic-gauche structure of N under ambient pressure,” *Phys. Rev. B*, vol. 73, p. 094105, Mar 2006.
- [12] H. L. Yu, G. W. Yang, X. H. Yan, Y. Xiao, Y. L. Mao, Y. R. Yang, and M. X. Cheng, “First-principles calculations of the single-bonded cubic phase of nitrogen,” *Phys. Rev. B*, vol. 73, p. 012101, Jan 2006.
- [13] J. Kotakoski and K. Albe, “First-principles calculations on solid nitrogen: A comparative study of high-pressure phases,” *Phys. Rev. B*, vol. 77, p. 144109, Apr 2008.
- [14] B. Boates and S. A. Bonev, “First-order liquid-liquid phase transition in compressed nitrogen,” *Phys. Rev. Lett.*, vol. 102, p. 015701, Jan 2009.
- [15] R. L. Mills and A. F. Schuch, “Crystal structure of gamma nitrogen,” *Phys. Rev. Lett.*, vol. 23, pp. 1154–1156, Nov 1969.
- [16] J. A. Venables and C. A. English, “Electron diffraction and the structure of α -N₂,” *Acta Crystallographica Section B*, vol. 30, pp. 929–935, Apr 1974.
- [17] F. D. Medina and W. B. Daniels, “Raman spectrum of solid nitrogen at high pressures and low temperatures,” *The Journal of Chemical Physics*, vol. 64, no. 1, pp. 150–161, 1976.
- [18] A. S. Zinn, D. Schiferl, and M. F. Nicol, “Raman spectroscopy and melting of nitrogen between 290 and 900 K and 2.3 and 18 GPa,” *The Journal of Chemical Physics*, vol. 87, no. 2, pp. 1267–1271, 1987.
- [19] M. I. Eremets, A. G. Gavriliuk, I. A. Trojan, D. A. Dzivenko, and R. Boehler, “Single-bonded cubic form of nitrogen,” *ESRF Highlights*, vol. 2004, pp. 34–35, 2005.
- [20] A. F. Goncharov, E. Gregoryanz, H.-k. Mao, Z. Liu, and R. J. Hemley, “Optical

evidence for a nonmolecular phase of nitrogen above 150 GPa,” *Phys. Rev. Lett.*, vol. 85, pp. 1262–1265, Aug 2000.

- [21] M. Kurt and H. Yurtseven, “Band-widths of the Raman stretching modes as a function of pressure in solid nitrogen,” *Trends in Applied Spectroscopy*, vol. 9, pp. 49–54, 2012.
- [22] E. Gregoryanz, A. F. Goncharov, R. J. Hemley, H.-k. Mao, M. Somayazulu, and G. Shen, “Raman, infrared, and x-ray evidence for new phases of nitrogen at high pressures and temperatures,” *Phys. Rev. B*, vol. 66, p. 224108, Dec 2002.
- [23] L. Tassini, F. Gorelli, and L. Ulivi, “High temperature structures and orientational disorder in compressed solid nitrogen,” *The Journal of Chemical Physics*, vol. 122, no. 7, p. 074701, 2005.
- [24] A. Goncharov and E. Gregoryanz, “Solid nitrogen at extreme conditions of high pressure and temperature,” Apr 2004.
- [25] R. D. Etters, V. Chandrasekharan, E. Uzan, and K. Kobashi, “High-pressure static and dynamic properties of the R3c phase of solid nitrogen,” *Phys. Rev. B*, vol. 33, pp. 8615–8621, Jun 1986.
- [26] J. Belak, R. LeSar, and R. D. Etters, “Calculated thermodynamic properties and phase transitions of solid N_2 at temperatures $0 \leq t \leq 300$ K and pressures $0 \leq p \leq 100$ GPa,” *The Journal of Chemical Physics*, vol. 92, no. 9, pp. 5430–5441, 1990.
- [27] R. Caracas and R. Hemley, “New structures of dense nitrogen: Pathways to the polymeric phase,” *Chemical Physics Letters*, vol. 442, no. 1-3, pp. 65–70, 2007.
- [28] R. Caracas, “Raman spectra and lattice dynamics of cubic gauche nitrogen,” *The Journal of Chemical Physics*, vol. 127, no. 14, p. 144510, 2007.
- [29] H. Yurtseven and S. Saritas, “Thermodynamic quantities at high pressures in the i and ϑ – phases of solid nitrogen deduced by Raman frequency shifts for the internal modes in literature,” *International Journal of Modern Physics B*, vol. 27, no. 09, p. 1350035, 2013.

- [30] E. Gregoryanz, A. F. Goncharov, C. Sanloup, M. Somayazulu, H.-k. Mao, and R. J. Hemley, “High P-T transformations of nitrogen to 170 GPa,” *The Journal of Chemical Physics*, vol. 126, no. 18, p. 184505, 2007.
- [31] S. K. Chatterjee, *Crystallography and the World of Symmetry*. Springer, Berlin, Heidelberg, 01 2006.
- [32] W. E. Streib, T. H. Jordan, and W. N. Lipscomb, “Single-crystal x-ray diffraction study of β nitrogen,” *The Journal of Chemical Physics*, vol. 37, no. 12, pp. 2962–2965, 1962.
- [33] D. Schiferl, S. Buchsbaum, and R. L. Mills, “Phase transitions in nitrogen observed by Raman spectroscopy from 0.4 to 27.4 GPa at 15 K,” *The Journal of Physical Chemistry*, vol. 89, no. 11, pp. 2324–2330, 1985.
- [34] B. M. Powell, G. Dolling, and H. F. Nieman, “Structure and intermolecular excitations of $b - N_2$ at 400 MPa and 55 K,” *The Journal of Chemical Physics*, vol. 79, no. 2, pp. 982–991, 1983.
- [35] A. F. Schuch and R. L. Mills, “Crystal structures of the three modifications of nitrogen 14 and nitrogen 15 at high pressure,” *The Journal of Chemical Physics*, vol. 52, no. 12, pp. 6000–6008, 1970.
- [36] D. T. Cromer, R. L. Mills, D. Schiferl, and L. A. Schwalbe, “The structure of N_2 at 49 kbar and 299 K,” *Acta Crystallographica Section B*, vol. 37, pp. 8–11, Jan 1981.
- [37] R. LeSar, S. Ekberg, L. Jones, R. Mills, L. Schwalbe, and D. Schiferl, “Raman spectroscopy of solid nitrogen up to 374 kbar,” *Solid State Communications*, vol. 32, no. 2, pp. 131 – 134, 1979.
- [38] B. Olinger, “The compression of solid N_2 at 296 K from 5 to 10 GPa,” *The Journal of Chemical Physics*, vol. 80, no. 3, pp. 1309–1311, 1984.
- [39] D. Schiferl, S. Buchsbaum, and R. L. Mills, “Phase transitions in nitrogen observed by Raman spectroscopy from 0.4 to 27.4 GPa at 15 K,” *The Journal of Physical Chemistry*, vol. 89, no. 11, pp. 2324–2330, 1985.

- [40] R. L. Mills, B. Olinger, and D. T. Cromer, “Structures and phase diagrams of N_2 and CO to 13 GPa by x-ray diffraction,” *The Journal of Chemical Physics*, vol. 84, no. 5, pp. 2837–2845, 1986.
- [41] R. Bini, L. Ulivi, J. Kreutz, and H. J. Jodl, “High-pressure phases of solid nitrogen by Raman and infrared spectroscopy,” *The Journal of Chemical Physics*, vol. 112, no. 19, pp. 8522–8529, 2000.
- [42] T. Westerhoff, A. Wittig, and R. Feile, “High-pressure Raman scattering of the stretching mode in nitrogen along the 300-K isotherm,” *Phys. Rev. B*, vol. 54, pp. 14–17, Jul 1996.
- [43] C. Mailhot, L. H. Yang, and A. K. McMahan, “Polymeric nitrogen,” *Phys. Rev. B*, vol. 46, pp. 14419–14435, Dec 1992.
- [44] T. W. Barbee, “Metastability of atomic phases of nitrogen,” *Phys. Rev. B*, vol. 48, pp. 9327–9330, Oct 1993.
- [45] M. M. G. Alemany and J. L. Martins, “Density-functional study of nonmolecular phases of nitrogen: Metastable phase at low pressure,” *Phys. Rev. B*, vol. 68, p. 024110, Jul 2003.
- [46] W. D. Mattson, D. Sanchez-Portal, S. Chiesa, and R. M. Martin, “Prediction of new phases of nitrogen at high pressure from first-principles simulations,” *Phys. Rev. Lett.*, vol. 93, p. 125501, Sep 2004.
- [47] M. Eremets, A. Gavriluk, I. Troyan, D. Dzivenko, and R. Boehler, “Single-bonded cubic form of nitrogen,” *Nature materials*, vol. 3, pp. 558–63, 08 2004.
- [48] M. I. Eremets, A. G. Gavriluk, and I. A. Trojan, “Single-crystalline polymeric nitrogen,” *Applied Physics Letters*, vol. 90, no. 17, p. 171904, 2007.
- [49] R. Reichlin, D. Schiferl, S. Martin, C. Vanderborgh, and R. L. Mills, “Optical studies of nitrogen to 130 GPa,” *Phys. Rev. Lett.*, vol. 55, pp. 1464–1467, Sep 1985.
- [50] F. Zahariev, A. Hu, J. Hooper, F. Zhang, and T. Woo, “Layered single-bonded nonmolecular phase of nitrogen from first-principles simulation,” *Phys. Rev. B*, vol. 72, p. 214108, Dec 2005.

- [51] H. Olijnyk, “High pressure x-ray diffraction studies on solid N_2 up to 43.9 GPa,” *The Journal of Chemical Physics*, vol. 93, no. 12, pp. 8968–8972, 1990.
- [52] D. Heberlein, E. Adams, and T. Scott, “Thermal expansion and isothermal compressibility of solid nitrogen,” *J Low Temp Phys.*, vol. 2, pp. 449–463, May 1970.
- [53] M. I. Bagatskii, V. A. Kucheryavy, V. G. Manzhelii, and V. A. Popov, “Thermal capacity of solid nitrogen,” *physica status solidi (b)*, vol. 26, no. 2, pp. 453–460, 1968.
- [54] T. D. D. Nguyen Quang Hoc, Nguyen Duc Quyen, “Thermodynamic properties of molecular cryocrystals of nitrogen type with fcc structure: Contribution from lattice vibrations and molecular rotational motion,” *Proc. Natl. Conf. Theor. Phys.*, vol. 37, pp. 150–156, 2012.
- [55] D. Tomasino, Z. Jenei, W. Evans, and C.-S. Yoo, “Melting and phase transitions of nitrogen under high pressures and temperatures,” *The Journal of Chemical Physics*, vol. 140, no. 24, p. 244510, 2014.
- [56] M. Ross and F. Rogers, “Polymerization, shock cooling, and the high-pressure phase diagram of nitrogen,” *Phys. Rev. B*, vol. 74, p. 024103, Jul 2006.
- [57] O. Akay and H. Yurtseven, “Calculation of the Raman and IR frequencies from the volume data at high pressures in N_2 ,” *Optik*, vol. 160, pp. 227 – 233, 2018.
- [58] H. Yurtseven and O. Akay, “Calculation of the phase diagrams for the fluid-solid and solid-solid (δ - δ_{loc} - ϵ) transitions in molecular nitrogen by using mean field model,” *Revue Roumaine de Chimie*, vol. 64, pp. 249–258, 12 2019.
- [59] O. Akay and H. Yurtseven, “Calculation of the Raman frequency and linewidth of vibrons using anharmonic self energy model for the ϵ , δ_{loc} and δ phases in solid nitrogen,” *Optik*, vol. 219, p. 165202, 2020.
- [60] H. Yurtseven and O. Akay, “Raman bandwidths calculated for the librational (α -phase) and internal (ϵ , δ_{loc} and δ phases) modes in solid N_2 using pseudospin-phonon coupling (PS) and energy-fluctuation (EF) models,” *Journal of Molecular Structure*, vol. 1217, p. 128451, 05 2020.

- [61] O. Akay and H. Yurtseven, “Calculation of the thermodynamic functions from the Raman frequency shifts close to the ϵ – δ loc– δ transitions and pippard relations in nitrogen,” *Modern Physics Letters B*, (in press).
- [62] Y. H. Roos and S. Drusch, “Chapter 1 - introduction to phase transitions,” in *Phase Transitions in Foods (Second Edition)* (Y. H. Roos and S. Drusch, eds.), pp. 1 – 17, San Diego: Academic Press, second edition ed., 2016.
- [63] G. Jaeger, “The ehrenfest classification of phase transitions: Introduction and evolution,” *Arch Hist Exact Sc.*, vol. 53, pp. 51–81, May 1998.
- [64] P. Papon, S. Schnur, J. Leblond, and P. Meijer, *The Physics of Phase Transitions: Concepts and Applications*. Advanced Texts in Physics, Springer Berlin Heidelberg, 2012.
- [65] I. K. Kamilov and K. K. Aliev, “Second-order phase transitions in ferromagnetic materials in weak fields near the Curie point,” *Soviet Physics Uspekhi*, vol. 26, pp. 696–712, Aug 1983.
- [66] T. M. McQueen, A. J. Williams, P. W. Stephens, J. Tao, Y. Zhu, V. Ksenofontov, F. Casper, C. Felser, and R. J. Cava, “Tetragonal-to-orthorhombic structural phase transition at 90 K in the superconductor $\text{Fe}_{1.01}\text{Se}$,” *Phys. Rev. Lett.*, vol. 103, p. 057002, Jul 2009.
- [67] L. Landau and E.M.Lifshitz, *Statistical Physics, Part I*. Course of Theoretical Physics, Pergamon Oxford, 1980.
- [68] L. P. Kadanoff, “Phases of matter and phase transitions ; from mean field theory to critical phenomena,” *Journal of Physics: Condensed Matter*, vol. 12, p. 1496, 2009.
- [69] C. Kittel, *Introduction to Solid State Physics*. Advanced Texts in Physics, 2004.
- [70] J. A. Gonzalo, F. J. de, and J. Garcia, *Solid state spectroscopies : basic principles and applications*. River Edge, N.J. : World Scientific, 2002.
- [71] D. Chowdhury and D. Stauffer, *Statistical Mechanics of Interacting Systems: Theory of Phase Transitions*. Wiley, 2004.

- [72] A. Umantsev, *Field Theoretic Method in Phase Transformations*. Lecture notes in Physics 840, 2012.
- [73] D. J. Gardiner and P. R. Graves, *Practical Raman Spectroscopy*. Springer, Berlin, Heidelberg, 1989.
- [74] E. Grüneisen, “Theorie des festen zustandes einatomiger elemente,” *Annalen der Physik*, vol. 344, no. 12, pp. 257–306, 1912.
- [75] T. Barron, “Grüneisen parameters for the equation of state of solids,” *Annals of Physics*, vol. 1, no. 1, pp. 77 – 90, 1957.
- [76] J. Zhang, J. Zhu, N. Velisavljevic, L. Wang, and Y. Zhao, “Thermal equation of state and thermodynamic Grüneisen parameter of beryllium metal,” *Journal of Applied Physics*, vol. 114, no. 17, p. 173509, 2013.
- [77] Y. Yamada, M. Mori, and Y. Noda, “A microscopic theory on the phase transitions in NH_4Br –an ising spin phonon coupled system–,” *Journal of the Physical Society of Japan*, vol. 32, no. 6, pp. 1565–1576, 1972.
- [78] J. Kanamori, M. Kataoka, and Y. Itoh, “Cooperative jahn-teller distortion in mixed chromites,” *Journal of Applied Physics*, vol. 39, no. 2, pp. 688–689, 1968.
- [79] M. Matsushita, “Anomalous temperature dependence of the frequency and damping constant of phonons near T_l in ammonium halides,” *The Journal of Chemical Physics*, vol. 65, no. 1, pp. 23–28, 1976.
- [80] I. Laulicht and N. Luknar, “Internal-mode line-broadening by proton jumps in KH_2PO_4 ,” *Chemical Physics Letters*, vol. 47, no. 2, pp. 237 – 240, 1977.
- [81] I. Laulicht, “On the drastic temperature broadening of hard mode Raman lines of ferroelectric KDP type crystals near T_c ,” *Journal of Physics and Chemistry of Solids*, vol. 39, no. 8, pp. 901 – 906, 1978.
- [82] G. Lahajnar, R. Blinc, and S. Zumer, “Proton spin-lattice relaxation by critical polarization fluctuations in KH_2PO_4 ,” *Physics of condensed matter*, vol. 18, pp. 301–316, 1974.

- [83] G. Schaack and V. Winterfeld, “Temperature behaviour of optical phonons near t_c in triglycine sulphate and triglycine selenate. ii. evidence of non-linear pseudospin-phonon interaction,” *Ferroelectrics*, vol. 15, pp. 35–41, 1977.
- [84] A. Pippard, *The Elements of Classical Thermodynamics*. Cambridge University Press, Cambridge, 1957.
- [85] H. Yurtseven and S. Ateş, “Pippard relations and the analysis of the specific heat for the α – β transition in quartz,” *International Journal of Chemistry*, vol. 2, p. 48, 2013.
- [86] A. Debernardi, F. de Geuser, J. Kulda, M. Cardona, and E. E. Haller, “Anharmonic self-energy of phonons: Ab initio calculations and neutron spin echo measurements,” 2002.
- [87] D. Wallace, *Thermodynamics of Crystals*. Dover books on physics, 2004.
- [88] F. D. Medina and W. B. Daniels, “Raman spectrum of solid nitrogen at high pressures and low temperatures,” *The Journal of Chemical Physics*, vol. 64, no. 1, pp. 150–161, 1976.
- [89] W. F. Sherman, “Bond anharmonicities, Gruneisen parameters and pressure-induced frequency shifts,” *Journal of Physics C: Solid State Physics*, vol. 13, pp. 4601–4613, sep 1980.
- [90] W. F. Sherman, “Pressure-induced changes in mode Gruneisen parameters and general equations of state for solids,” *Journal of Physics C: Solid State Physics*, vol. 15, pp. 9–23, jan 1982.
- [91] H. Olijnyk and A. P. Jephcoat, “Vibrational dynamics of isotopically dilute nitrogen to 104 GPa,” *Phys. Rev. Lett.*, vol. 83, pp. 332–335, Jul 1999.
- [92] P. Bell, H. Mao, and R. Hemley, “Observations of solid H_2 , D_2 and N_2 at pressures around 1.5 Mbar at 25°C,” *Physica B+C*, vol. 139-140, pp. 16 – 20, 1986.
- [93] H. Schneider, W. Häfner, A. Wokaun, and H. Olijnyk, “Room temperature Raman scattering studies of external and internal modes of solid nitrogen at

- pressures $8 \leq p \leq 54$ GPa,” *The Journal of Chemical Physics*, vol. 96, no. 11, pp. 8046–8053, 1992.
- [94] G. D. Mukherjee and R. Boehler, “High-pressure melting curve of nitrogen and the liquid-liquid phase transition,” *Phys. Rev. Lett.*, vol. 99, p. 225701, Nov 2007.
- [95] A. Jephcoat, R. Hemley, H. Mao, and D. Cox, “Pressure-induced structural transitions in solid nitrogen,” *Bull. Am. Phys. Soc.*, vol. 33, p. 522, 1988.
- [96] R. Brout, *Phase transitions*. Benjamin, New York USA, 1965.
- [97] M. Brith, A. Ron, and O. Schnepp, “Raman spectrum of α - N_2 ,” *The Journal of Chemical Physics*, vol. 51, no. 4, pp. 1318–1323, 1969.
- [98] J. E. Cahill and G. E. Leroi, “Raman spectra of solid CO_2 , N_2O , N_2 , and CO,” *The Journal of Chemical Physics*, vol. 51, no. 4, pp. 1324–1332, 1969.
- [99] P. M. Mathai and E. J. Allin, “Low frequency raman spectra of $\alpha_{16}O_2$, $\alpha_{18}O_2$, and α -N .,” *Can. J. Phys.* 49: No. 15, 1973-5(1 Aug 1971).
- [100] U. D. Yurtseven, H., “Temperature and pressure effect on the Raman frequencies calculated from the crystal volume in the γ -phase of solid nitrogen,” *Journal of Applied Spectroscopy*, vol. 82, p. 700, 2015.
- [101] M. I. M. Scheerboom and J. A. Schouten, “Anomalous behavior of the vibrational spectrum of the high-pressure δ phase of nitrogen: A second-order transition,” *Phys. Rev. Lett.*, vol. 71, pp. 2252–2255, Oct 1993.
- [102] W. L. Vos and J. A. Schouten, “Improved phase diagram of nitrogen up to 85 kbar,” *The Journal of Chemical Physics*, vol. 91, no. 10, pp. 6302–6305, 1989.
- [103] Y. Tao, L. Wei-Peng, L. Ying-Zhe, W. Bo, G. Zhong-Xue, and B. Jian-Hua, “The outlook for platonic and cubic gauche nitrogens,” *Computational Materials Science*, vol. 123, pp. 31 – 39, 2016.
- [104] H. Yurtseven, z. Tiryaki, and O. Tari, “Pippard relations for cubic gauche nitrogen,” *Anadolu University Journal of Science and Technology A - Applied Sciences and Engineering*, vol. 17, pp. 741 – 746, 2016.

- [105] X. Wang, F. Tian, L. Wang, T. Cui, B. Liu, and G. Zou, “Structural stability of polymeric nitrogen: A first-principles investigation,” *The Journal of Chemical Physics*, vol. 132, no. 2, p. 024502, 2010.
- [106] X. L. Wang, Z. He, Y. M. Ma, T. Cui, Z. M. Liu, B. B. Liu, J. F. Li, and G. T. Zou, “Prediction of a new layered phase of nitrogen from first-principles simulations,” *Journal of Physics: Condensed Matter*, vol. 19, p. 425226, sep 2007.
- [107] J. Hooper, A. Hu, F. Zhang, and T. K. Woo, “Genetic algorithm and first-principles DFT study of the high-pressure molecular ζ phase of nitrogen,” *Phys. Rev. B*, vol. 80, p. 104117, Sep 2009.
- [108] G. G. Raju, *Dielectric Loss and Relaxation—I*, ch. chapter3, pp. 1–55. CRC Press, 2016.

CURRICULUM VITEA

PERSONAL INFORMATIONS

Surname, Name: Akay,Özge

Nationality: Turkish (TC)

Date and Place of Birth: 25 March 1985, Kocaeli/Turkey

Phone: +90 (554) 465 0856

EDUCATION

Degree	Institution	Year of Graduation
Ph.D.	Physics, Middle East Technical University	2020
M.S.	Physics, Bilkent Üniversitesi	2013
B.S.	Physics, Middle East Technical University	2010

PROJECT

2011/2012	Differential Microfluidic Sensors, supported by The Scientific and Technological Research Council of Turkey , TUBITAK 1001, 110T304.
-----------	--

PROFESSIONAL EXPERIENCE

2018/2019 (Fall-Spring)	Lecturer, Qatar Naval Academy, Doha-Qatar Freshman Physics I-II
2015-	Teaching Assistant, Physics Group, PiriReis University, Freshman Physics Laboratory (101-102)
2010-2013	Teaching Assistant, Department of Physics, Bilkent University, Freshman Physics Laboratory
2011-2013	Project assistant, Advanced Research Laboratories, Bilkent University <ul style="list-style-type: none">• Clean room experience (Mask Aligner, PECVD, RIE).• Nanofabrication techniques (lithography, phase shift lithography).• Metallization (Box Coater).• Graphane growth.

PUBLICATIONS

- H.Yurtseven, Ö.Akay Analysis of the Raman Frequency Shifts for the Lattice Modes and Vibrons related to the Thermodynamic Quantities in the η phase of solid nitrogen. High Temperature Materials and Processes, 32 (4) 383–389 (2013).
- Ö.Akay, H. Yurtseven, Calculation of the Raman and IR frequencies from the volume data at high pressures in N_2 , International Journal for Light and Electron Optik, 160 227-233 (2018).
- H. Yurtseven, Özge Akay, Calculation of the phase diagrams for the fluid-solid and solid-solid (δ - δ_{loc} - ϵ) transitions in molecular nitrogen by using mean field model, Revue Roumaine de Chimie, 64(3) 249-258 (2019).
- Ö.Akay, H. Yurtseven, Calculation of the thermodynamic functions using a mean field model for the fluid-solid transition in nitrogen, Revue Roumaine de Chimie, , 65(5), 425-432 (2020).

- H.Yurtseven, Ö.Akay, Liquid-(Solid+Liquid) Transitions in a Two-component system of $(CH_3)CCl_3 + CCl_4$, Journal of Solution of Chemistry, 49 (2) 195-209 (2020).
- H.Yurtseven, Ö.Akay, Raman bandwidths calculated for the librational (α -phase) and internal (ϵ , δ_{loc} and δ phases) modes in solid N_2 using pseudospin-phonon coupling (PS) and energy-fluctuation (Ef) models, Journal of Molecular Structure, 1217 128451 (2020).
- Ö.Akay, H.yurtseven, Calculation of the Raman frequency and linewidth of vibrons using anharmonic self energy model for the ϵ , δ_{loc} and δ phases in solid nitrogen, Optik, 219 165202 (2020).
- Ö.Akay, H. Yurtseven, Calculation of the thermodynamic functions from the Raman frequency shifts close to the ϵ - δ_{loc} - δ transitions and Pippard relations in nitrogen, Modern Physics letter B, 2020 (in press).
- H. Yurtseven, Ö.Akay, Calculation of the inverse relaxation time and the activation energy as a function of temperature for the Raman modes close to the phase transitions in solid nitrogen, Journal of Molecular Structure,1226 129347(2021).

CONFERENCES, MEETINGS AND COURSES ATTENDED

- Course attended,Theoretical Physics, Utrecht University,28 July - 14 August 2010, Holland
- Oral presentation on “A Microfluidic based Hydrodynamic Modulation Voltammetry (Electrochemical Sensor) ” in the NANOTR8 - 8th Nanoscience and Nanotechnology Conference, Hacettepe University, Ankara,27 June–01 July 2012, TURKEY
- Oral presentation on “Calculation of the Raman and IR Frequencies from the volume data at high pressures in N_2 ” in the The 3rd International Turkish Congress on Molecular Spectroscopy, Bodrum,26-29 August 2017, TURKEY.

- Oral presentation on “Calculation of the Melting Temperatures at high Pressures in Nitrogen using a Mean Field Model” in the 21. Sıvı Hal Sempozyumu ,Piri Reis University, İstanbul,21 December 2017, TURKEY
- Poster presentation on “Calculating Phase Diagram of Solid Nitrogen by using Mean Field Theory “ in the 23. Yoğun Madde Fiziği Toplantısı, METU, Ankara,22 December 2017, TURKEY
- Oral presentation on “Calculation of The T-X Phase Diagram in a Two-Component System by using Mean Field Model” in the 22. Sıvı Hal Sempozyumu ,Piri Reis University, İstanbul,07 December 2018, TURKEY
- Poster presentation on “Calculation of the Raman frequency and linewidth of vibrons using anharmonic self energy model for the ϵ , δ_{loc} and δ phases in solid nitrogen “ in the 24. Yoğun Madde Fiziği Toplantısı, Bilkent University, Ankara,21 December 2018, TURKEY